

Breathing Life Into Dinosaurs: Tackling Challenges of Soft-Tissue Restoration and Nasal Airflow in Extinct Species

JASON M. BOURKE,^{1*} WM. RUGER PORTER,¹ RYAN C. RIDGELY,²
TYLER R. LYSON,³ EMMA R. SCHACHNER,⁴ PHIL R. BELL,⁵
AND LAWRENCE M. WITMER²

¹Department of Biological Sciences, Ohio University, Athens, Ohio

²Department of Biomedical Sciences, Heritage College of Osteopathic Medicine, Ohio University, Athens, Ohio

³Department of Earth Sciences, Denver Museum of Nature and Science, Denver, Colorado

⁴Department of Veterinary Clinical Sciences, Louisiana State University School of Veterinary Medicine, Baton Rouge, Louisiana

⁵Department of Environmental and Rural Science, University of New England, Armidale, New South Wales, Australia

ABSTRACT

The nasal region plays a key role in sensory, thermal, and respiratory physiology, but exploring its evolution is hampered by a lack of preservation of soft-tissue structures in extinct vertebrates. As a test case, we investigated members of the “bony-headed” ornithischian dinosaur clade Pachycephalosauridae (particularly *Stegoceras validum*) because of their small body size (which mitigated allometric concerns) and their tendency to preserve nasal soft tissues within their hypermineralized skulls. Hypermineralization directly preserved portions of the olfactory turbinates along with an internal nasal ridge that we regard as potentially an osteological correlate for respiratory conchae. Fossil specimens were CT-scanned, and nasal cavities were segmented and restored. Soft-tissue reconstruction of the nasal capsule was functionally tested in a virtual environment using computational fluid dynamics by running air through multiple models differing in nasal soft-tissue conformation: a bony-bounded model (i.e., skull without soft tissue)

Abbreviations used: acPM = anastomotic canal in premaxilla; aEth = ethmoid artery; air = airway; anas = anastomosis between palatine, lateral nasal, and dorsal alveolar vessels; aSO + LN = anastomosis between supraorbital and lateral nasal vessels; aSph = sphenopalatine artery; at = potential accessory turbinate; bch = bony choana (fenestra exochoanalis); bLN = branches of lateral nasal vessels; bMN = branches of medial nasal vessels; cap = cartilaginous nasal capsule; caud co = caudal concha; cDA = dorsal alveolar canal; ch = choana (fenestra endochoanalis); cLN = canal for lateral nasal vessels; cMN = canal for medial nasal vessels; co = concha; cPM = canal in premaxilla; cSO + LN = canal for anastomosis between supraorbital and lateral nasal vessels; cSO = canal for supraorbital vessels; DA = dorsal alveolar vessels; f = frontal; fSO = suborbital fenestra; gLN = groove for lateral nasal vessels; j = jugal; lac = lacrimal; Lc = lacrimal canal; LN = lateral nasal vessels; max = maxilla; mid co = middle concha; MN = medial nasal vessels; mu = mucosa; nar = naris; nas = nasal; nc = nasal capsule; ng = nasal gland; npd = ductus nasopharyngeus; ns = nasal septum; ob = olfactory bulb; OfC = olfactory conchal vessels; olf e = olfactory epithelium; om = olfactory meatus; ot = olfactory turbinate; p = parietal; PA = palatine vessels; pl = palatine; pm = premaxilla; po = postorbital; post = postvestibular ridge; preco = preconcha; preco rec = preconchal recess; prf = prefrontal; ps = parasphenoid rostrum; pt = pterygoid; q = quadrate; qj = quadratojugal; RC = respiratory conchal vessels; res e = respiratory epithelium; sDS = dorsal

sagittal sinus; so1 = supraorbital 1; so2 = supraorbital 2; som = supraorbital bone (mineralized supraorbital membrane); sOf = olfactory sinus; SO = supraorbital vessels; sq = squamosal; t = tongue; turb = turbinate; v = vomer; vest = vestibulum nasi; vp = ventromedian process.

This article includes AR WOW Videos, which can be viewed at <http://bcove.me/k1si0ck1>.

Grant sponsor: National Science Foundation; Grant number: IOB-0517257 and IOS-1050154; Graduate Research Fellowship; Grant sponsor: Jurassic Foundation grant; Grant sponsor: The University of Pennsylvania Summer Research Stipend in Palaeontology.

This article was published online on October 14, 2014. An extraneous sentence was added just before the Acknowledgement section and it has since been removed. This notice is included in the online version to indicate that both have been corrected October 15, 2014.

*Correspondence to: Jason M. Bourke, Department of Biological Sciences, Ohio University, Athens, OH 45701. E-mail: jb513009@ohio.edu

Received 24 June 2014; Accepted 25 June 2014.

DOI 10.1002/ar.23046

Published online in Wiley Online Library (wileyonlinelibrary.com).

and then models with soft tissues added, such as a paranasal septum, a scrolled concha, a branched concha, and a model combining the paranasal septum with a concha. Deviations in fluid flow in comparison to a phylogenetically constrained sample of extant diapsids were used as indicators of missing soft tissue. Models that restored aspects of airflow found in extant diapsids, such as appreciable airflow in the olfactory chamber, were judged as more likely. The model with a branched concha produced airflow patterns closest to those of extant diapsids. These results from both paleontological observation and airflow modeling indicate that *S. validum* and other pachycephalosaurids could have had both olfactory and respiratory conchae. Although respiratory conchae have been linked to endothermy, such conclusions require caution in that our re-evaluation of the reptilian nasal apparatus indicates that respiratory conchae may be more widespread than originally thought, and other functions, such as selective brain temperature regulation, could be important. *Anat Rec*, 297:2148–2186, 2014. © 2014 Wiley Periodicals, Inc.

Key words: dinosaurs; pachycephalosaurs; computational fluid dynamic; turbinates; conchae; physiology; soft tissue; reconstruction

Dinosaur nasal cavities present a diverse array of shapes and sizes, ranging from seemingly simple nostril-to-throat passages, all the way to elaborate convoluted pathways (Coombs, 1978; Witmer, 2001; Vickaryous and Russell, 2003; Witmer and Ridgely, 2008a; Evans et al., 2009; Miyashita et al., 2011). A number of functions have been proposed for this elaboration of the nasal apparatus including thermoregulatory benefits (Maryańska, 1977; Wheeler, 1978; Witmer and Sampson, 1999), enhanced olfaction (Ostrom, 1961, 1962; Miyashita et al., 2011), phonation (Weishampel, 1981; Evans et al., 2009), and osmoregulation (Osmólska, 1974). None of these functions are mutually exclusive, and the diversity of dinosaurs throughout the Mesozoic makes it likely that different species emphasized different functions.

Early dinosaur nasal reconstructions focused on specimens that represented extremes of narial architecture such as sauropods (Osborn, 1898; Romer, 1933; Coombs, 1975) and hadrosaurs (Ostrom, 1961, 1962; Weishampel, 1981). Soft-tissue reconstruction in extinct animals has relied heavily on the bony features of fossils along with comparative anatomy of similar, related taxa (e.g., Romer, 1922, 1924; Simpson and Elftman, 1928; Colbert, 1946; Haas, 1955). Much of this work has focused on muscle reconstruction as the relationship between muscle and bone is often the most observable. However, other soft tissues have also been reconstructed in this fashion, including blood vessels (Lehman, 1996) and general neuromorphology (Hopson, 1979). Incorporation of the extant phylogenetic bracket (EPB) with its inverted pyramid of inference (Witmer, 1995a) greatly increased the confidence of soft-tissue reconstructions by providing a stable, evolutionarily-grounded framework. Reconstructions that have followed from it have produced the most accurate inferences of soft tissues in extinct animals to date (Witmer, 1997a; Carrano and Hutchinson, 2002; Snively and Russell, 2007; Holliday and Witmer, 2008; Witmer and Ridgely, 2008a, b, 2009; Witmer et al., 2008; Evans et al., 2009; Hieronymus et al., 2009; Holliday, 2009; Tsuihiji, 2010; Schachner et al., 2011a).

Despite these improvements, the soft-tissue relations of the nasal region remain elusive due to the preservational biases of the fossil record. Whereas the nasal cavity is composed of bone, its contents—the cartilaginous nasal capsule and associated structures (turbinates, mucosa, etc.)—are mostly composed of soft tissues that rarely fossilize (Fig. 1). These soft tissues support critical, physiologically relevant functions in extant taxa. Reconstructions have typically used the internal bony boundaries of the nasal cavity to determine the shape of the nasal capsule (Witmer and Ridgely, 2008a; Evans et al., 2009). These results have produced nasal cavity shapes that faithfully represent the outermost extent of the nasal capsule adjacent to the bone, but leave the inner boundaries adjacent to the air spaces unresolved, producing a large empty shell (Fig. 2). Our previous work comparing the effects of shape between bony-bounded nasal capsules and soft-tissue nasal capsules of extant diapsids has shown that not taking into account these missing soft tissues greatly changes the patterns of respired airflow, resulting in underestimated physiological capabilities in the animals studied (Bourke and Witmer, 2011). Study of the osteological correlates (OC) for these missing tissues has not received adequate attention previously, limiting our understanding of extinct animal physiology.

One potential means of testing hypotheses on the possible locations of nasal soft-tissue structures in extinct taxa is to use airflow patterns through the nasal capsule as a guide. Shared nasal airflow patterns observed in the extant relatives (birds, crocodylians, and lizards) of extinct dinosaurs provide evidence for phylogenetic constraint, highlighting regions of similarity among taxa. Given the causative role that nasal soft tissues play in determining airflow patterns, hypotheses of soft tissues in the nasal cavities of extinct taxa can be tested via their effects on modeled airflow in comparison to phylogenetically conserved airflow patterns present in extant outgroups. This method of soft-tissue reconstruction is somewhat similar to Rudwick's (1964) "paradigm

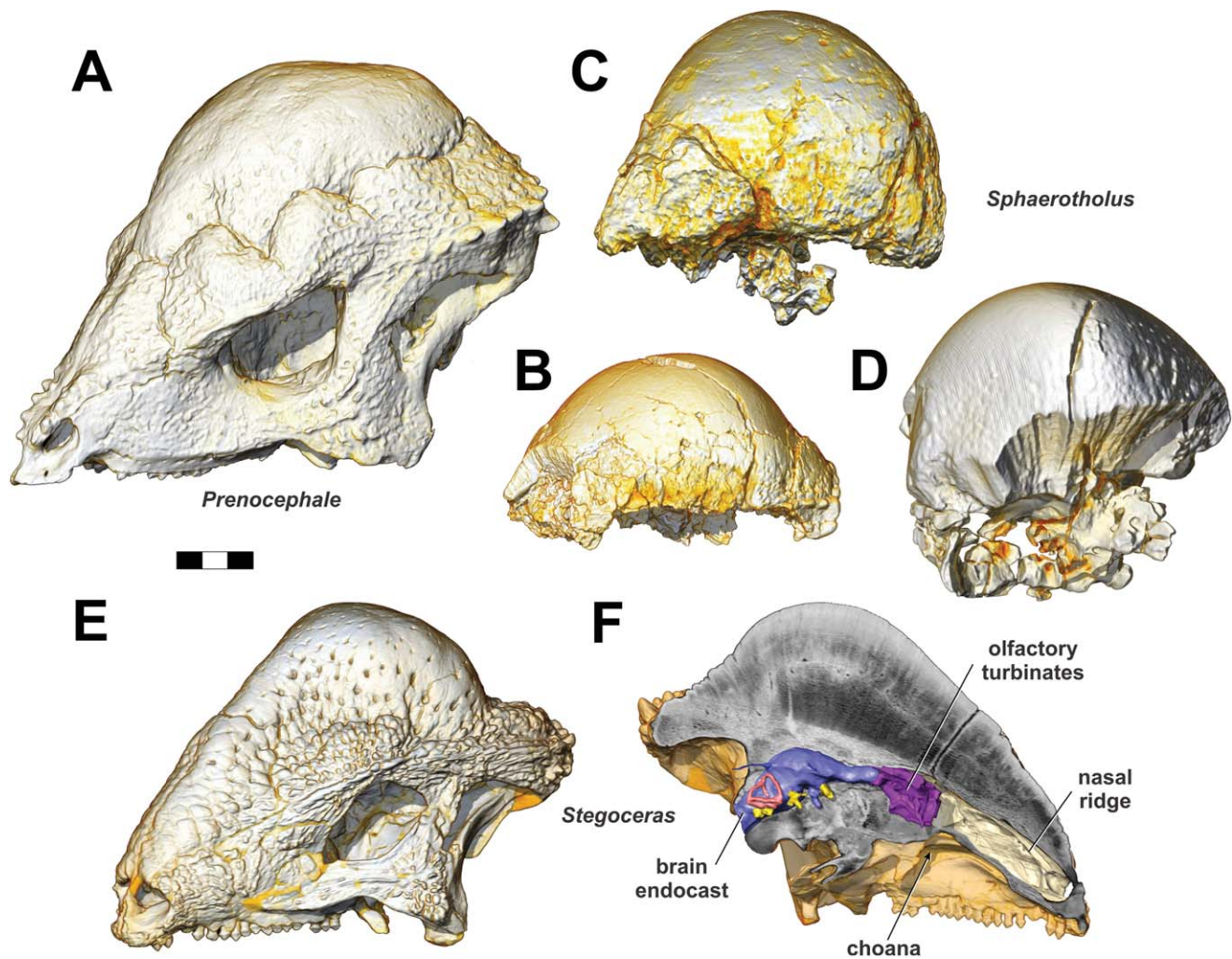


Fig. 1. Pachycephalosaurid skulls discussed in this article, based on volume-rendered CT-scan data, in oblique left rostralateral view, except for F which is a medial view of the left half of a sagittally sectioned skull. **A:** *P. prenes*, ZPAL MgD-1/104. **B:** *S. edmontonensis*, MRF 360. **C:** *S. edmontonensis*, MRF 361. **D:** *S. goodwini*, NMMNH

P-27403. **E:** *S. validum*, UALVP 2. **F:** *S. validum*, UALVP 2, sagittally sectioned to reveal putative respiratory turbinate ridge on the nasal and segmented surfaces of brain endocast and mineralized olfactory turbinates. Scale bar = 3 cm. See text for full taxon names.

approach” in which one assesses the function of a structure in an animal or animal group, by comparing it to its “idealized” form. However, unlike Rudwick’s paradigm, we do not assume that the nasal capsule is optimized for any particular function. The nose serves a variety of functions, all of which are phylogenetically constrained and some of which conflict with one another (e.g., respiration vs. olfaction), thus limiting the optimality of any one function. Instead of optimization, airways of extinct animals are judged based on how consistent their airflow pattern is compared to observed or modeled airflow patterns in extant animals. As a trivial example, given that inspired air travels from nostril to throat in all extant outgroups, any soft-tissue hypotheses in dinosaurs that disallowed such flow would be falsified on phylogenetic grounds. As a more sophisticated example, the hypothesis that the caudodorsal region of the nasal capsule adjacent to the olfactory bulb of the brain was ventilated in extinct dinosaurs may be tested by study-

ing airflow patterns in extant outgroups with similar associations. Should these outgroups show airflow in this olfactory region, any nasal-capsule soft-tissue hypotheses in dinosaurs that fail to produce olfactory airflow would be falsified. Thus, phylogenetically constrained airflow patterns can be used as a standard by which airflow in extinct taxa can be compared, tested, and potentially restored. Unlike many functional properties that rely on a suite of attributes that do not preserve in the fossil record (e.g., the detailed functioning of the feeding apparatus depends on attributes like muscle architecture and neural motor activation patterns), airflow is ultimately the outcome of well-understood physical parameters (fluid dynamics), making it useful for soft-tissue reconstruction. To simulate airflow, models can be subjected to a computational fluid dynamic (CFD) analysis. CFD is an engineering technique used extensively in industry (Agarwal, 1999; Brzustowicz et al., 2002, 2003; Mirade and Daudin, 2006; Yam et al., 2011),

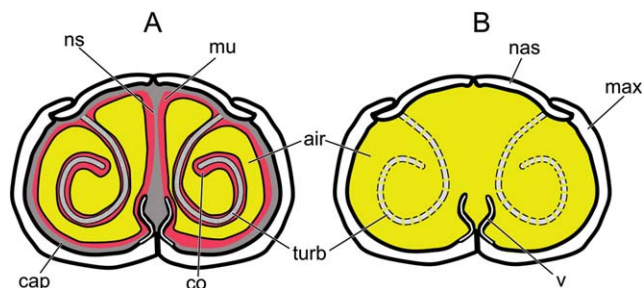


Fig. 2. Diagrammatic cross sections through the nasal region of a generalized amniote. **A:** The nasal passage can be broken down into a series of nested layers starting with the bones surrounding the nasal cavity (white). Deep to the bones of the nasal cavity is the cartilaginous nasal capsule and nasal septum (gray) as well as cartilaginous or mineralized turbinates (hatched). Deep to this layer lies the mucosa (red) and conchae. The deepest region is the open space of the nasal airway where respired air travels (yellow). **B:** In contrast, fossilized airways rarely retain evidence of the soft tissue within, resulting in a much lower fidelity, bony-bounded airway. Even mineralized turbinates may not preserve due to their delicate architecture.

as well as in medicine (Hoi et al., 2004; Guilherme et al., 2007; Chen et al., 2009). CFD uses numerical simulation techniques that typically utilize either the finite element or finite volume method. Models are broken into thousands, or even millions of discrete elements collectively referred to as a computational mesh. Governing equations for fluid flow are discretized and then numerically solved across this mesh. The ability of CFD to simulate fluid flow in a digital environment reduces the costs associated with creating elaborate flume structures or from acquiring and maintaining the machinery needed for digital particle image velocimetry (Lauder et al., 2003). The largest limiting factor for CFD comes down to computational power.

Even with airflow-aided nasal reconstructions, the fidelity of reconstructed airflow achievable in extinct species will be limited by the taxa chosen, quality of fossil preservation, and overall skull architecture. For instance, the nasal capsule of many theropod dinosaurs was only partially bounded by the bones of the nasal cavity, leaving large areas of the nasal capsule bounded only by other soft tissues. The same limitation is seen in large sauropods (Fig. 3). Although evidence for a rostrocaudal extended nasal vestibule has been discovered in sauropods (Witmer, 2001), these results only indicated rostrocaudal extent, leaving the nasal roof, or tectum nasi, completely unbounded and potentially quite variable. Further complicating matters are the large sizes of most dinosaur species (O’Gorman and Hone, 2012), many of which were larger than any terrestrial animal today. These large size discrepancies make it problematic to predict physiological parameters for dinosaurs based on the osteology of extant animals as such predictions require extrapolation beyond the empirical data.

Nasal soft-tissue reconstructions benefit from a “best case” scenario that utilizes taxa that fall within the size range of extant animals while also having nasal passages that are osteologically well defined. Pachycephalosaurs appear to provide this ideal case (Fig. 1). The group is composed of small to moderate sized species (Maryańska and Osmólska, 1974). Although much focus has been placed on the enlarged domes and their role in

paleobiology (Fastovsky and Weishampel, 2005; Snively and Cox, 2008; Horner and Goodwin, 2009; Schott et al., 2011; Snively and Theodor, 2011), pachycephalosaurs are also known for extensive mineralization of soft tissues, contributing to the supraorbital ridge of the skull (Maidment and Porro, 2009) and continuing to the tail where mineralized myosepta have recently been discovered (Brown and Russell, 2012). Few pachycephalosaurs preserve much more than a dome, but skulls or partial skulls are known for some species. Computerized Tomography (CT) scan data of the exceptionally well preserved holotype skull of *Stegoceras validum* (UALVP 2) revealed the presence of mineralized olfactory turbinates in the nasal cavity (Fig. 1E,F). Similar turbinates were also found in two specimens of the derived pachycephalosaur *Sphaerotholus* spp.: *S. edmontonensis* (MRF 360, Fig. 1B) and *S. goodwini* (NMMNH P-27403, Fig. 1D). Moreover, as is discussed below, ridges preserved on the nasal bones of both *Stegoceras* (Fig. 1F) and two specimens of *Sphaerotholus edmontonensis* may represent the mineralized bases of respiratory turbinate or conchal structures. Mineralization of these turbinates provides a rare glimpse of the soft tissues that were present in the nasal passages of a dinosaur. They also allow for direct comparisons with other diapsids, testing hypotheses of turbinate shape in dinosaurs. Such well defined structures make the nasal cavity of pachycephalosaurs the most amenable for soft-tissue reconstruction. Other published examples of mineralized olfactory turbinates (e.g., ankylosaurs; Witmer and Ridgely, 2008a) or mineralized olfactory and respiratory turbinates (e.g., tyrannosaurids; Witmer and Ridgely, 2010) come from large dinosaurs outside the range of extant empirical data, and so pachycephalosaurs may indeed provide our strongest case for restoring and interpreting nasal function in extinct dinosaurs.

The work presented here is an extension of prior work that has been conducted on a variety of extant diapsid species including crocodylians (Bourke and Witmer, 2010), birds (Bourke and Witmer, 2011) and lizards. This work has been extended to dinosaurs previously, with preliminary models of airflow in *Majungasaurus*, *Diplodocus*, and *Camarasaurus* (Bourke and Witmer, 2012). The use of pachycephalosaurs in this study provides the most complete reconstruction of nasal soft tissues in a dinosaur to date.

APPROACH

We set out to test the effects of soft-tissue configurations in the nasal capsule of pachycephalosaurs. We started by first reconstructing the most conservative interpretation of the nasal anatomy, which was accomplished using CT-scan data and segmentation software to reconstruct the nasal capsule based on only the bony-boundaries of the surrounding nasal cavity. The result produced a nasal capsule that hugged the surrounding bones and was reminiscent of previous soft-tissue nasal capsule reconstructions in extinct animals (e.g., Witmer and Ridgely, 2008a). From this original model, the nasal capsule was progressively modified by the addition of potential soft-tissue structures—including turbinates—based on the shapes observed in the extant relatives of dinosaurs. CFD was used to assess the functional implications of these different anatomical variants by comparing nasal flow patterns between the different models and against previous CFD models of related extant animals.

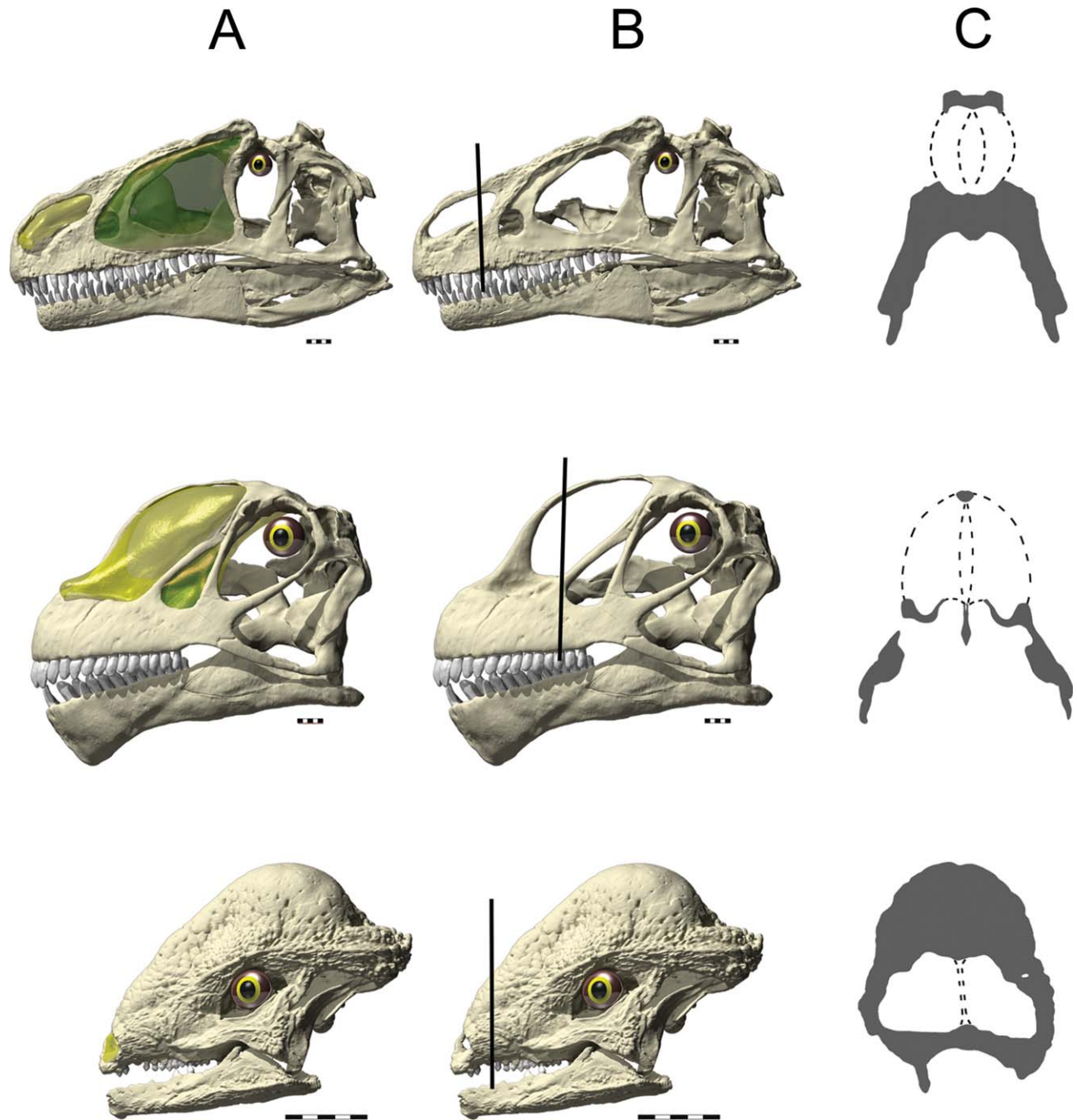


Fig. 3. Comparison of nasal cavity boundaries in the dinosaur genera *Allosaurus* (top), *Camarasaurus* (middle), and *Stegoceras* (bottom). **A:** Skulls with nasal capsule and paranasal sinuses restored. **B:** Skulls without restored nasal passages. Black line indicates the location of **(C)** cross sections taken through the nasal passage. Dotted lines indicate the bound-

aries of conservatively restored nasal passages. Note the extensive unbounded regions of the nasal cavity in *Allosaurus* and *Camarasaurus* compared to *Stegoceras*. The well-constrained nasal cavity of *Stegoceras* is more amenable to soft-tissue restoration. Scale bar = 5 cm.

TERMINOLOGY

Bony Nasal Cavity

We use this general term to incorporate the outermost border of the bony nasal passage and everything within it. It is bounded by the bones of the facial skeleton,

which for diapsids typically consist of the premaxilla, maxilla, nasal, prefrontal, lacrimal, palatine, and vomer. Its rostralmost extent ends at the bony narial aperture whereas the caudal extent usually ends at the lacrimal, prefrontal, and palatines (extending as far back as the pterygoids in crocodylians).

Bony and Fleishy Nostril

The bony nostril is the rostral opening of the bony nasal cavity, bounded by the premaxilla, nasal, and maxilla. This bony structure is often called the “naris” by paleontologists, but that term technically refers to the fleshy nostril and the formal term is bony narial aperture [apertura nasi ossea (Baumel and Witmer, 1993; Waibl et al., 2012)]. The distinction is important here as we will use the terms fleshy and bony nostril (Witmer, 2001).

Bony and Fleishy Choana

As with nostrils, the term choana has often been applied to both the bony opening of the nasal cavity within the palate as well as the fleshy opening of the nasal cavity into the pharynx. However, these are two structurally distinct anatomical features. The bony choana is the skeletal structure surrounding the smaller fleshy choana [fenestrae exochoanalis and endochoanalis, respectively (Jarvik, 1942; Bellairs, 1949)]. Rarely are these two structures identical. As such, we will distinguish between the two when necessary.

Nasal Capsule

This cartilaginous structure is deep to the bony nasal cavity and serves as the main point of attachment or outgrowth for most of the soft tissues inside the nasal passage (e.g., turbinates, mucosa, and conchae). The rostral extent of the nasal capsule may continue as a cartilaginous extension beyond the bony borders of the bony narial aperture as external nasal cartilages.

Conchae and Turbinates

The terms turbinate (or turbinal) and concha are often used interchangeably, but we prefer to separate the two. The turbinates are the cartilaginous outgrowths of the nasal capsule that project into the nasal cavity, whereas the conchae comprise the overlying mucosa that covers the turbinates. Turbinates can be viewed as the internal support of the conchae, although sometimes conchae can be entirely mucosal with no internal support. Turbinates often take the form of thin scrolls or lamellae (branched or unbranched) of cartilage that sometimes mineralize and thus are occasionally preserved within the bony nasal cavity in dried skulls and fossils, providing some indication of the presence and disposition of the conchal mucosa. Functionally, the conchae are more important, being the physiological players that increase the available surface area for respired air to pass over, allowing them to function in countercurrent heat exchange as well as odorant analysis. The functions of conchae vary depending on location in the nasal passage and what epithelial layers they support (e.g., respiratory vs. olfactory epithelium).

Mucosal Layer

Resting on the inner surfaces of the nasal capsule and conchae is the nasal epithelium. Various epithelial types and their corresponding submucosal neurovascular bundles are found here. Three basic epithelial types can be distinguished in the nasal passage, in roughly rostral to caudal order: cornified stratified epithelium, ciliated

columnar (respiratory) epithelium, and olfactory epithelium (identified by the presence of olfactory receptor neurons and Bowman’s glands).

Airway

This is the deepest space within the nasal passage and is occupied by respired air. The nasal airway passes from the fleshy nostril to the fleshy choana.

Divisions of the Nasal Passages

Diapsid nasal passages received special attention in the works of Parsons (1959, 1967, 1970), Bang (1960, 1971), Bang and Wenzel (1985), and Witmer (1995b). Diapsid nasal passages vary greatly in size and shape, but their gross underlying structure shows consistent and predictable morphologies. This structure allows for separation of the nasal capsule into the following three compartments. (1) Vestibulum nasi: The nasal vestibule is the rostralmost portion of the nasal capsule just deep to the fleshy nostril. It is typically a tubular region that is smaller in diameter than the succeeding cavum nasi proprium. (2) Cavum nasi proprium (CNP): Continuing caudally from the vestibulum nasi and rostral to the ductus nasopharyngeus, the cavum nasi proprium (= main nasal cavity) typically occupies a more capacious portion of the nasal capsule. Conchae, both respiratory and olfactory, tend to lie within the CNP. The olfactory chamber resides within the cavum nasi proprium at its caudalmost extent and is typically outside of the main respiratory flow. (3) Ductus nasopharyngeus: Following the terminology of Parsons (1970), the nasopharyngeal duct is defined as any connection from the cavum nasi proprium that leads to the choana. It varies in length and complexity between taxa.

INSTITUTIONAL ABBREVIATIONS

MRF, Marmarth Research Foundation, Marmarth, ND; NMMNH, New Mexico Museum of Natural History, Albuquerque, NM; OUVC, Ohio University Vertebrate Collections, Athens, OH; UALVP, University of Alberta Laboratory for Vertebrate Paleontology, Edmonton, AB; ZPAL, Institute of Paleobiology, Polish Academy of Sciences, Warsaw.

FOSSIL SPECIMENS AND CT SCANNING

We primarily focused on two pachycephalosaurid species, *Stegoceras validum* and *Sphaerolitholus edmontonensis*, supplemented with data from another species of *Sphaerolitholus* (*S. goodwini*; Williamson and Carr, 2002) and *Prenocephale prenes* (Maryńska and Osmólska, 1974). Sullivan (2003, 2006) formally referred the two species of *Sphaerolitholus* to the Mongolian genus *Prenocephale*, and this assignment was followed by Schott et al. (2009) and Watabe et al. (2011). The name *Sphaerolitholus*, however, was retained by Maryńska et al. (2004), Longrich et al. (2010), and Evans et al. (2013), and we follow this taxonomy. Likewise, some workers synonymize *S. edmontonensis* with *S. buchholtzae* (Williamson and Carr, 2002), but we provisionally follow Sullivan (2003, 2006), Schott et al. (2009), Longrich et al. (2010), and Watabe et al. (2011) in accepting the validity of the species epithet *edmontonensis*. All recent authors

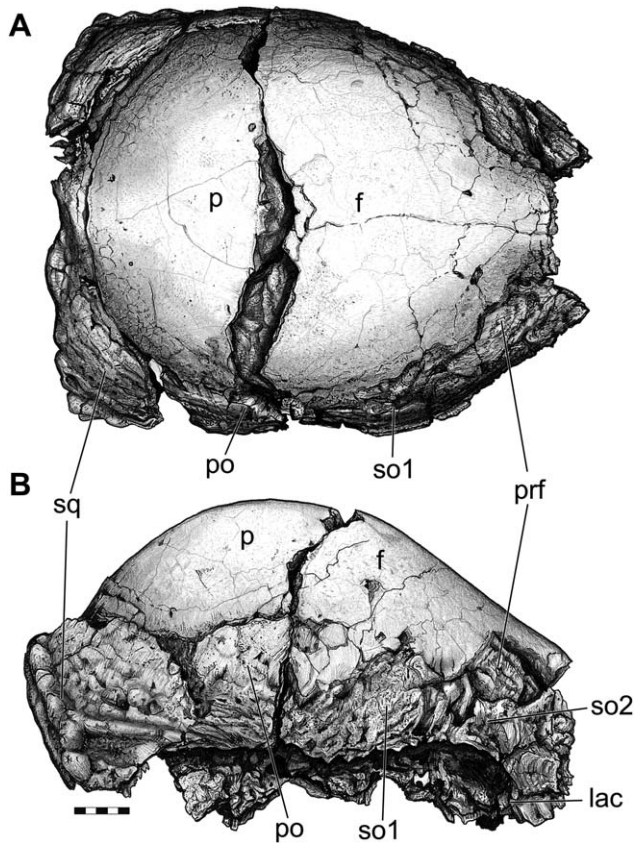


Fig. 4. Preserved dome of *S. edmontonensis*, MRF 360, in dorsal (A) and right lateral view (B).

regard *Stegoceras* as a relatively basal pachycephalosaurid and *Sphaerotholus* as part of a diverse clade of more derived pachycephalosaurine taxa including *Prenocephale* (Sereno, 2000; Williamson and Carr, 2002; Sullivan, 2003, 2006; Maryańska et al., 2004; Schott et al. 2009; Longrich et al., 2010; Watabe et al., 2011).

Stegoceras validum

Specimen UALVP 2 (Fig. 1E,F) was collected from the Upper Cretaceous (Campanian) Dinosaur Park Formation of Alberta, Canada, and was first described by Gilmore (1924). This specimen remains the best preserved skull for *Stegoceras* and is one of the few pachycephalosaur species known from a complete skull. Only slight taphonomic distortion was observed for UALVP 2, including slight right skew to the entire skull along with minor dorsal displacement of the vomers and palatines. The nasal passage was well defined in this taxon and well bounded by the bones of the nasal cavity. Metaplastic ossification of the overlying dermis was extensively present in this species. Both the supraorbital membrane and the dermis surrounding the bony narial aperture, often regarded as “dermal sculpturing” (Witzmann, 2009), were preserved in UALVP 2. The narial dermal ossification provided a hard limit to nostril size and position. As described below, mineralization or ossification of soft tissues extended to portions of the cartilaginous

nasal capsule, such as the tectum nasi, septum, and turbinates.

Sphaerotholus edmontonensis

MRF 360 (Fig. 1B), 361 (Fig. 1C), 362 are new specimens collected in a poorly lithified iron-rich sandstone in the lower third of the Upper Cretaceous Hell Creek Formation (latest Maastrichtian) of southwestern North Dakota. The most complete and informative specimen, MRF 360, is assigned to *S. edmontonensis* based on the triangular arrangement of three nodes on the caudolateral corner of the squamosal and the placement of the first node over the contact between the parietal and squamosal (Sullivan, 2000). Open sutures on the skull suggest that this specimen represents a juvenile. It is incompletely preserved in two pieces that were separated along the frontoparietal suture (Fig. 4). The frontoparietal dome and portions of the braincase are preserved, but the palate, quadrates, and nasals were lost due to erosion, exposing the caudal regions of the nasal cavity, revealing preserved soft-tissue structures. The nasal cavity structures of MRF 360 were preserved by the rapid precipitation of siderite (identified by scanning electron microscopy equipped with energy dispersive X-ray spectroscopy [SEM/EDX]) onto the external surfaces of the structures. Subsequent decay of the cartilage left behind a high-fidelity siderite mould and thin voids, which denote the morphology and location of the presumably cartilaginous turbinates. CT scans indicate that the voids left behind after complete decay of the structures are not merely superficial, but extend well into the skull. The requisite rapid siderite precipitation rate (Allison and Pye, 1994) and slow decay of cartilage (Coe, 1978) for this type of preservation have been noted in modern reducing environments and decaying carcasses, respectively.

Two other pachycephalosaurid specimens found near MRF 360 are also referable to *S. edmontonensis*. MRF 361 is similar to MRF 360 in preserving the dome and some of the braincase, but nasal soft tissues are not preserved. MRF 362 preserves a portion of the nasal bones. Although it is a very fragmentary specimen, it provides important details on the internal structure of the bony nasal cavity.

S. goodwini

NMMNH P-27403 (Fig. 1D) is the holotype specimen of *S. goodwini* and was collected from the Upper Cretaceous (Campanian) Kirtland Formation of the San Juan Basin, New Mexico (Williamson and Carr, 2002). It consists of a complete frontoparietal dome, as well as much of the braincase, and, much like MRF 360, preserves portions of what are here interpreted as mineralized olfactory turbinates.

P. prenes

ZPAL MgD-1/104 (Fig. 1A) is the holotype specimen of *P. prenes* and was collected from the Upper Cretaceous Nemegt Formation of Mongolia. The skull is virtually complete. It is the best known skull anatomically (Maryańska and Osmólska, 1974; Sereno, 2000; Maryańska et al., 2004; Sullivan, 2006). Only a cast of the skull was

available for CT scanning, but the original specimen was studied by one of the authors (LMW).

CT Scanning Protocols

All principal pachycephalosaur fossil specimens discussed here were scanned at the University of Texas High-Resolution X-ray CT Facility (UTCT) in Austin, Texas, with the exception of MRF 362, which was scanned at the Ohio University MicroCT Scanning Facility (OU μ CT) in Athens, Ohio. The *S. validum* specimen (UALVP 2) was scanned axially on the UTCT's ACTIS system at a slice thickness of 250 μ m, 450 kV, 1.3 mA, and 1400 views for a total of 514 slices. Both *S. edmontensis* crania were scanned axially on UTCT's ACTIS system, MRF 360 at a slice thickness of 237 μ m, 215 kV, 0.15 mA, and 1800 views for a total of 531 slices, and MRF 361 at a slice thickness of 500 μ m, 400 kV, 3.7 mA, and 1000 views for a total of 262 slices. The *S. edmontensis* nasal fragment (MRF 362) was scanned axially on OU μ CT's GE eXplore Locus *in vivo* Small Animal MicroCT Scanner at a slice thickness of 90 μ m, 80 kV, 498 μ A, 3600 views for a total of 730 slices. The holotype specimen of *S. goodwini* (NMMNH P-27403) was not a major specimen for this study, but scan data were made available by T. E. Williamson; the specimen was scanned at the State of New Mexico Office of the Medical Investigator on a Philips Brilliance Big-Bore scanner at a slice thickness of 400 μ m, 120 kV, and 166 mA for a total of 398 slices. All scan data were imported into Avizo 7 (FEI Visualization Sciences Group, Burlington, MA) on 64-bit PC workstations for analysis. Anatomical features of interest (e.g., nasal cavity, turbinates, cranial endocast, endosseous labyrinth, etc.) were highlighted and digitally extracted using Avizo's segmentation tools for quantification and visualization.

Brief Anatomical Description

We present some brief descriptions here to provide the pertinent anatomical framework for the airflow modeling. The full extent of the nasal cavity is preserved only in *Stegoceras* (UALVP 2) among the specimens analyzed here with CT scanning, supplemented with observations of *Prenocephale*. It is bounded by the premaxillae rostrally and the maxillae and lacrimals laterally (Fig. 5A). The greatly expanded nasals provide much of the dorsal limit to the nasal cavity, with the prefrontals participating at the caudalmost extent of the nasal cavity. The caudal border is composed of a mineralized ethmoid ossification that separates the nasal cavity from the orbital cavity (Maryńska and Osmólska, 1974). Ventrally the nasal cavity is bordered by medial extensions of the maxillae, the palatines, and the vomer at the midline. Caudally the vomer contacts an unusual ventromedian process as well as the pterygoids, which are sutured to medial extensions of the highly arched palatines (Fig. 5B,C). This triangular ventromedian process projects ventrally at the rostrocaudal level of the caudal extremities of the bony choanae and tooth rows. Gilmore (1924) regarded this median process as deriving from the vomer, but could not rule out it being part of the parasphenoid (his "presphenoid"), and Maryńska and Osmólska (1974) agreed with the parasphenoid interpretation. Analysis of the CT scan data, however, does not

reveal any clear continuity of this ventromedian process with the vomer, pterygoid, or parasphenoid, but rather appears to be sutured to separate adjacent bones. The other well preserved pachycephalosaurid skull that of *P. prenes* (ZPAL MgD-1/104), lacks a ventromedian process, but has a tuberosity on the pterygoids in a similar location. Therefore, the process in *Stegoceras* may represent mineralization of a perhaps more widely distributed soft-tissue structure, which is discussed further below in the context of restoration of the soft palate.

The well-constrained nasal cavity of *Stegoceras* allows for interpretation of the extent of the cartilaginous nasal capsule and the locations of the major regions of the nasal cavity. The vestibulum nasi appears to have been short, whereas the CNP comprised the majority of the nasal capsule, extending from the rostral aspect of the maxillae and continuing caudally to the mesethmoid. The border of the bony choana was formed by the maxilla laterally and the vomer and palatine medially (Fig. 5C). The vaulting of the palatines produced a noticeable concavity within the oral region. A ventral concavity shared by the palatine and pterygoid caudal to the bony choana (here termed the choanal fossa) suggests that the nasal passage continued beyond the bony choanal border, pushing the fleshy choana—that is, the transition from nasopharynx to oropharynx—further toward the throat (Fig. 5D). We regard the ventromedian process and choanal fossae as OCs of a soft palate, with the fleshy choanae opening immediately caudal to the ventromedian process. This inference is functionally consistent in that the soft palate would extend caudally to about the distal end of the tooth row. It also receives support from a comparison with extant relatives (birds and lizards) that also have extensive bony choanae with much smaller, caudally placed, fleshy choanae (Rieppel et al., 2008; Crole and Soley, 2010). In these extant species, the much larger bony choana is partially or completely floored over by a tight-fitting sheet of oral mucosa, leaving only slit-like openings for the fleshy choana. A similar situation was likely present in *Stegoceras*. The result of this anatomical arrangement would be an extensive nasopharyngeal duct somewhat similar to the nasopharyngeal duct seen in extant crocodylians (Witmer, 1995b), as well as some mammals and turtles.

As noted above, CT scans of the skull of *Stegoceras* (UALVP 2) revealed the presence of mineralized turbinates within the caudal region of the nasal cavity. This caudal location—recessed dorsally away from the rest of the nasal cavity and adjacent to the olfactory bulbs—indicates that this region was the olfactory recess, which would have housed the olfactory chamber. Thus, the turbinates found here likely supported olfactory conchae, clothed in olfactory epithelium. This specimen also preserved portions of the tectum nasi and lateral nasal wall, providing a clear picture of nasal capsule shape in pachycephalosaurs. Likewise, as noted above, one of the *Sphaerotholus* specimens (MRF 360) preserves very comparable turbinates. Moreover, this specimen also preserves parts of the lateral nasal wall, tectum nasi, and a perforated caudal wall separating the olfactory bulbs from the olfactory chamber of the nasal cavity. This perforated wall appears equivalent to the cribriform plate seen in mammals and is the first time such a structure has been observed in a dinosaur fossil. The presence of a cribriform plate so close to the preserved turbinates,

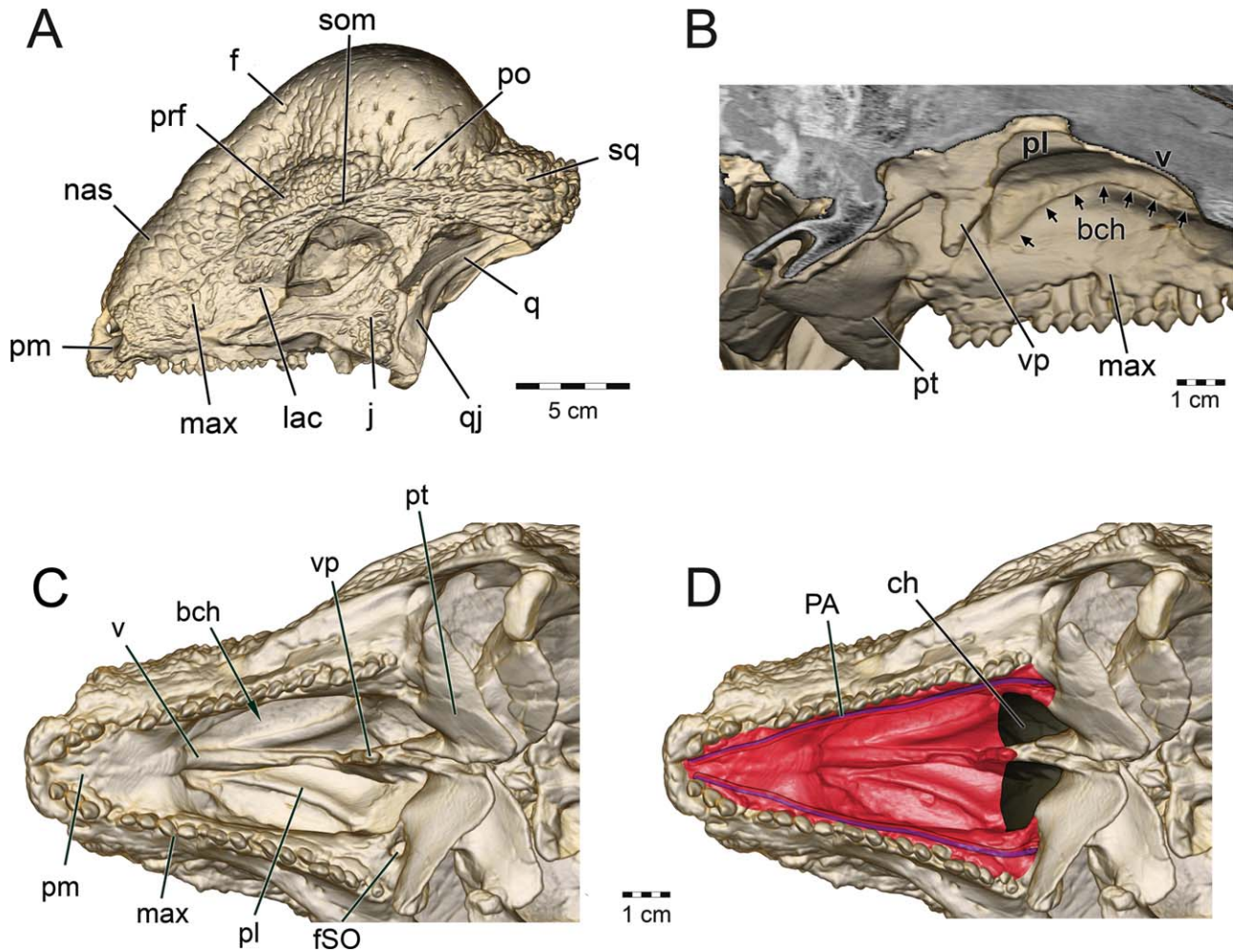


Fig. 5. *S. validum*, UALVP 2, and cranium. **A**: Lateral view. **B**: Left medial view of the sagittally sectioned skull highlighting neomorphic ventromedian process of palate. **C**: Ventral view of skull. **D**: Same view as C but with restored soft palate and vasculature.

coupled with their location within the caudalmost aspect of the nasal cavity, suggests that these turbinates indeed supported olfactory conchae.

The turbinates in *Stegoceras* and *Sphaerotherolus* appear very similar to each other, which is significant in that the two taxa are not particularly closely related, suggesting that potentially all pachycephalosaurids had such structures. The nasal septum in *Stegoceras* has a spade-shaped base and is overall wider than in *Sphaerotherolus*. In both taxa, the turbinates are vertically oriented, shell-like, lamellar structures that arc convex-medially toward the septum. The turbinates in *Stegoceras* are slightly more dorsoventrally splayed when viewed rostrally (Fig. 6), but this splaying was likely a preservational artifact of the deteriorating nasal capsule prior to fossilization. Portions of the right olfactory turbinate appear to be torn, whereas the left olfactory turbinate has been completely separated from the rest of the nasal capsule. Reattaching these structures reduces the splay seen in the turbinates, making them approach the shape seen in *Sphaerotherolus*. A region of unidentified preserved soft tissue was observed in the nasal cavity of *Sphaerotherolus*

ventrolateral to the olfactory turbinates. It consists of a coiled shape with the left side preserving more coils than the right. These structures may be a second set of turbinates. Exactly what function these potential turbinates would play has been difficult to assess. Extant archosaurs generally have a single olfactory turbinate (but see Discussion), suggesting that these secondary turbinates may have housed respiratory conchae. The placement of these potential turbinates, however, is out of the predicted flow region of the airfield (generally between the nasal septum and the next most lateral tissue). Further, the scroll-shaped secondary structures are angled 49° ventral to the olfactory concha (Fig. 7), which suggests that if air did enter these structures it did so from a steep angle. This situation may indicate that *Sphaerotherolus* had a relatively vaulted nasal cavity compared to other pachycephalosaurs. Connections between these extra tissues and the olfactory turbinates occur only at the caudalmost aspect of the olfactory chamber. Unfortunately, the lack of facial bones for *Sphaerotherolus* hamper any further attempts to reconstruct the shape of its nasal capsule.

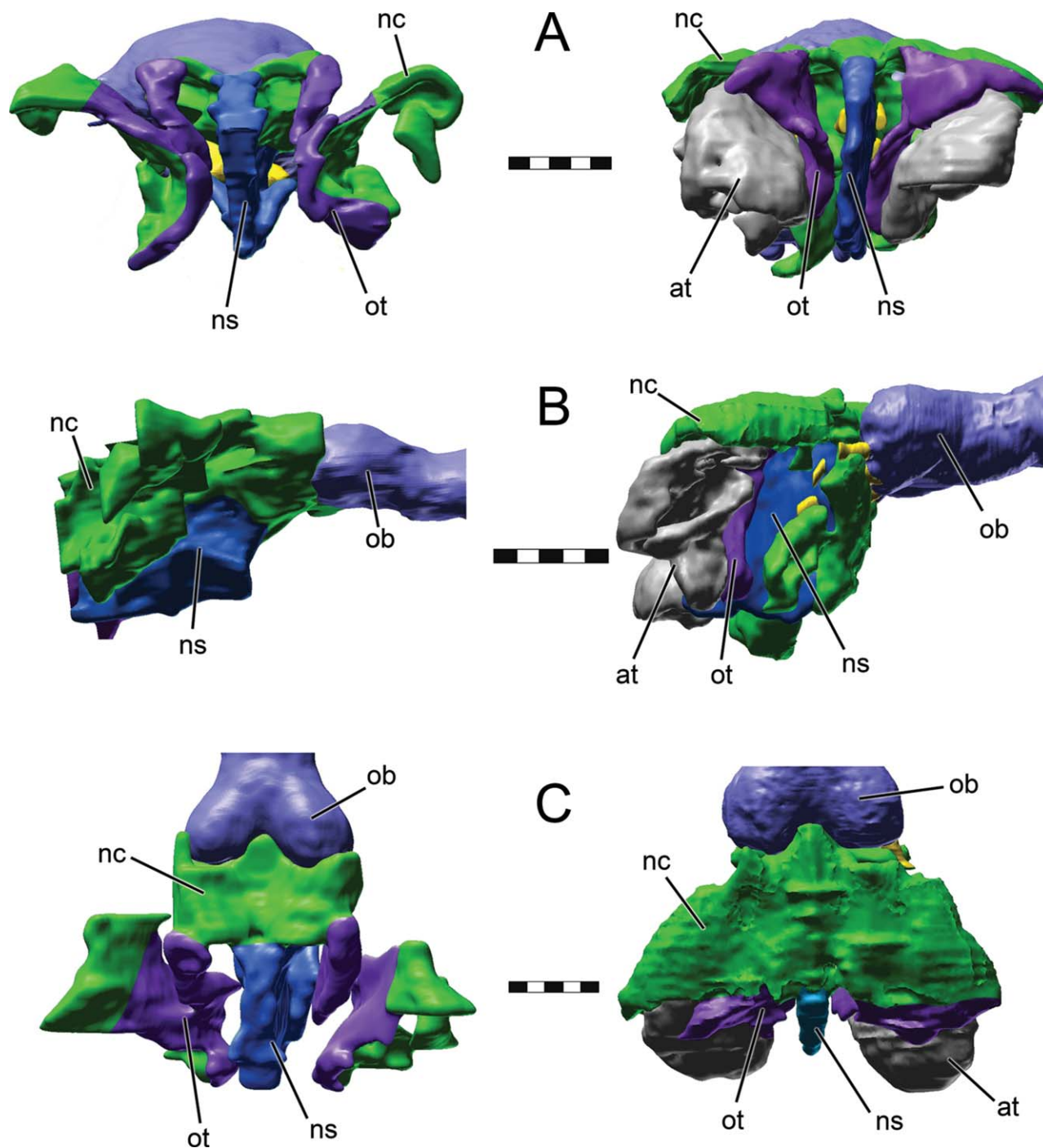


Fig. 6. Preserved nasal capsule morphology compared between *S. validum* (UALVP 2; left) and *S. edmontonensis* (MRF 360; right) in (A) rostral, (B) left lateral, and (C) dorsal views. Scale bars = 1 cm.

METHODS FOR CFD ANALYSES

Model Creation

As noted above, skulls were CT-scanned and segmented using the 3D visualization software Avizo 7.1. Taphonomic distortion is a common problem with fossilized bones (Dunlavey et al., 2004; Angielczyk and

Sheets, 2007), necessitating the use of retrodeformation techniques to restore original shape (Motani et al., 2005; Witmer and Ridgely, 2008b; Arbour and Currie, 2012). The hypermineralized nature of pachycephalosaur skulls made them more resistant to taphonomic distortion than other dinosaurs. For *Stegoceras* (UALVP 2), a slight dorso-medial skew of the right side was present (Fig. 8).

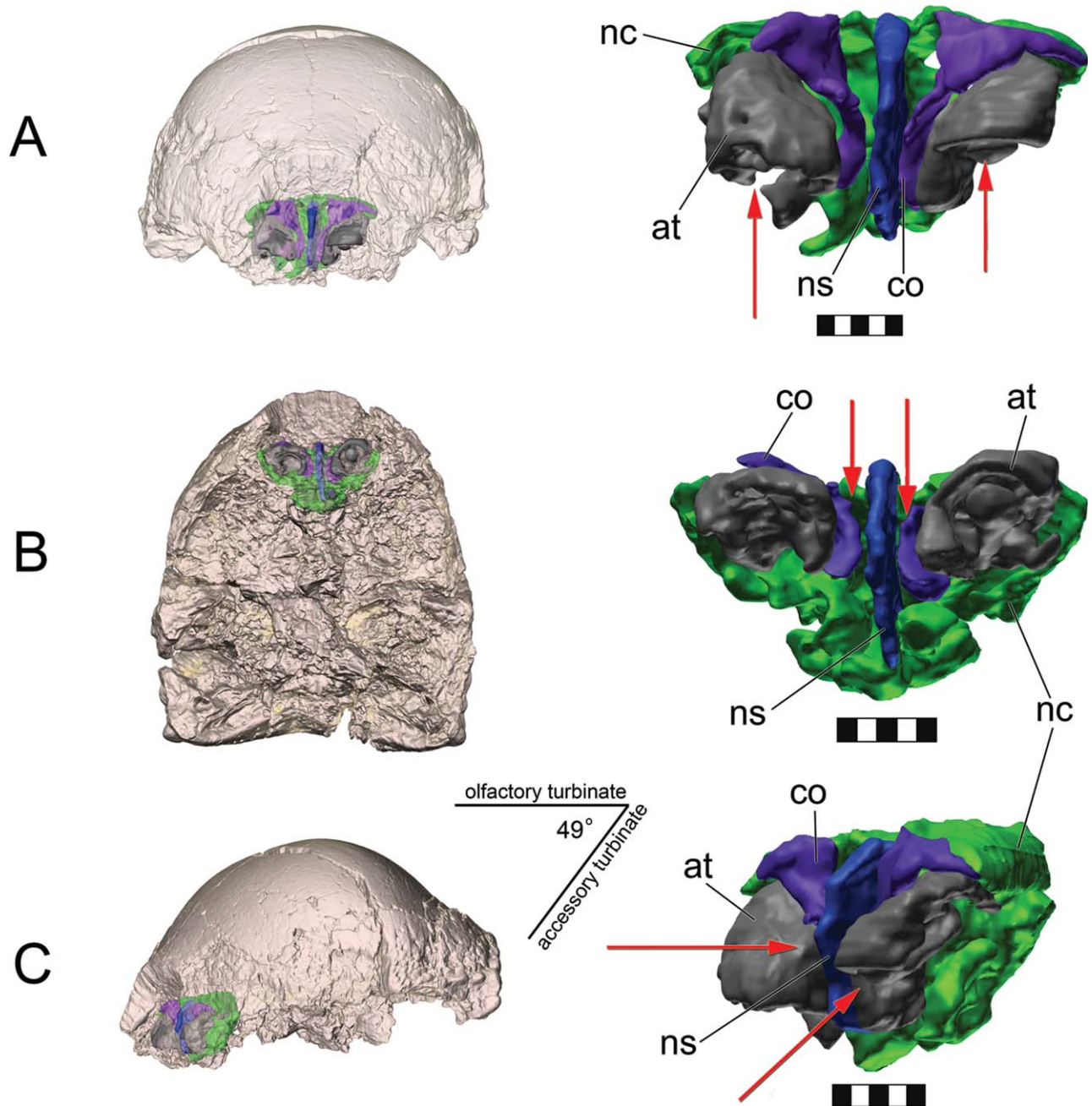


Fig. 7. Turbinate anatomy for *S. edmontonensis*, MRF 360 shown *in situ* within the semitransparent cranium (left) and isolated (right) in (A) rostral, (B) ventral, and (C) left lateral oblique views. Airflow direction (red arrows) between the olfactory turbinates (purple) and septum (blue) is compared with flow through the potential accessory turbinates (gray), which are offset from the rest of nasal tissues by 49°. Scale bars = 1 cm.

This skew had little effect on the nasal region, requiring minor retrodeformation in Maya (Autodesk 2013) to ameliorate.

A 3-dimensional surface model of the nasal cavity was segmented from the CT data. This surface model was essentially a cast that comprised the negative space between the bones bounding the nasal cavity and represented the potential spaces through which the respired

airfield could have moved (Fig. 9). A distinct septal sulcus could be discerned from the CT data. This sulcus suggested that *S. validum* had a complete nasal septum similar to its extant relatives. Further evidence for this complete septum could be seen in the olfactory chamber where, as noted above, the septum had become mineralized. The presence of a complete septum would have separated the right and left nasal capsules from one

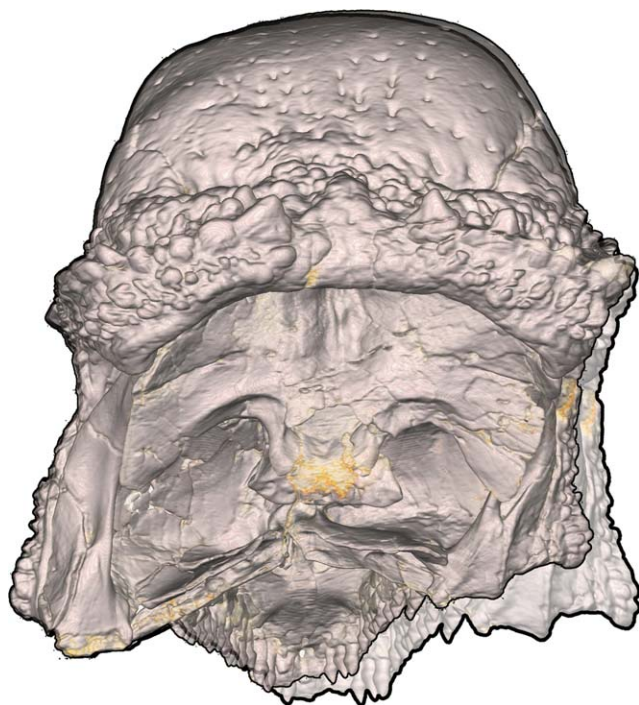


Fig. 8. Caudal view of skull for *S. validum* (UALVP 2). The thinner outline shows the skull as preserved, with taphonomic deformation causing a slight dorsomedial skew of the right side. The thicker outline indicates the corrected, retrodeformed skull. Most deformation occurred on the right side of the skull leaving the left side relatively untouched.

another such that air passing through one nasal capsule would interact independently from air entering the other nasal capsule. This independence allowed for modeling of only one side of the nasal capsule as flow patterns should be basically identical in the opposing side. This first-pass nasal reconstruction took into account only the bony boundaries of the nasal cavity and its associated paranasal sinuses (Fig. 9). This low-fidelity nasal capsule model was thus referred to as the bony-bounded model (BBM). The presence of mineralized turbinates allowed for further refinement of the nasal capsule. The location of the olfactory turbinates relative to the segmented airway indicated that the caudal portion of the nasal capsule was much more constricted than the BBM model would indicate. The extra space within the nasal capsule likely represented portions of the paranasal sinus system. In this case, the expanded caudal region of the nasal capsule likely represented a cavum conchae, inflating the olfactory turbinate as it does in birds and crocodylians (Witmer, 1995b).

CFD Preparation

Before models could be subjected to a fluid dynamic analysis, they first needed to be cleaned of any artifacts of segmentation. These artifacts included low-resolution areas of segmentation that produced “stair-stepping” regions to the model, as well as areas where an insufficient number of triangles were used to represent parts of the morphology, introducing a high skew (triangles

with extremely acute angles) into the model. Surface models were cleaned using the smoothing and noise reduction algorithms in Geomagic Studios 10 (Geomagic). Surface models were then recalculated (remeshed) in Avizo 7.1 to reduce skew by covering the model in as many equilateral triangles as possible.

Models were assigned a series of boundary conditions that would induce physiologically realistic airflow through the model (Fig. 10). These boundary conditions consisted of a pressure inlet located at the nostril, a pressure outlet located at the fleshy choana, and an impermeable wall boundary over the rest of the model. Surface models were transformed into volumetric meshes for fluid dynamic analysis (Fig. 10). A hybrid mesh consisting of a tetrahedral shell with a hexahedral core was created for each model. This meshing technique provided the efficiency of hexahedral cells (Aftosis et al., 1994; Biswas and Strawn, 1998) without the difficulties associated with fitting hexahedra to unstructured grids (Blacker, 2001; Ruiz-Gironés, 2011). Mesh creation was done using the program ICEM CFD (ANSYS). Fluid dynamic analysis was performed using the fluid dynamics program Fluent 13 (ANSYS).

Environmental Parameters

Standard sea level atmospheric pressure (101,325 Pa) was used for the area surrounding the nostrils. The wall boundary incorporated a “no-slip” condition indicating a lack of movement at the solid-fluid boundary. Although the mucous and cilia that comprise the respiratory epithelia will contribute to some movement of the airfield, these movements are often so slow (≤ 1 cm/min) and their thickness so slight that they can essentially be ignored (Craven et al., 2009). In Fluent, the “target-mass-flow-rate” option was used to obtain estimated volumetric flow rates at the pressure outlet, allowing the program to determine the pressure gradient necessary to obtain these rates. A 3D double-precision solver was chosen for model analysis. A segregated pressure-based PISO algorithm was used to solve the steady-state continuity and Navier-Stokes equations. A node-based discretization gradient was used on all models. A second-order accurate spatial discretization scheme was used for both pressure and momentum (Fluent, 2006). Iterative models ran until all normalized residuals of error had converged to 10^{-4} . Point surface monitors placed at various locations on the models were also employed as a secondary means of determining convergence independent of continuity and momentum. Results were analyzed using Fluent 13 and Avizo Wind 7.1. Models were tested during resting inspiration and expiration.

To ensure that grid resolution would not affect the final results, a grid convergence index (GCI) for each model was calculated based on three grid resolutions (grid refinement ratio = 2) for each model of nasal morphology (Fig. 10). GCI calculations followed the methods of Roache (1994) and Craven et al. (2009).

Physiological Variables

A key requirement for any simulation of respiration is the necessary empirical data to justify the flow rates being simulated. For many extant taxa, respiratory data are either readily available in the literature or are

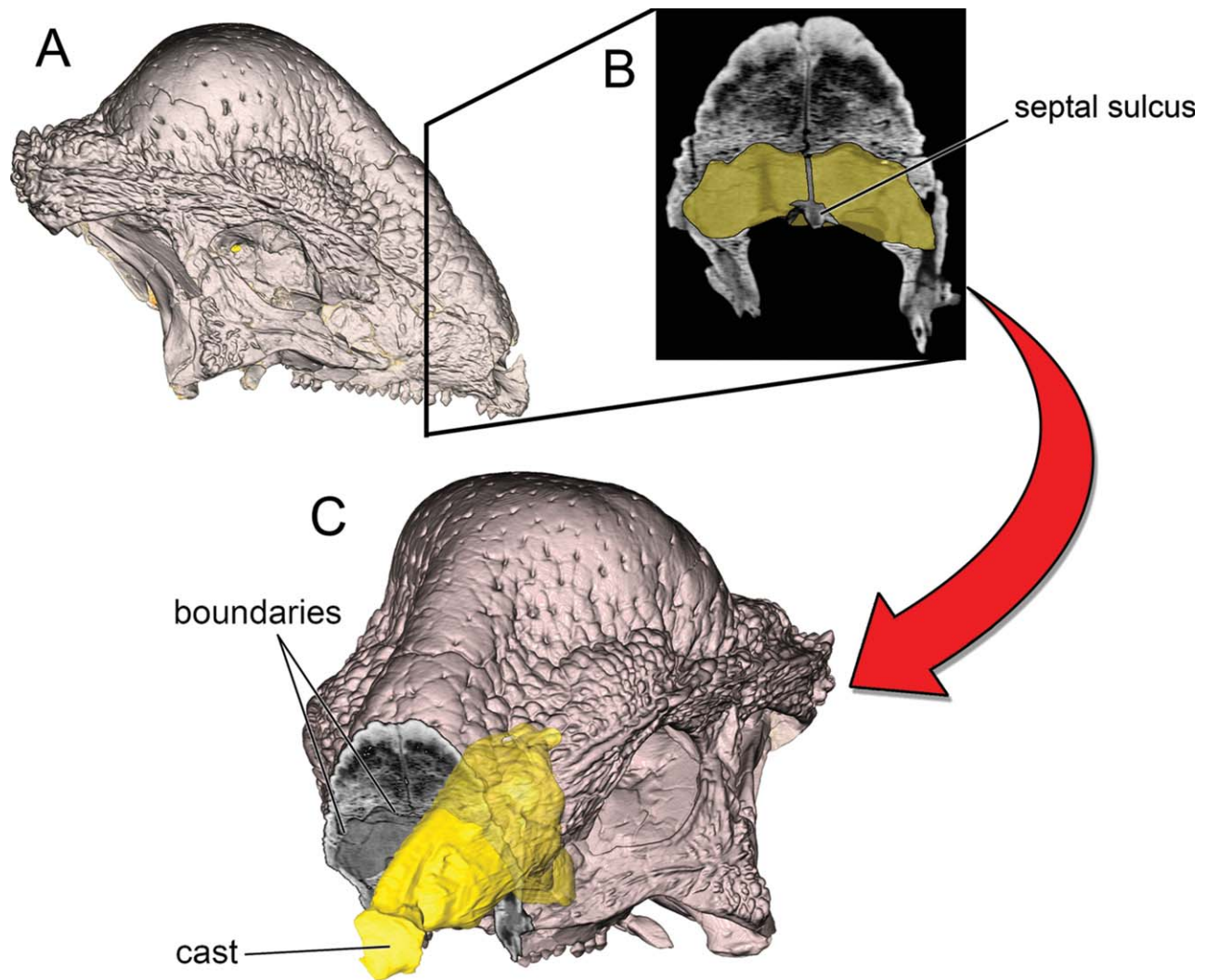


Fig. 9. Segmentation of the air spaces on the left side of *S. validum* (UALVP 2). The skull (A) was CT scanned and from the CT data (B), the airway was segmented out using OCs for its boundaries (e.g., the septal sulcus). The presence of a complete septum was used to justify segmentation of only the left side of the airway (C).

obtainable via experimentation. Obviously, neither of these options are available for extinct taxa. Certain aspects of the respiratory system, such as air sac placement (Wedel, 2003; O'Connor and Claessens, 2005; O'Connor, 2006, 2009), respiratory muscles (Carrier and Farmer, 2000a, b), and overall lung mobility (Schachner et al., 2009, 2011b), may be inferred from OCs found on the skeleton. However, they tell us very little of the dynamic variables required to simulate flow rates (i.e., tidal volume and respiratory frequency, which are required to determine respiratory drive), which thus requires respiratory variables to be inferred. To ensure confidence in our inferences, we used the EPB approach (Witmer, 1995a) to aid in estimates of respiration values for pachycephalosaurs. This was accomplished by searching the literature for data on resting respiratory variables in extant diapsids. Although this group is not as well studied as mammals, there are a handful of stud-

ies that proved useful for obtaining physiologically viable resting respiration values.

The most comprehensive collection of respiration data on diapsids comes from Frappell et al. (2001), who surveyed resting respiratory variables in 50 species of birds spanning a broad phylogenetic range of extant Neornithes. Their data was corrected for phylogeny, making it the most rigorous look at respiratory variables for any diapsid taxon to date. However, these data only covered one half of the dinosaur EPB. No similar comprehensive study has been performed for crocodylians. The works of Farmer and Carrier (2000a, b) and Farmer (2006), however, come the closest, although the data are limited to one crocodylian taxon (*Alligator mississippiensis*). Farmer (2006) discovered an apparent constraint on tidal volume in extant archosaurs. Taking data from a variety of alligator studies, Farmer (2006) discovered that the equation relating tidal volume to body mass in

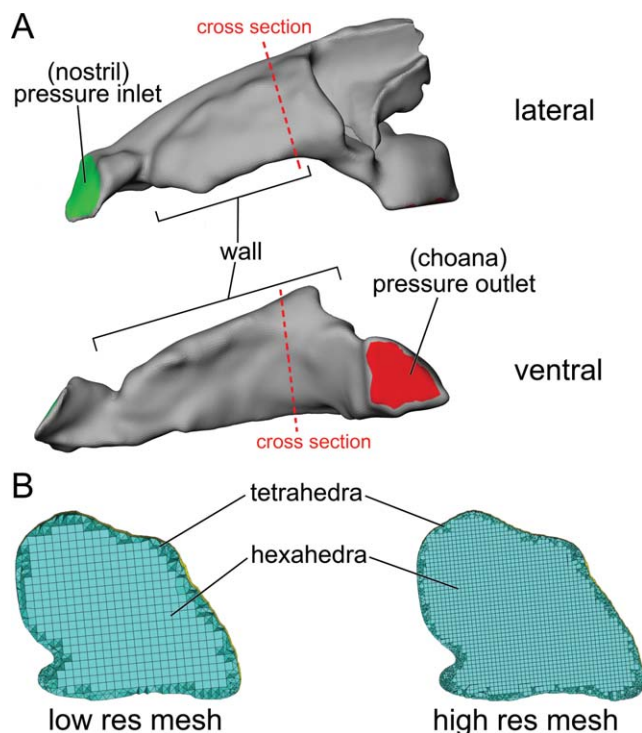


Fig. 10. **A:** Boundary condition placement on models. Boundary setup reflects inspiration. Inlets and outlets were swapped for expiration. **B:** Cross sections from location shown in “A” demonstrate the distribution of tetrahedra and hexahedra within models. Multiple resolutions of each model were run to ensure grid independence.

crocodylians was almost identical to the same equation in birds obtained by Frappell et al. (2001).

$$V_T = 20.3M^{1.06} \text{ (Frappell et al., 2001)}$$

$$V_T = 20.7M^{1.06} \text{ (Farmer, 2006)}$$

The differences between the equations are slight enough that they are likely the result of the limited taxon sampling for crocodylians. These data suggest that it may be possible to predict tidal volume in extinct archosaurs such as dinosaurs.

Determining respiratory rate was more difficult due to a general lack of broadly comparative data for diapsids other than birds. Individual respiratory variables have been recorded previously for alligators (Hicks and White, 1992; Farmer and Carrier, 2000a). These data show that alligators between 1.34 and 3.4 kg at 30°C, had a respiratory frequency of 7.5–7.3 breaths/min respectively. These values fall within the range of values for bird taxa of similar size [e.g., 8.6–8.4 breaths/min for a 1 kg penguin and pheasant, respectively (Frappell et al., 2001)]. To further aid in reconstructing respiratory physiology, we looked at resting respiratory variables in squamates, the immediate outgroup to archosaurs. To date there has only been one preliminary study of respiratory variables in squamates (Bennett, 1973). This study looked at 16 species of lizards ranging in size from 0.1 to 1 kg. Results of that study found tidal volume to be shallower in lizards compared to archosaurs.

TABLE 1. Estimated resting respiratory variables for *S. validum* based on data from Frappell et al. 2001

Estimated mass (kg)	Frequency (breaths/min)	Tidal volume (mL)	Inspiratory drive (mL/sec)
10	7.64	233	73
40	4.67	1013	169

However, respiratory frequency (at 37°C) for the size range studied did fall within the respiratory frequency range of similar sized non-passerine birds (17–35 breaths/min). These data suggest that diapsids, as a group, breathe in a similar manner regardless of thermophysiology. This breathing frequency is substantially different from that of mammals, which take approximately three times as many breaths during an equal period of time (Frappell et al., 2001). Based on the similarities of these studies, the equations from Frappell et al. (2001) were used, as they provided a physiologically reasonable set of respiratory values (Table 1). These equations required an estimate of body mass. To account for the fact that precise body masses of extinct animals are currently unknowable, we used a high and low end for body mass estimates so as to incorporate a range of values that were likely to encompass the “true value” of the living animal (Hutchinson et al., 2011). Minimum and maximum mass estimates for *S. validum* were obtained from Peczki (1995).

Model Assumptions

Fluid dynamic modeling—like all modeling—requires initial assumptions be met prior to running an analysis. Two of these assumptions are the viscosity model chosen for the fluid and the steadiness of the flow over time. To determine which viscosity model to use, it was necessary to ascertain the type of fluid flow (laminar or turbulent) that was likely present in the airway, which can be approximated by calculating the Reynolds number throughout the airway. Reynolds numbers are dimensionless ratios of inertial-to-viscous forces within a fluid. Reynolds numbers below 2,000 indicate that viscous forces dominate the flow field, making fluid flow laminar (Vogel, 1994). As the Reynolds numbers increase above 2,000, the orderliness of the flow deteriorates, resulting in laminar flows that contain partially formed turbulence (Vogel, 1994). At Reynolds numbers of 4,000 and higher, inertial forces dominate the flow field resulting in fully formed turbulent flow (Vogel, 1994).

It is difficult to calculate Reynolds numbers for biological systems as the fractal nature of the shapes involved make it difficult to obtain a characteristic length (typically the diameter). A way around this problem is to borrow a technique from civil engineering and use the wetted perimeter of the object, as was performed by Holmes et al. (2011).

$$Re = \frac{4Q}{Pv}$$

where Q = the volumetric flow rate measured (m^3/sec), P = the wetted perimeter in meters (Foss, 1998), and v = the kinematic viscosity of air ($1.6036e-05 m^2/sec$ at 30°C).

TABLE 2. Average Reynolds and Womersley numbers across all the nasal capsule morphologies in *S. validum* under two estimated flow rates

Mass (kg)	Flow Rate (L/min)	Reynolds number	Womersley number
10	4.4	128 (43–214)	1.2 (0.6–2.2)
40	10	297 (100–496)	0.9 (0.4–1.7)

Data range in parentheses.

Using cross sections taken approximately every 3 mm, and assuming the volumetric flow rates obtained from Frappell et al. (2001), the resulting Reynolds numbers suggested that a laminar viscosity model was the best choice for all the models studied (Table 2).

The second assumption that needed to be met was the steadiness of the flow field. The steadiness of a flow determines how often it is able to assume the classic parabolic profile under oscillating conditions (e.g., the pulsation of blood flow or the pendular pattern of breathing). To determine this, we used the dimensionless Womersley number (Womersley, 1955), as defined for the respiratory system (Craven et al., 2009).

$$Wo = \frac{Dh}{2} \sqrt{\frac{2\pi f}{\nu}}$$

where f = the frequency of oscillation (Hz), and Dh is the hydraulic diameter of the airway defined as:

$$Dh = \frac{4A}{P} \quad (\text{Foss, 1998})$$

where A = the area of the cross section being measured (m^2).

The Womersley number is a function of a structure's size, the frequency of oscillation, and the kinematic viscosity of the fluid being moved (Loudon and Tordesillas, 1998). At $Wo \leq 1$ the flow field may be considered to exist in a quasi-steady state, which suggests that the fluid is capable of reaching and maintaining the standard parabolic profile. Furthermore, it also implies that instantaneous flow rate can be determined by the corresponding instantaneous pressure gradient (Loudon and Tordesillas, 1998), allowing a steady-state solution to be modeled. As Wo increasingly deviates from unity, the flow becomes more unsteady. At $Wo > 10$ inertial forces dominate once more, forcing a flattened “plug” profile to the fluid flow (Ku, 1997). This flow type is considered to be completely unsteady, making its shape for a given pressure gradient unknown *a priori*, necessitating the use of a transient model for flow calculations.

Based on the breathing frequency data obtained from Frappell et al. (2001), Womersley data from all our pachycephalosaur models fell between 0.2 and 2.6, indicating that a steady-state solution would be a valid modeling scenario (Table 2).

RESULTS

Qualitative comparisons of airflow profiles across all of the grid resolutions used here revealed gross overall similarity in airflow patterns. GCI data indicated that the highest grid resolutions were largely independent of

TABLE 3. Grid convergence index (GCI) for the finest grid based on impedance (Δ pressure) during inspiration for a given flow type

Nasal morphology	Converged variable	GCI _{finest} (4.4 L/min)	GCI _{finest} 10 (L/min)
Bony bounded	ΔP	0.1698	0.149
Paranasal septum	ΔP	1.3087	8.9628
Scrolled turbinate	ΔP	1.0628	1.6692
Branched turbinate	ΔP	1.5421	4.4215
Septum and concha	ΔP	0.045	0.04

grid error at both high and low flow velocities (Table 3; Fig. 11).

Airflow in the BBM

Air movement through the BBM airway consisted of slow moving air traversing the nasal capsule from nostril to choana. Pressure values and associated velocities were exceedingly low (maximum pressure drop < 2 Pa) resulting in a slow moving air stream throughout the nasal capsule. Despite being a largely open space, some slight stratification of the airfield was observed. Air entered the nostril where it proceeded through the small vestibulum nasi. The shape of the vestibulum nasi directed air medially as it entered the enlarged CNP. The sudden transition from the relatively confined vestibulum nasi to the larger CNP resulted in a Venturi effect, jetting air further into the nasal capsule where it fanned out to encompass the larger space. This effect created a noticeable pocket of relatively stagnant air within the lateral aspect of the CNP. As the inspired airfield approached the olfactory chamber it veered ventrolaterally toward the ductus nasopharyngeus, which imparted a low-velocity swirling motion to the airfield. Portions of this swirling forced the lateral-most air streams to flow caudally to rostrally along the ventrolateral aspect of the CNP, filling up this portion of the nasal capsule and creating a barrier to entry for other inspired air (Fig. 12). This pattern was observed under both estimated flow rates, with the higher flow rate serving only to enforce the pattern observed under the slower flow regime (Fig. 13). Upon expiration flow spiraled through the CNP to exit through the nostril.

Comparing these data with previously published works on mammals (Craven et al., 2010; Doorly et al., 2008; Jiang and Zhao, 2010), as well as our own work on sauropsids (Bourke and Witmer, 2010, 2011), some notable differences were observed. Flow rate in the nasal capsule of *Stegoceras* was substantially slower and more uniform than the inspiratory flows seen in extant amniotes. The near lack of olfactory flow in the BBM of *S. validum* is clearly unrealistic and a sign that the BBM was not accurately capturing the flow pattern within the nose. This determination was based on multiple lines of evidence including the presence of a well-developed olfactory region in this taxon. The preservation of well-developed olfactory turbinates (Fig. 6) further suggested that olfaction was, if anything, a large sensory component of this animal's repertoire. Large olfactory bulbs on the endocast of *S. validum* likewise indicated that olfactory sensitivity was, at the very least, not reduced in this specimen. Furthermore, extant

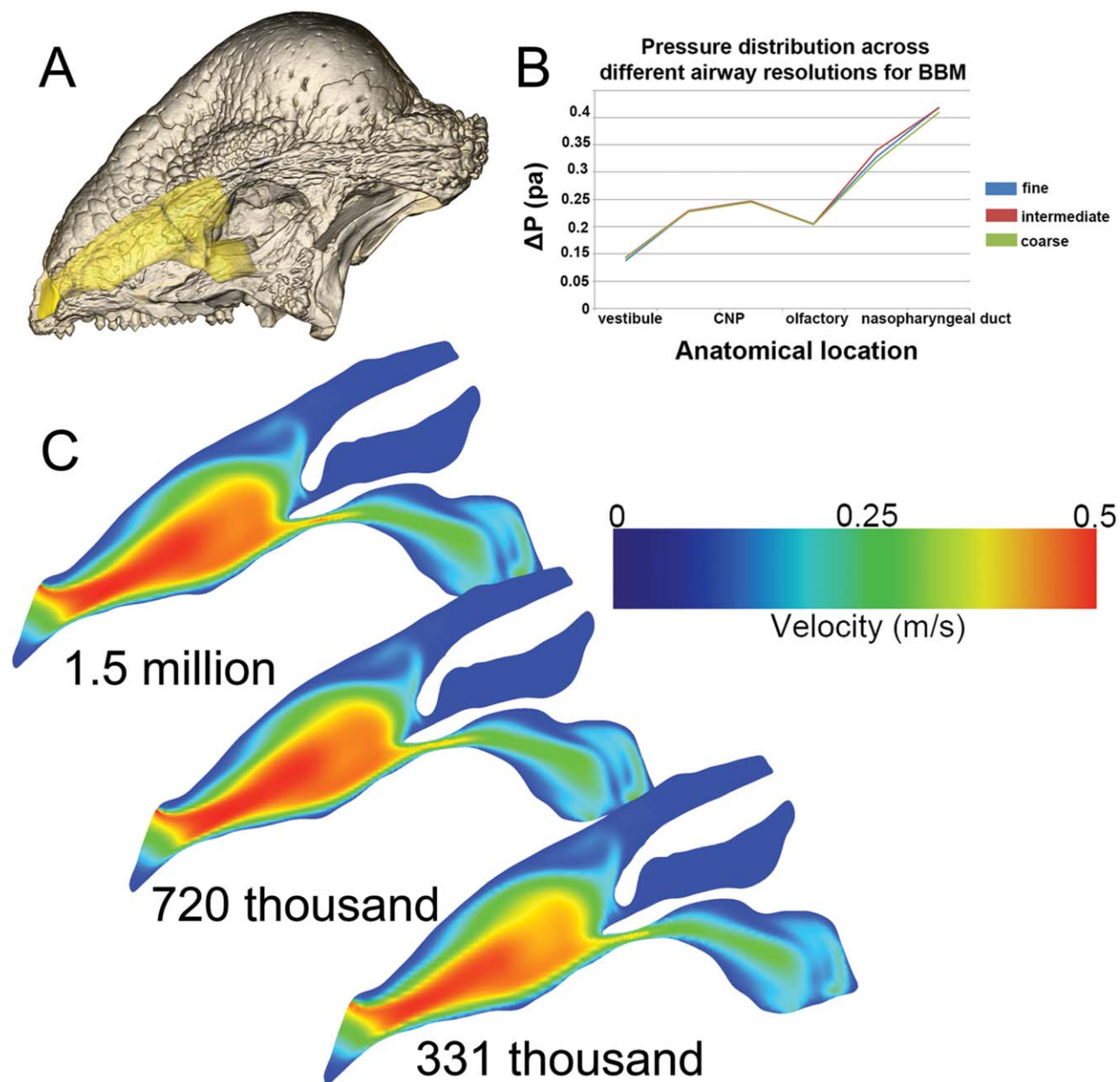


Fig. 11. Grid Convergence Index (GCI) results from a three grid refinement study to determine solution independence. **A:** Sagittal cross sections through the nasal cavity of *Stegoceras* (UALVP 2) were taken from each model resolution. **B:** Magnitude of pressure distribu-

tion throughout the nasal capsule of the bony bounded airway grids. **C:** Velocity profiles taken from the same location along each grid resolution reveal extensive similarity between grids, indicating that the solution obtained was largely free of grid error.

amniotes with even moderately developed olfaction (e.g., humans) routinely show air moving through their olfactory chambers during resting respiration (Kimbell et al., 1997; Guilherme et al., 2007; Craven et al., 2009). In contrast, airflow during resting respiration in the BBM of *S. validum* dropped quickly in velocity shortly upon entering the olfactory chamber. This air did not proceed far before being drawn back into the ductus nasopharyngeus (Fig. 13). Higher inspiratory flow speeds allowed for greater olfactory chamber penetration, but always at exceedingly low speeds (<1.5 cm/sec). That the flow pat-

tern observed in our BBM was in disagreement with these morphological criteria suggests that the BBM was inadequate for revealing airflow patterns in the living animal. These results were not unexpected in that the bony-bounded airway is largely an empty space with no reconstructed soft tissues (other than the soft palate to provide the position of the fleshy choana). Extant taxa use various soft-tissue conformations to manipulate the respired airfield, directing it to different regions of the nasal capsule before exiting the choana. *Stegoceras* would have had similar structures in its nasal capsule,

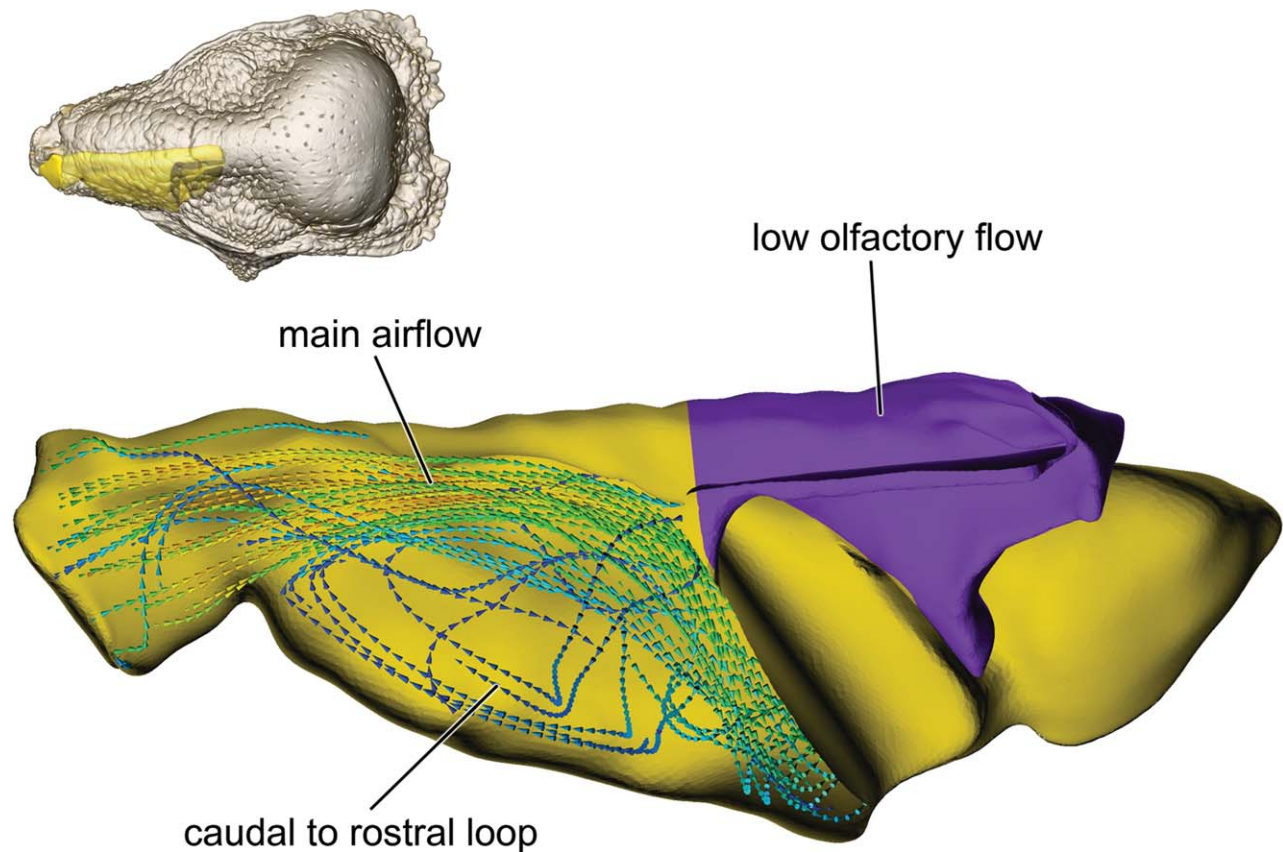


Fig. 12. Dorsal view of bony-bounded airway in *S. validum* (UALVP 2). Little olfactory flow was noted in the airway under both flow rates. Furthermore, a caudal-to-rostral loop was observed in the lateral aspect of the cavum nasi proprium.

in particular a region near the olfactory chamber that would have aided in pushing air further in. Ultimately, the results of the BBM analyses show that nasal soft tissues must be considered to provide valid tests of hypotheses of nasal airflow and physiology.

Reconstructing Soft-Tissue Structures

All extant diapsids fill the majority of their nasal cavities with mucocartilaginous tissues that come with associated neurovasculature and glands. The current conformation of the bony-bounded nasal capsule in *S. validum* did not take into account the neurovasculature or glands that would have been present. These structures would have taken up varying amounts of space that would limit the extent of the nasal capsule.

Mineralization/ossification of many of the periorbital elements in pachycephalosaurids provides key information on the broad patterns of blood flow entering and exiting the nasal region. In *Stegoceras*, the nasal region was likely supplied by the ethmoid arteries, similar to extant archosaurs. In crocodylians, the ethmoid arteries are branches of the caudal cerebral arteries, whereas in birds the ethmoid arteries are branches of the rostral cerebral arteries (Baumel, 1993; Sedlmayr, 2002; Almeida and Campos, 2011). During crocodylian development, the connection of the rostral cerebral arteries to

the ethmoid arteries obliterates, leaving the caudal cerebral arteries to form the ethmoid arteries (Burda, 1969). The osteological evidence that would inform which condition occurred in *Stegoceras* is currently unavailable, but the ethmoid arteries were restored in *Stegoceras* on a level I' inferential basis (i.e., a homologous condition present minimally in both extant outgroups [level I] but lacking OCs, hence the I' designation; Witmer, 1995a; Fig. 14). In extant archosaurs, the ethmoid arteries form the nasal vessels rostral to an anastomosis between the ethmoid and supraorbital arteries (Sedlmayr, 2002). In *Stegoceras*, a canal was found that represents the course of the supraorbital vessels as they entered the nasal region and anastomosed with the nasal vessels, similar to *Prenocephale* (Maryańska and Osmólska, 1974). Maryańska and Osmólska (1974) reported in *Prenocephale* that two foramina between accessory orbital ossifications 1 and 2 transmitted the ethmoid arteries. Maryańska and Osmólska (1974) reconstructed these blood vessels according to squamate vascular anatomy, where the supraorbital vessels supply a majority of the blood to the nasal region and the cerebral arterial contribution is overshadowed by extracranial blood vessels, specifically, the supraorbital arteries (Burda, 1966; Porter and Witmer, 2012). In *Stegoceras*, we used archosaur vascular anatomy to inform the restoration of the supraorbital vessels anastomosing with one of the nasal vessels. This

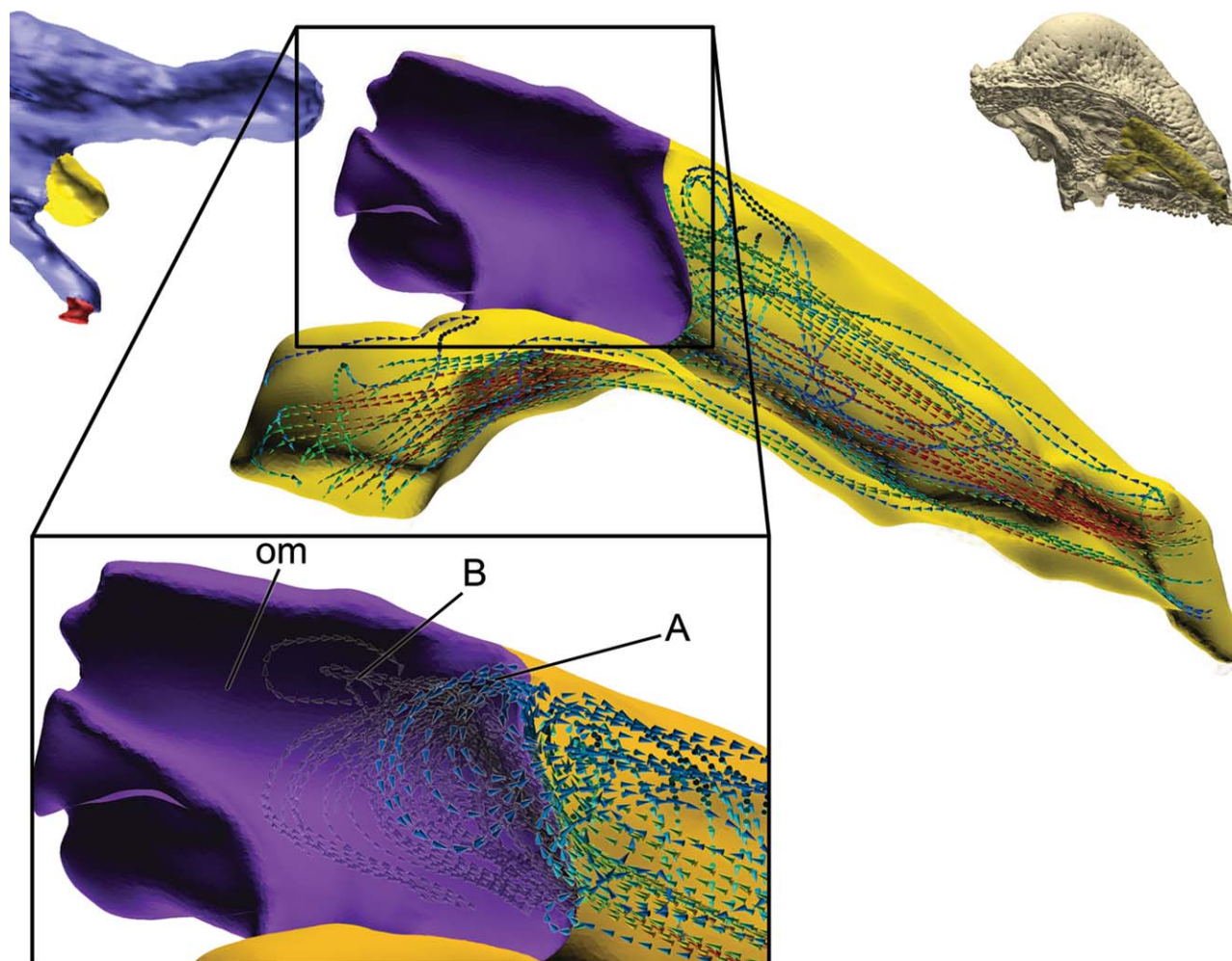


Fig. 13. Medial view of left bony-bounded airway under inspiratory flow conditions. The brain endocast placement (top left) shows the close association of the olfactory bulbs with the olfactory chamber. Inset: Olfactory flow within the olfactory meatus (om) under a flow regime of (A) 4.4 L/min and (B) 10 L/min.

anastomosis likely occurred with the lateral rather than the common or medial nasal vessels, as canals that transmitted branches of the medial nasal vessels were found within the suture between the nasal bones. These canals indicated that the bifurcation of the common nasal vessels occurred caudal to the supraorbital vessels, excluding the common nasal vessels from the anastomosis. The restoration of this anastomosis is a level I' inference (Fig. 14).

The common nasal arteries bifurcate into medial and lateral nasal arteries ventral to the olfactory bulbs in extant archosaurs (Sedlmayr, 2002). The medial nasal vessels (arteries and veins) travel within the mucosa along the nasal septum, leaving few OCs. They course rostroventrally with the medial nasal nerve along the nasal septum from the olfactory region to canals in the premaxilla, where they usually anastomose with terminal branches of the dorsal alveolar blood vessels. In *Stegoceras*, canals were found between the nasal bones that initially coursed rostr dorsally and then curved caudodorsally. These canals indicated the location of the medial nasal vessels as they passed along the nasal sep-

tum and indicated the caudalmost location of the medial nasal vessels after they branched from the common nasal vessels. Canals and grooves within the premaxilla of both *Stegoceras* and *Prenocephale* were found along the ventrolateral aspect of the nasal process. These canals and grooves transmitted the medial nasal neurovascular bundle through the premaxilla, where they ultimately anastomosed with the dorsal alveolar, palatine, and lateral nasal vessels. Based on the presence of these OCs, the medial nasal blood vessels were restored in *Stegoceras* on a level I basis, although parts of the vessels require a level I' inference (Fig. 14).

In extant archosaurs, the lateral nasal arteries branch from the common nasal artery and then join the lateral nasal nerve after it exits the nasal capsule through the foramen epiphaniale (Witmer, 1995b; Sedlmayr, 2002). The lateral nasal neurovascular bundle then courses rostrolaterally along the dorsolateral aspect of the nasal capsule, where it supplies the nasal gland (Witmer, 1995b; Sedlmayr, 2002). After supplying the nasal gland, the lateral nasal neurovascular bundle courses rostroventrally to supply the plexus surrounding the

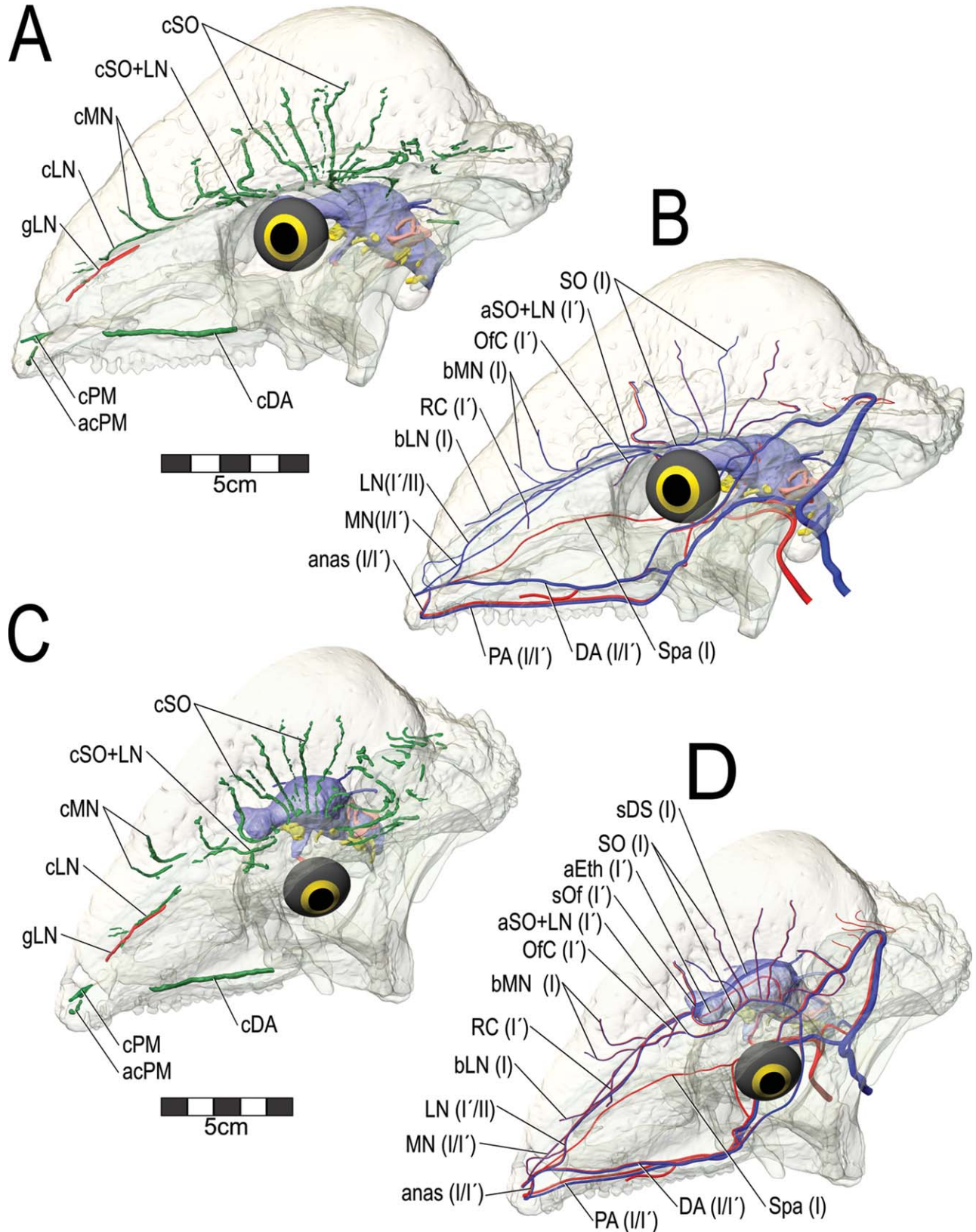


Fig. 14. Restoration of the blood vessels within the nasal region of *S. validum* (UALVP 2). **A:** Left lateral view and **(C)** left dorsolateral view, showing OCs (e.g., vascular canals and grooves) found in the nasal region. **B:** Left lateral view and **(D)** left dorsolateral view showing the restored blood vessels that supply and drain the nasal region. Levels of inference follow abbreviations parenthetically.

vestibulum nasi. The lateral nasal neurovascular bundle has different OCs in birds (the lateral orbitonasal foramen; Witmer 1995b) and crocodylians (e.g., canals in the nasal bones of alligators). *Stegoceras* resembles the crocodylian condition in having branches of the lateral nasal vessels passing through canals in the nasal bones to reach the dorsal aspect of the skull. The main trunk of the lateral nasal vessels would connect these branches, indicating the course of the lateral nasal vessels through the nasal region. These vessels were restored in *Stegoceras*, again requiring both level I' and level II inferences (level II inferences draw phylogenetic support from only one extant outgroup, in this case crocodylians; Fig. 14).

In extant diapsids, the lateral nasal vessels anastomose with the dorsal alveolar vessels just caudal to the bony narial aperture. They form an anastomotic loop around the vestibulum nasi that has been shown to contain cavernous tissue (Stebbins, 1948; Oelrich, 1956; Witmer, 2001; Sedlmayr, 2002). These blood vessels curve dorsally around the nostril and anastomose with the premaxillary vessels (the continuation of the dorsal alveolar vessels ventrally) and the medial nasal vessels within the premaxilla (Sedlmayr, 2002). In extant diapsids, an anastomosis between the dorsal alveolar, nasal, and palatine vessels was found within a canal near the premaxilla and maxilla articulation. A nerve was not found within this canal in the extant sample and is likely an exclusively vascular OC. In *Stegoceras*, a similar canal within the premaxilla likely transmitted anastomotic branches of the palatine, dorsal alveolar, and nasal blood vessels. The restoration of this anastomosis was a level I or I' inference (Fig. 14).

In extant archosaurs, the veins of the nasal region usually course with the artery of the same name. The medial and lateral nasal veins are tributaries of the olfactory sinus and its caudal continuation, the dorsal sagittal sinus (Baumel, 1993; Sedlmayr, 2002). The venous drainage from the medial and lateral nasal vein that contained cooled blood from the nasal region could drain directly into the dorsal sagittal sinus. The olfactory sinus was restored in *Stegoceras* as a level I' inference, and the dorsal sagittal sinus was restored as a level I inference (Fig. 14).

A closer examination of the CT data for *Stegoceras* revealed the presence of a ridge projecting ventromedially and running along the ventral surface of the nasals. This ridge was observed on both sides of the skull suggesting that it was not an artifact of preservation. It runs from the rostral tip of the nasals, caudally toward the lacrimal in the caudal region of the nasal cavity (Fig. 15). Further support for this ridge structure came from two other *Sphaerotherolus edmontonensis* specimens found near MRF 360 (MRF 361 and MRF 362). Each specimen exhibits similar ridges running down the ventral aspect of the nasals. Finally, a similar ridge is present in *Prenocephale* (ZPAL MgD-1/104) as well, although its full extent cannot be determined without CT scanning. Thus, the presence of these ridges in these three pachycephalosaurid taxa further supports the interpretation that these were not artifacts of preservation. The presence of a ridge running within the length of the nasal cavity suggests that a soft-tissue structure was present. Ridges within the nasal cavities of mammals function as attachment sites for turbinates

and have been used as OCs for respiratory turbinates in extinct synapsids (Hillenius, 1992). The turbinates of diapsids rarely mineralize, but the cartilaginous skeleton may still pull on its attaching bone with enough force to form a process or ridge, especially if the animal is large (Fig. 16). Thus, we hypothesize that the ridges observed within the nasal cavities of pachycephalosaurids supported turbinates, specifically respiratory turbinates, given their location. The exact size and shape of these turbinates currently cannot be worked out, but comparisons with extant diapsids offer potential shapes that could have been present. Among extant birds, turbinate shapes are typically limited to variations of scrolls or branches (Bang, 1971). Thus, to assess the effects of turbinate placement within the airway of *Stegoceras*, two separate digital models were made. One model contained a scrolling turbinate whereas the other model contained a branched turbinate (Fig. 17C,D). As we were assessing the effect of these shapes on the respired airfield in life, we were actually looking at the effect of the innermost structures of the nasal capsule—the conchae.

In extant archosaur taxa, the conchae are supplied primarily by the medial nasal vessels. The crocodylian concha and avian caudal concha are supplied by branches of the medial nasal vessels and the ventral aspects of these olfactory conchae are supplied by the sphenopalatine artery (Oelrich, 1956; Sedlmayr, 2002). In birds, the lateral nasal vessels supply the rostral concha and the rostral aspect of the middle concha (Sedlmayr, 2002). In crocodylians, only the medial nasal vessels have been found to supply the conchae. In *Stegoceras*, conchal branches of the medial nasal vessels were restored as a level I' inference. The sphenopalatine artery was restored in *Stegoceras* as a level I inference, based on canals found in extant taxa and in *Prenocephale* within the orbit and passing into the nasal region through the sphenopalatine foramen. This foramen is located “dorsal to the tongue of the Pterygoid, which underlies the palatine and ventral to several small ossifications” (Maryńska and Osmólska, 1974, p. 83). In extant archosaurs and squamates, the sphenopalatine artery supplies the mucosa of the nasal septum. These blood vessels would have supplied the restored concha, increasing vascularization of soft tissues in the airfield.

Although bony ridges in the nasal cavity and the lateral expansion of the nasal capsule may be related to the presence of turbinates, it is also possible that they might be related to other soft-tissue structures, as well. For example, based on phylogenetics *Stegoceras*, like almost all archosaurs, should have had a well-developed paranasal air sinus known as the antorbital sinus (Witmer, 1997b). *Prenocephale* (ZPAL MgD-1/104) has an extensive antorbital sinus running the length of the maxilla (Maryńska and Osmólska, 1974; Witmer, 1997b; Maryńska et al., 2004). Thus, the lateral expansion of the nasal capsule in *Stegoceras* noted above may actually represent the antorbital sinus. If so, the ridge seen in *Stegoceras* may have been associated with a largely unossified or unmineralized wall that separated the nasal capsule from the paranasal sinus. In *Prenocephale*, a medial lamina of the maxilla provides a partial bony wall, but in *Stegoceras* the CT scan data clearly indicate that such a wall, if present, must have been composed of soft tissue (cartilage and/or mucosa). Many extant birds have a largely cartilaginous medial wall of

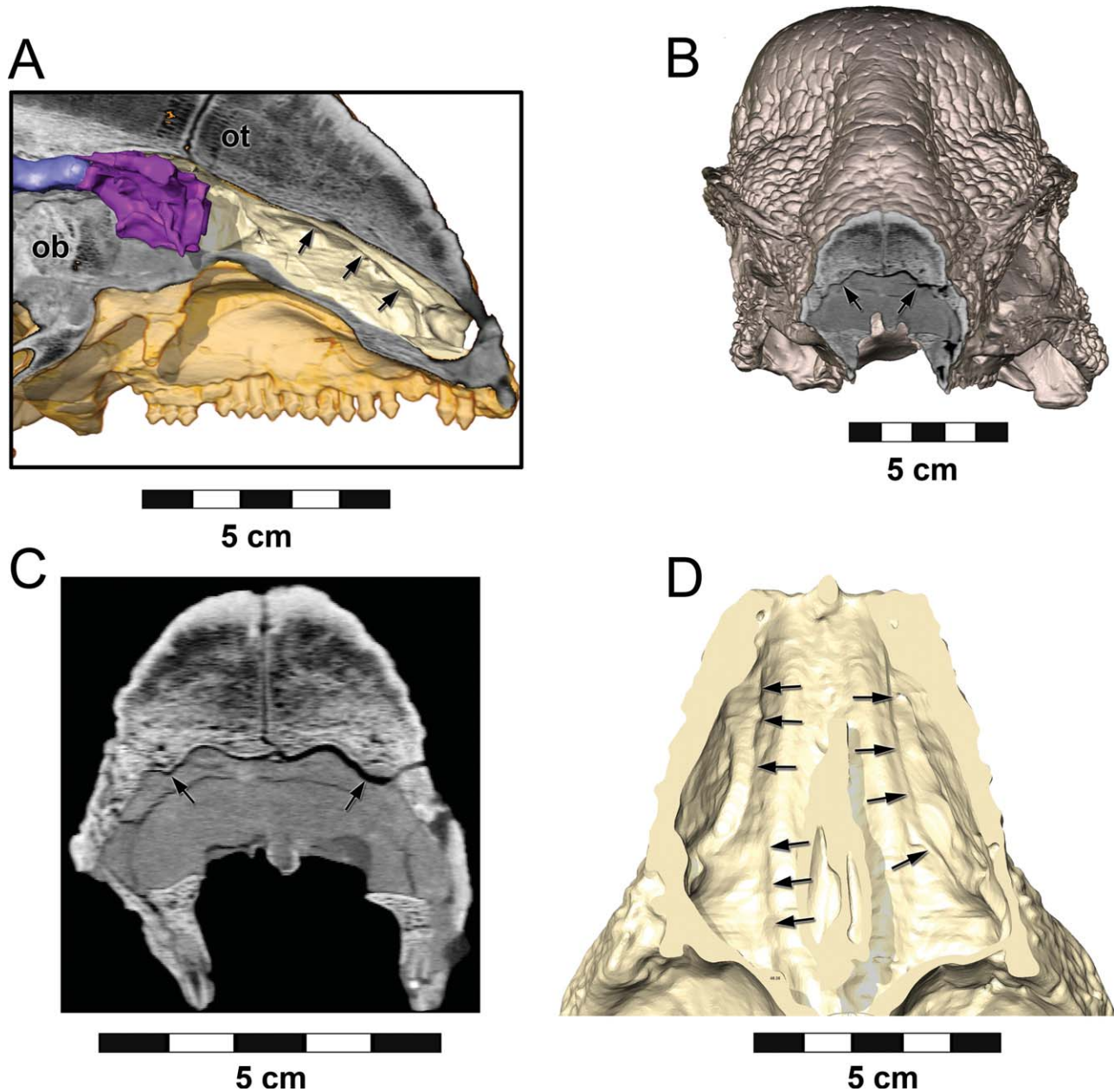


Fig. 15. Putative turbinate ridge within the nasal cavity of *S. validum* (UALVP 2). **A**: Left medial view with brain endocast and olfactory turbinates in place. **B**: Rostral view with axial slice shown. **C**: CT image of axial slice from **B**. **D**: Ventral view of the roof of the nasal cavity. Arrows point to the ridge.

the antorbital sinus (Witmer, 1995b), as did many extinct saurischians (Witmer, 1997a), and so this condition in *Stegoceras* would not be that unusual. As such, it was decided that a third digital model of nasal capsule variation should be made that incorporated an extended paranasal septum (Fig. 17B).

Finally, a fourth model was created to test the possibility that the ridge seen in *Stegoceras* (UALVP 2) incorporated both a paranasal septum and a nasal turbinate (Fig. 17E). As noted above, in *Prenocephale* (ZPAL MgD-1/104), the paranasal septum is preserved as a lamina of maxilla medial to the antorbital sinus. This lamina

approaches, and indeed contacts in some areas, a ridge that seems comparable to (and likely homologous with) the ridge in *Stegoceras*. As preserved, the ridge in *Prenocephale* is not associated with the maxillary paranasal septum throughout its entire length, perhaps lending support to the notion that the ridge could simultaneously function to demarcate the walls of the antorbital sinus and to support a respiratory turbinate. Indeed, in many extant amniotes, nasal conchae are closely associated with paranasal air sinuses (Witmer, 1995b, 1997a).

To test the impact of these different soft-tissue hypotheses on nasal airflow, the 3D modeling program

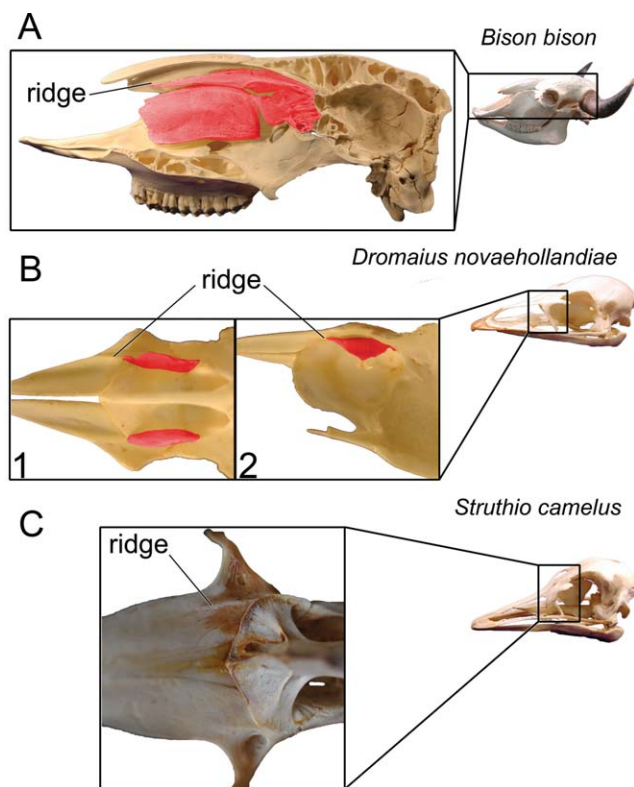


Fig. 16. **A**: Mineralized nasal turbinates (red) in a representative mammal (*Bison bison*, OUVc 9557 [inset], 09489). **B**, **C**: Ridges for turbinates are rare in diapsids, but large paleognaths sometime show turbinate ridges for attachment of their middle and caudal turbinates. **B**: Although rarely mineralized, the caudal nasal turbinates (red) in some birds will mineralize. (1) Ventral view of nasals in emu (*Dromaius novaehollandiae*, OUVc 10539 [inset], 10534). (2) Left lateral view of nasals and mesethmoid in the same specimen. **C**: Ventral view of nasals and mesethmoid of an ostrich (*Struthio camelus*, OUVc 10464 [inset], 10526).

Maya was used to model conchae of different conformations (scrolled and branched), as well as a paranasal septum walling off the antorbital sinus (with and without a turbinate), in *Stegoceras*. These models were converted into fluid dynamic models, which were then subjected to CFD analysis following the criteria listed above.

Results of Modeling a Paranasal Septum

As just noted, a paranasal septum was digitally modeled and placed along the path of the nasal ridge (Fig. 17B). The septum completely separated the lateral expansion of the bony-bounded nasal capsule. Justification for this was based on the relationship of the paranasal sinuses to the air passages of extant amniotes. The antorbital sinus in *Stegoceras* joined with the nasal capsule via an ostium, probably in a position similar to that described for *Prenocephale* (Maryńska and Osmólska, 1974; Witmer, 1997b). However, this ostium would have been small and arranged orthogonal to respired airflow (Witmer, 1995b; Witmer and Ridgely, 2008a), resulting in very little air exchange taking place during respiration.

Results of CFD analysis revealed a substantial change in airflow pattern. Both pressure drop and flow velocity

greatly increased over the BBM (Table 4). Similar to the bony-bounded airway, the airfield continued to exhibit a medial bias as air moved from the vestibulum nasi to the CNP. However, unlike the BBM, the airfield never formed a caudal-to-rostral loop, which represents an advance in that the loop was regarded as being unrealistic. Rather, inspired air arced mediolaterally as it traveled through the CNP to the ductus nasopharyngeus. Air in the dorsalmost portion of the airway moved the slowest, whereas air nearer to the nasal capsule floor—i.e., closer to the ductus nasopharyngeus—moved fastest. These flow patterns were true for both flow rates tested. Under the flow rate estimated for a 10 kg individual, airflow was remarkably slow, with air in the nasal capsule averaging 16 cm/min. This low-velocity air imparted a weak momentum to the air streams entering the olfactory chamber, keeping air from overcoming the relatively high pressure in the olfactory chamber, resulting in stagnation. This pattern changed somewhat under the flow rate estimated for a 40 kg individual. Under this flow regime, some air did enter the olfactory chamber where it circulated dorsally, then rostrally (Fig. 18). Airflow upon expiration was nearly identical to airflow in the BBM, with air spiraling through the nasal capsule toward the nostril (Fig. 19).

Results of Modeling a Scrolled Concha

Using the middle concha of turkeys (*Meleagris gallopavo*) as a typical template for conchal shape, a simple scrolled concha was inserted into the nasal capsule of *Stegoceras* along the length of the nasal ridge. The concha scrolled mediolaterally 1.5 times before opening into the ductus nasopharyngeus. The concha left 1–4 mm of space within the nasal capsule for respired air to traverse. These are typical values for extant amniotes.

Pressure drop was uneven across the nasal capsule. Placement of the scrolled concha served to function as a barrier separating a relatively low-pressure gradient medially from a relatively steeper pressure gradient laterally. During inspiration, air followed a path similar to that observed in the BBM, with the vestibulum nasi largely directing the flow of air into the CNP. The concha split the airfield into three different channels. One channel took a ventral route to the ductus nasopharyngeus, wrapping around the outside of the concha (Fig. 20). A second channel entered the concha where it followed a straight path towards the ductus nasopharyngeus (Fig. 20). Very little twisting or cyclonic motion of the air was observed in the concha at either the estimated low or high flow rates. The final air channel proceeded medially along the outside of the concha toward the olfactory chamber. As with the paranasal septum model, airflow at the estimated low flow rate did not penetrate the olfactory chamber but stopped just short of it before wrapping ventrally around the concha and exiting into the ductus nasopharyngeus. However, under the high flow-rate estimate, air was able to slightly penetrate the olfactory chamber (Fig. 20). Airflow on expiration initially spiraled out of the ductus nasopharyngeus where it encountered the concha. Air entering the concha straightened shortly upon entry. Other air channels proceeded ventrally or medially around the concha. Very little air proceeded along the dorsal aspect of the concha.

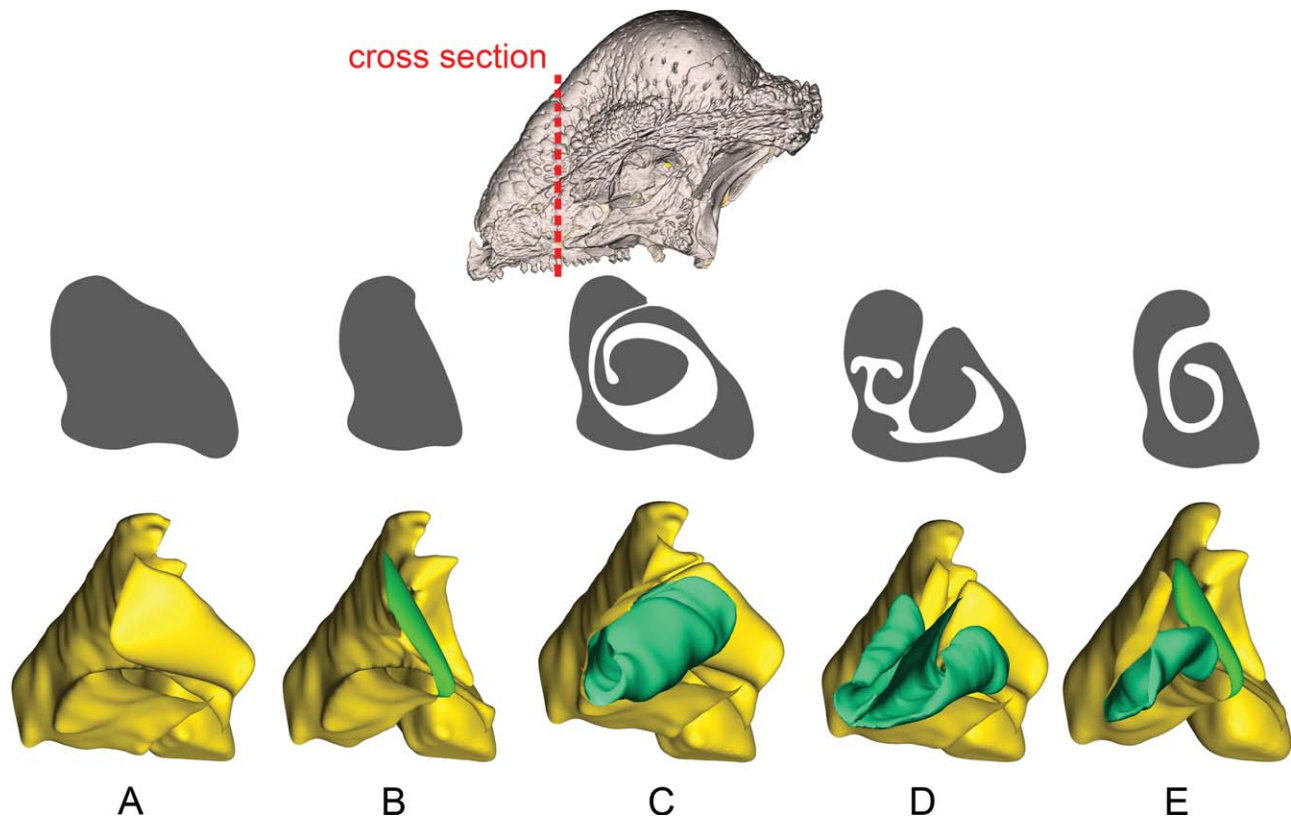


Fig. 17. Four potential morphologies of *S. validum* (UALVP 2) were tested and had airflow patterns compared with (A) the bony-bounded airway morphology, which did not take into account any unpreserved soft tissue. B: Nasal morphology composed of a paranasal septum walling off the antorbital paranasal air sinus from the the CNP. C: Nasal morphology that incorporated a scrolled nasal concha. D: Nasal

morphology that incorporated a branched nasal concha. E: Nasal morphology that incorporated both an antorbital septum and a scrolled nasal concha. Models are shown with the front-facing triangles hidden, allowing a view of the inside of the airway. Paranasal septum = green. Conchae = aquamarine.

TABLE 4. Maximum pressure and velocity magnitudes in different configurations of the nasal capsule at 10 L/min

Model	Max Pressure (Pa)	Max velocity (m/s)	Resistance (Pa*sec/mL)
Bony-bounded	1.807289	1.39497	0.010841566
Paranasal septum	5.419671	2.283075	0.032511524
Scrolled concha	3.001694	1.693192	0.018006563
Branched concha	4.424924	2.286139	0.026544235
Septum + concha	4.108988	2.14766	0.024648998

Results of Modeling a Branched Concha

The middle concha of an ostrich (*Struthio camelus*) was used as a typical template for construction of the branched concha for *Stegoceras*. As with the scrolled concha, the branched concha ran the length of the nasal ridge prior to termination near the ductus nasopharyngeus. The more open nature of the branched shape provided more room for the airfield (1–6 mm space between the concha and the capsule walls).

Similar to the scrolled concha, inspired air broke into multiple (3–4) separate channels as it came into contact

with the branched concha (Fig. 21). The first channel proceeded ventrolaterally with occasional air streams noted dorsally along the outside of the concha. These dorsal streams were relatively slow moving as they proceeded caudally toward the ductus nasopharyngeus. The second channel entered the lateral branch of the concha where it proceeded toward the ductus nasopharyngeus in a relatively straight line. The third channel entered the medial branch of the concha where it proceeded caudally towards the olfactory chamber. At 4.4 L/min (10 kg), air moved slowly through the medial branch and was unable to penetrate the olfactory chamber before wrapping around the outside of the concha and dumping into the ductus nasopharyngeus. At 10 L/min (40 kg), effectively no air was found moving through the medial branch of the concha. The fourth and final channel proceeded along the outside of the medial branch where it moved caudally into the olfactory chamber. At 4.4 L/min, olfactory flow deteriorated 8 mm into the 25 mm deep olfactory chamber. At 10 L/min, this olfactory chamber penetration was slightly better with average olfactory flow faster than before. Airflow upon expiration was more evenly distributed than in the scrolled conchal morphology, with air streams readily passing around and through the branched concha. This included air

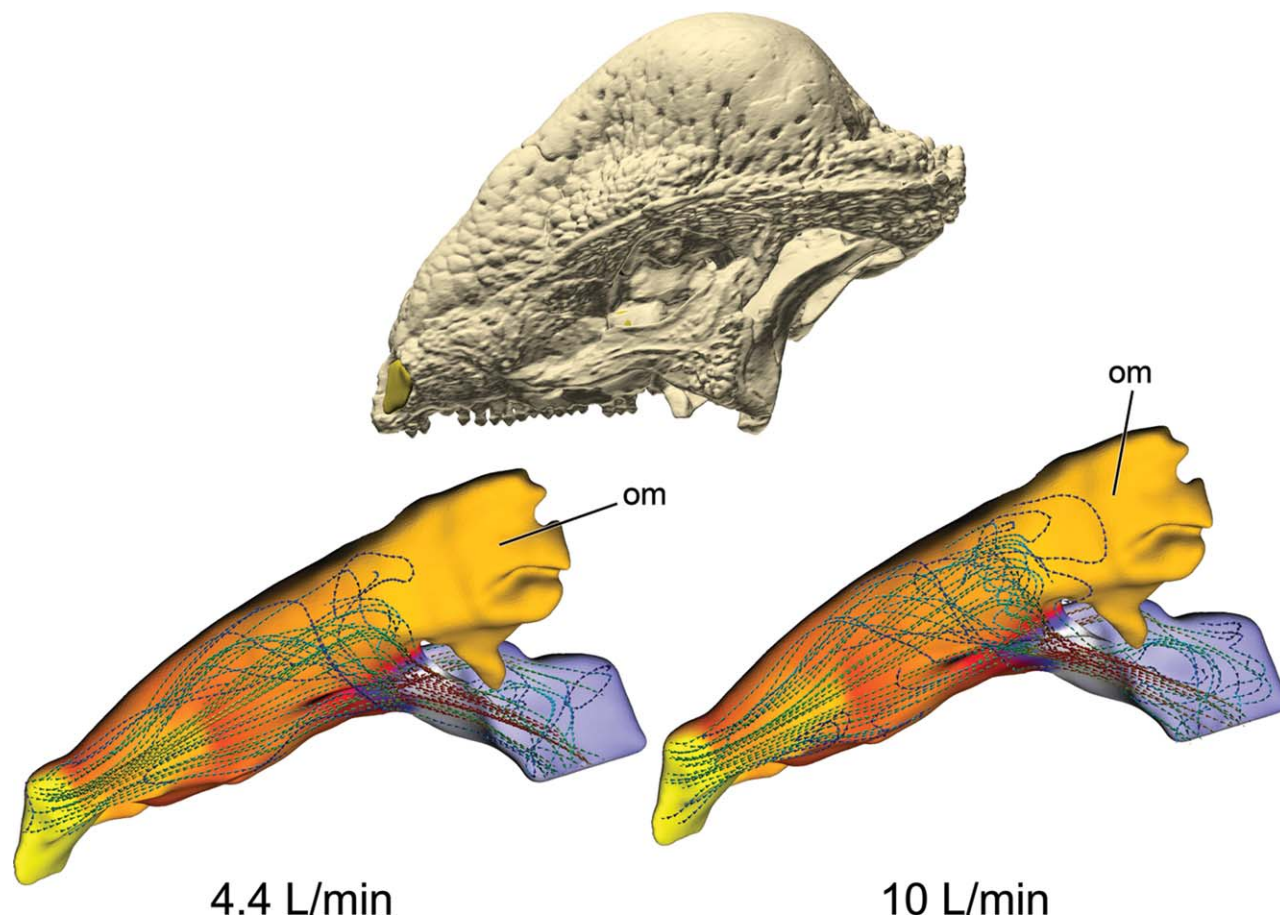


Fig. 18. Lateral view of the nasal capsule of *S. validum* (UALVP 2) modeled with a paranasal septum at both high (right) and low (left) flow rates. Nasal capsule is color-coded to reflect the pressure distribution through the airway. Hotter colors represent higher pressures (lower flow velocities).

moving through the olfactory chamber, indicating olfactory washout was taking place.

Results of Modeling a Concha with a Paranasal Septum

This airway model used the antorbital sinus configuration with the modeled paranasal septum described above but with the addition of a mediolaterally scrolled concha. Surprisingly, despite the reduced size of the airway with the combined structures, distance from the center of the air stream to the nearest wall was very comparable to the other conchal arrangements (<4.5 mm).

Inspired air broke into three channels shortly after entering the CNP. Most air traveled ventrally along the outside of the concha, towards the ductus nasopharyngeus. A second channel moved through the scroll where it followed the contours but never really developed a spiraling motion. The third channel of inspired air ran towards the olfactory chamber between the nasal septum and the medial wall of the concha. This channel exhibited slower airflow than the rest of the nasal capsule, with air meandering towards the olfactory chamber

before being drawn ventrally towards the ductus nasopharyngeus. Similarly to the scrolled concha model, air movement became stagnant upon entry into the olfactory chamber (Fig. 22). Airflow on expiration jetted out of the ductus nasopharyngeus where it was split into several channels by the concha. A weak spiraling motion was observed in the air channel that proceeded along the ventral aspect of the concha. The majority of expired air passed ventral to or within the scroll of the concha, leaving most of the medial aspect of the nasal capsule relatively undisturbed (Fig. 22).

DISCUSSION

Critique of Methods

The results obtained from our airflow simulations are ultimately dependent on the assumptions used to make them. For instance, the use of a laminar viscosity assumption may have placed excessive restrictions on our airflow models, limiting the ability of respired air to mix within the nasal capsule, or push inspired air into the olfactory chamber via vortex shedding. Although laminar flow is considered orderly, the restrictions of our viscosity model would not necessarily negate the

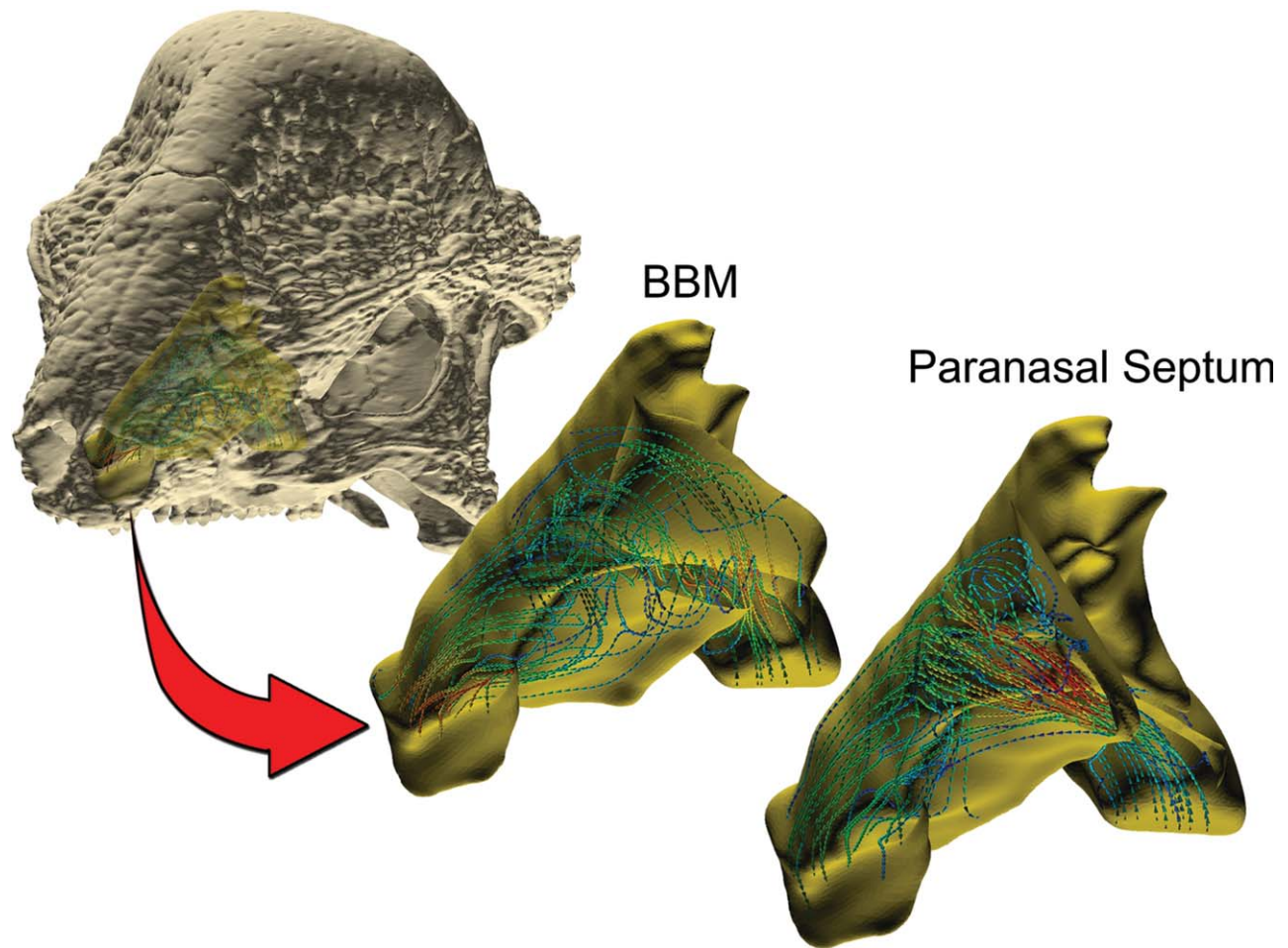


Fig. 19. Comparison of airflow of *S. validum* (UALVP 2) during expiration at 10 L/min in the bony-bounded airway model and airway modeled with a paranasal septum. Airways both exhibited a distinct lateromedial swirl to the airfield. Swirling was narrower and less developed in the airway modeled with a paranasal septum.

formation and shedding of low Reynolds number, laminar vortices such as Von Kármán trails (Vogel, 1994, 2003). Contortions within the airway may also produce laminar “mixing” as well as vortex shedding (Vogel, 1994). Our work on extant diapsid airways have produced models that exhibit such vortices using the same laminar viscosity assumption used in this study. Thus, we feel confident that the assumptions used in these analyses, while potentially too conservative, should not negate the formation of airflow patterns that would promote olfactory flow. We prefer to err on the side of conservative estimates.

A large caveat for our results comes from the predicted flow rates used, which were based on rates obtained from regression equations relating respiratory variables to body mass in birds. Birds are not pachycephalosaurs, yet still can be informative for dinosaur studies. Birds are generally small-bodied, volant endotherms. In contrast, pachycephalosaurs were larger-bodied, terrestrial animals of controversial metabolic status. Thus, it is possible that the airflow rates predicted might be overestimated. The metabolism of pachycephalosaurs—

or any extinct animal—currently remains, strictly speaking, unknown. However, we argue that it would have little bearing on the respiratory parameters used in the modeling methods used here. Although oxygen demand in tachymetabolic, endothermic birds may be over 20 times higher than similar sized bradymetabolic ectotherms (Nagy et al., 1999), the arrangement of the avian respiratory system allows birds to extract more oxygen per breath, and at lower concentrations, than similar sized mammals (Schmidt-Nielsen, 1997), which results in avian breathing frequencies being one-third those of similar sized mammals (Frappell et al., 2001). For non-passerine birds, this breathing frequency falls within the same range as similar sized lizards (Bennett, 1973), assuming a monophasic breathing pattern (Milsom, 1988). In turn, the large tidal volume in birds has been shown to be almost identical to the tidal volume in similar sized crocodylians (Farmer, 2006). Moreover, recent studies indicate that some key aspects of the avian respiratory system, such as unidirectional pulmonary airflow, may be deeply nested within diapsids (Farmer and Sanders, 2010; Schachner et al., 2013).

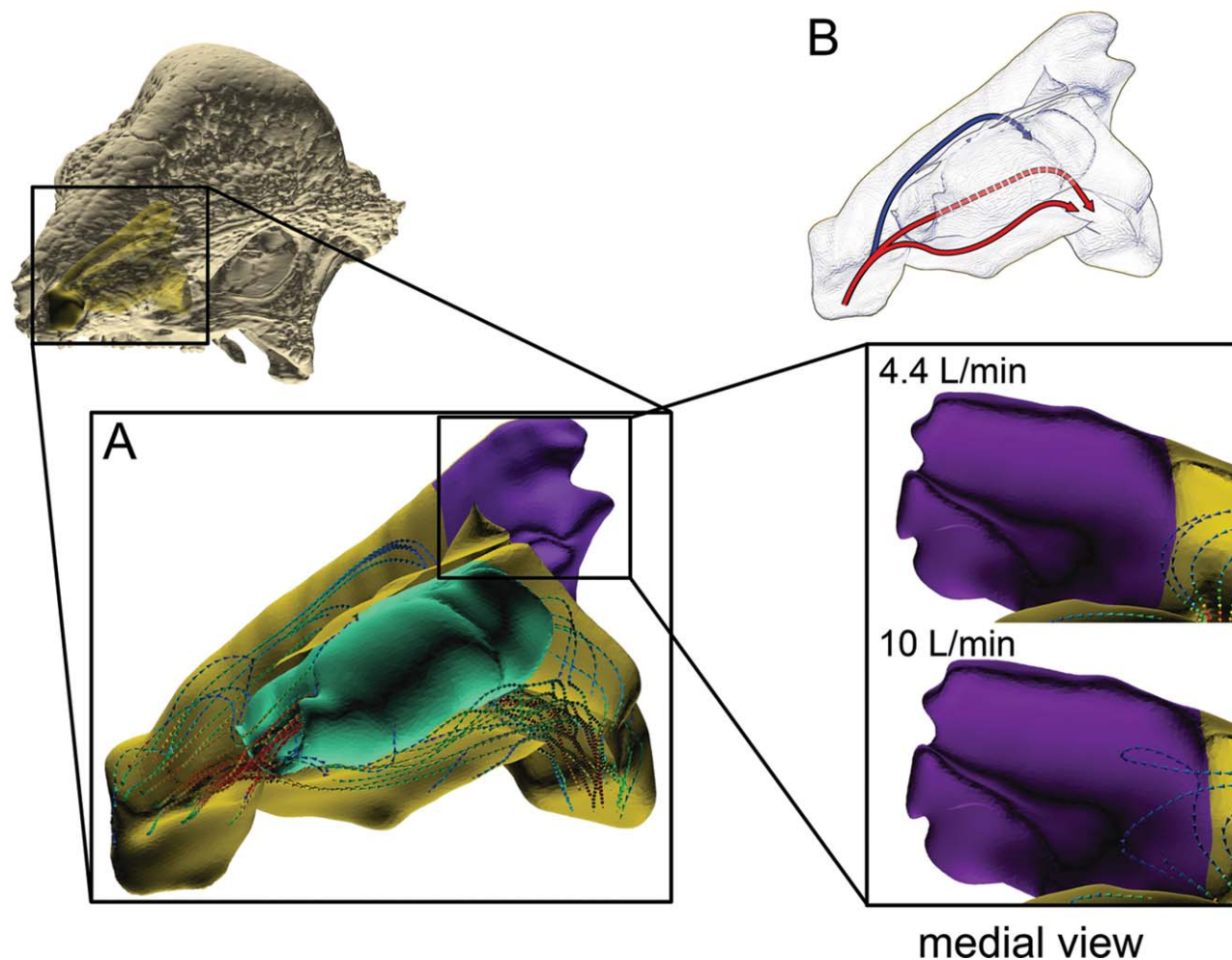


Fig. 20. Nasal capsule of *S. validum* (UALVP 2) modeled with a scrolled concha. **A**: Inspiratory airflow through the scrolled concha (aqua) model. Arrows are color-coded for velocity with hotter colors representing higher velocities. **B**: Inspired air broke into three channels upon entering the CNP. Inset: Very little olfactory flow was observed under both flow regimes with olfactory mixing being less at the lower flow rate.

Given all these similarities in respiratory variables, the inspiratory drive estimated for *Stegoceras* likely falls within the range of physiological relevance for an animal its size regardless of its metabolic status.

It remains possible that the volumetric flow rate in *Stegoceras* is underestimated based on the combined nature of the equations from Frappell et al. (2001). The authors provided several allometric equations for resting respiratory variables, including equations that could have been derived from other variables, in this case breathing frequency and tidal volume. Using the estimates obtained from these individual equations, the calculated volumetric flow rates for a 10 kg and 40 kg *Stegoceras* would be 1.3 and 1.6 times higher, respectively, than the combined inspiratory drive equation. However, using these higher inspiratory flow rates would have had a negligible effect on the results reported. Our study analyzed airflow through the same nasal morphology at flow rates that differed from each other by a factor of almost three. Despite this large dif-

ference in volumetric flow, the overall flow pattern remained essentially the same.

Lastly, the models used in these simulations were based on segmentation of CT scan data. Although likely higher in resolution than wax or latex casts, it still remains likely that the segmented data did not fully capture the shape of the nasal cavity. Vagaries of preservation and preparation, combined with technical factors in the segmentation program (e.g., smoothing algorithms, Hounsfield spectra, and tolerance values), may result in reconstructions that are flawed to some extent. Still, the segmentations, resulting nasal capsule models, and all the CFD analyses constitute a nested series of hypotheses that are amenable to testing via new or better data on pachycephalosaur nasal anatomy. Likewise, although we cannot directly compare the results obtained here with data from a living individual of *S. validum*, the error ranges provided by the grid convergence index do suggest that we are close enough to the original structure that—given the conditions specified by the

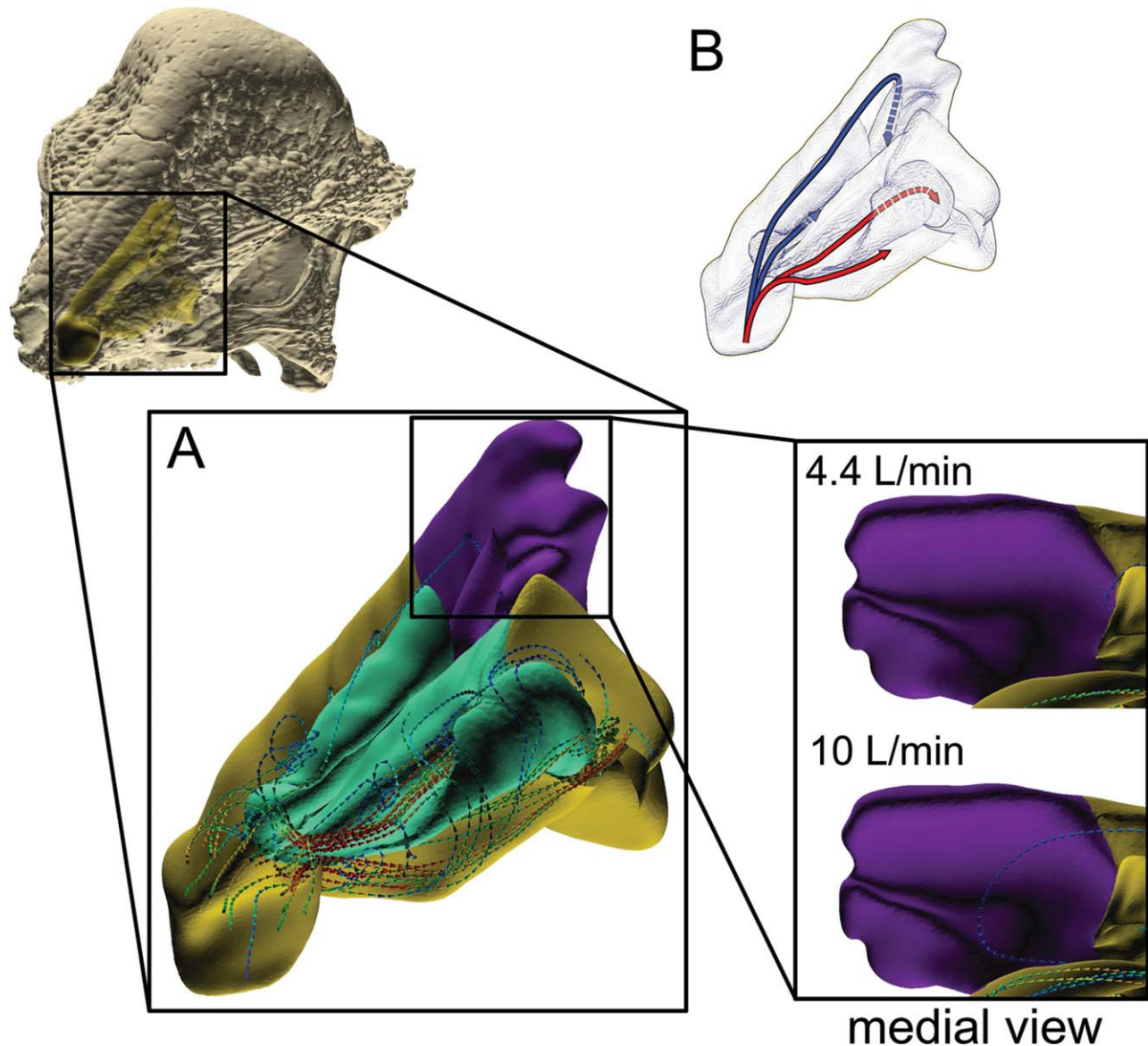


Fig. 21. Nasal capsule of *S. validum* (UALVP 2) modeled with a branched concha. **A**: Inspiratory airflow in the branched concha (aqua) model. Arrows are color-coded for velocity with hotter colors indicating higher velocity. **B**: Inspired air broke into 3–4 separate channels upon entering the CNP. Inset: Some olfactory mixing was observed at the low flow rate whereas substantial mixing was observed at the higher flow rate.

program—the results obtained from our simulations should not be affected by the resolution of the airway models used.

Flow Analysis

Under all nasal conformations tested the estimated flow rate for a 10 kg *S. validum* (4.4 L/min) was too slow to be entirely effective at ventilating the nasal capsule, especially the olfactory chamber. As noted at the outset, restoration of credible, phylogenetically constrained airflow patterns, such as appreciable olfactory airflow, is a powerful test of these models. This discrepancy in our results suggests either that 10 kg was too

low of a body-mass estimate for this specimen or that, as discussed above, the difference in body shape between birds and pachycephalosaurs was large enough that the predicted estimates provided by the bird equation were not directly comparable to those of the pachycephalosaur. The intent of these analyses was not to iteratively refine the airway models until they precisely matched extant findings. Such an effort would be largely wasted in that the precise conformation of the nasal structures in any extinct animal is ultimately unknowable, and so cannot be tested rigorously. Rather our intent was to explore the general effects of different conformations, and the clear outcome was that an airway modeled with conchae (whether scrolled or

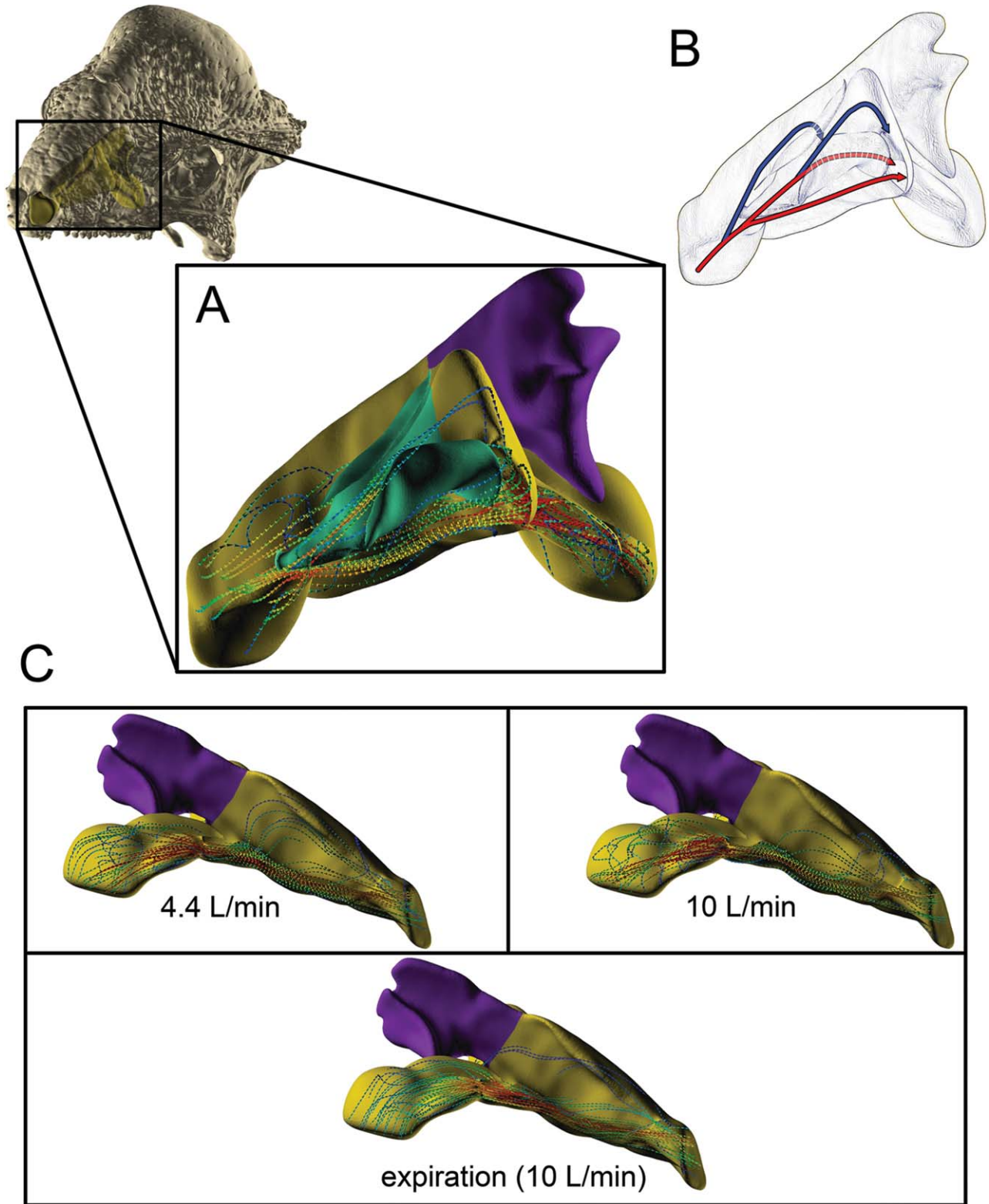


Fig. 22. Nasal capsule of *S. validum* (UALVP 2) modeled with a scrolled concha and a paranasal septum. **A:** Airflow during resting inspiration through the model with both scrolled concha (aqua) and a paranasal septum. **B:** Airflow was observed breaking into three different channels during inspiration. Arrows are color-coded for velocity with hotter colors indicating greater velocities. **C:** Left medial views of

the nasal capsule during high and low volume inspiration. Under both scenarios, flow within the olfactory chamber (purple) was essentially stagnant. This pattern was repeated upon expiration as well (regardless of flow rate). This nasal morphology produced very little olfactory flow during all phases of respiration.

branched) provided more realistic flow patterns whereas airways without conchae were less credible or not credible at all.

For example, the BBM of *Stegoceras* resulted in greatly reduced airflow velocities through the nasal capsule, complete with some unrealistic flow patterns (e.g., caudal-to-rostral flow in the lateral aspect of the CNP, lack of olfactory flow in the olfactory chamber). Incorporating soft tissue into the nasal capsule produced results more in line with what is seen in extant diapsids. Such improvements are expected in that living animals have nasal soft tissues that greatly modify airflow, and the BBM essentially revealed that the fossils themselves cannot be taken at face value. Soft tissues matter.

Given that the olfactory chamber was largely devoid of airflow under most nasal configurations, it is tempting to ask how certain we are of the chamber's configuration. For many dinosaurs, the shape of the olfactory chamber can only be partially ascertained. However, due to the remarkable preservation seen in *Stegoceras* and other pachycephalosaurs, the olfactory turbinates and even portions of the nasal capsule wall have remained largely intact. Thus, unlike most other dinosaurs, we are relatively certain of the overall shape of the olfactory chamber in this group. The difficulty of moving air into this region of the nasal capsule was more likely the result of missing soft tissues rostral to the olfactory chamber. Based on our work on extant diapsids, various soft-tissue structures are used to direct air into the olfactory chamber. In birds, conchal shape and a raised ridge known as the crista nasalis help separate flow streams and direct air into the olfactory chamber (Fig. 23C, top). Similarly, in lizards, an airway constriction called the postvestibular ridge reduces the aperture of the nasal capsule just prior to entering the CNP, which results in inspired air jetting into the CNP, allowing air to reach the olfactory chamber (Fig. 23C, bottom). In crocodylians, the junction of the primary choana and ductus nasopharyngeus is highly compressed laterally, which occurs just prior to the entrance to the olfactory chamber. Air in this region shows a similar jetting effect to that of lizards (Fig. 23C, middle). Likewise, in macrosmatic mammals, the lamina transversa and dorsal meatus have been shown to provide similar olfactory segregating functions (Craven et al. 2007, 2010). The distance between the vestibulum nasi and the olfactory chamber in pachycephalosaurs suggests that some soft-tissue structure must have been present to help guide air toward the olfactory chamber.

Studies on extant taxa have shown that the airway takes up a relatively small amount of space within the nasal capsule (e.g., Jackson and Schmidt-Nielsen, 1964; Murrish and Schmidt-Nielsen, 1970; Langman et al., 1979). By reducing the lumen of the nasal conduit, local pressure drops considerably, resulting in an increased flow speed for any given flow rate, which is beneficial for decreasing the travel time for air to pass from the nostril to lungs, ensuring successful ventilation. However, the reduced lumen also increases the resistance of air to movement through the nasal capsule. Resistance of fluid to movement within a pipe is directly proportional to pipe length and inversely proportional to pipe diameter raised to the fourth power (Vogel, 1994). For instance, if a pipe's diameter is decreased by half, its resistance will increase 16 fold. Thus, the upper respiratory tract must

balance keeping the airway small enough to maintain high flow rates for efficient lung ventilation and other physiological processes (e.g., thermoregulation), but large enough that resistance to air movement does not require an inordinate amount of muscular effort. Such compromises have been noted in the trachea of giraffes, which are smaller in diameter than equivalent sized mammals (Hugh-Jones et al., 1978), as well as in the often convoluted tracheae of birds, which are wider for a given neck length resulting in the same resistance as an equivalent-sized mammal with a shorter trachea (Hinds and Calder, 1971). Studies on extant taxa have revealed that the distance between the center of the air stream and the nearest wall of the nasal airways is rarely >5 mm (Jackson and Schmidt-Nielsen, 1964; Murrish and Schmidt-Nielsen, 1970; Schmidt-Nielsen et al., 1970; Langman et al., 1979). These short distances are required for the efficient transfer of heat and moisture within the nasal capsule (Collins et al., 1971) and thus would be expected to be present within the nasal capsule of *Stegoceras*. Under the BBM, the distance between the center of the air stream and the capsular wall was rarely <5 mm (Fig. 24), except for the region of the olfactory turbinate.

Addition of a paranasal septum reduced airway volume by 23%, slightly increasing the surface area to volume ratio and decreasing the distance to the nearest wall to <4 mm in many places. However, large portions of the airfield still remained above the 5 mm mark, suggesting that the improvements to the airway from this morphology were only slight. In contrast, the incorporation of a respiratory concha greatly changed the composition of the respired airfield, contracting the volume by 10–29%, increasing overall surface area, and dividing the nasal capsule into distinct respiratory and olfactory regions. Distance from the center of the airfield was reduced to 0.22–4.3 mm throughout the cavum nasi proprium (Fig. 24).

Placement of a concha, whether branched or scrolled, created two distinct pressure gradients. A relatively steep, low-pressure gradient pushed the majority of the airfield into the lateral aspect of the nasal capsule where it entered the ductus nasopharyngeus. A much shallower gradient formed on the medial aspect of the nasal capsule, leading to the olfactory chamber. This pressure separation was very similar to the pressure distribution observed in extant, concha-filled birds. The scroll-shaped concha's separation of the medial and lateral sides of the nasal capsule resulted in the medial (olfactory) side having an extended high-pressure zone. This zone posed a barrier to entry for inspired air (Fig. 25). Olfactory information is acquired mostly on inspiration (Schoenfeld and Cleland, 2005). Thus, for our tests olfactory flow during inspiration was more informative of model effectiveness than flow available upon expiration. These data suggested that the coiled conchal shape was not very effective at moving air into the olfactory chamber. In contrast olfactory flow was highest under the branched concha model. The shape of the branched concha, with its curled medial projection, created a transverse partition to the airfield that reduced ventral migration of air around the concha and into the ductus nasopharyngeus (Fig. 25). This produced a conveyor belt-like function along the medial branch of the branched concha, forcing air to ride along it, pushing

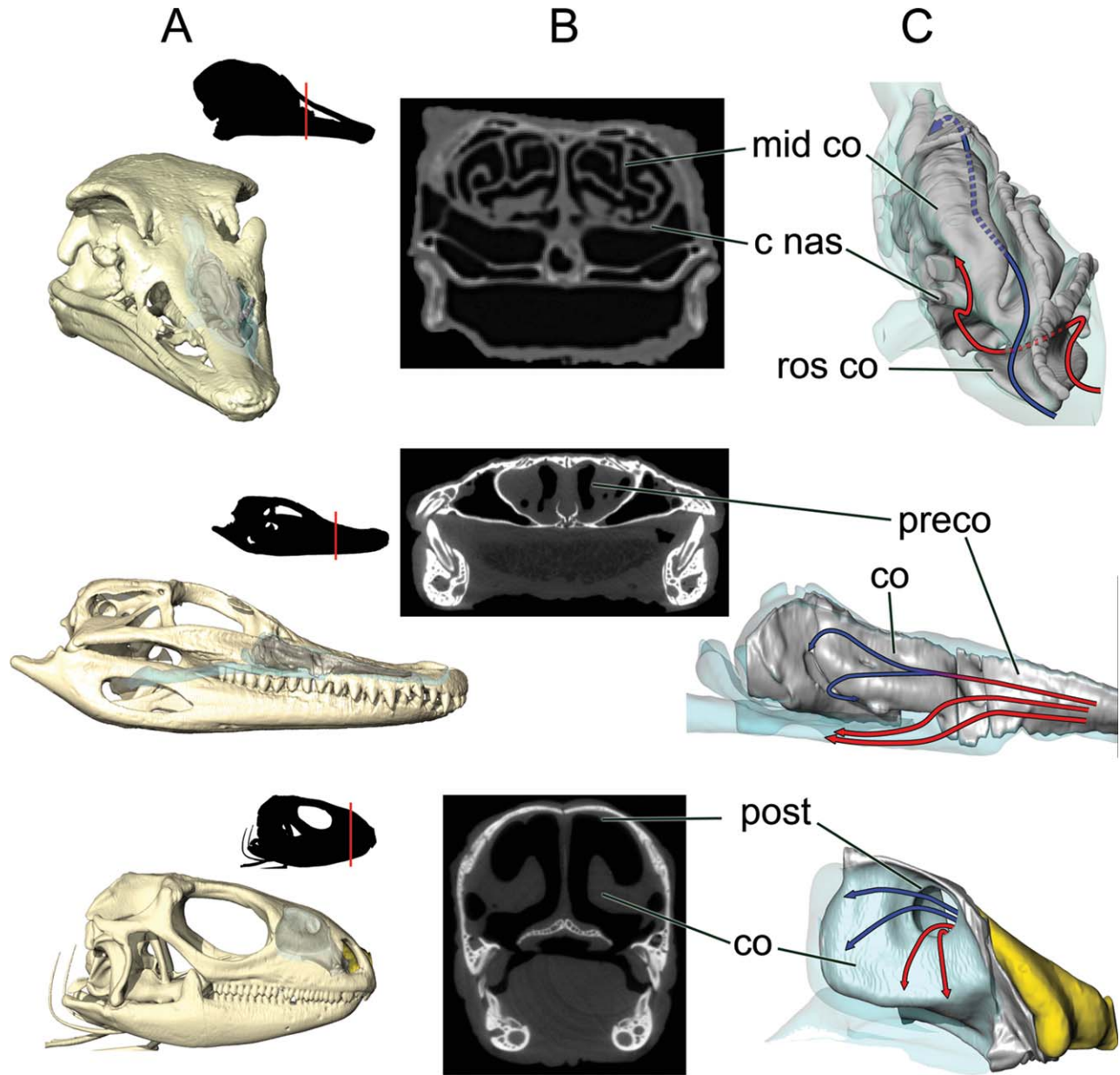


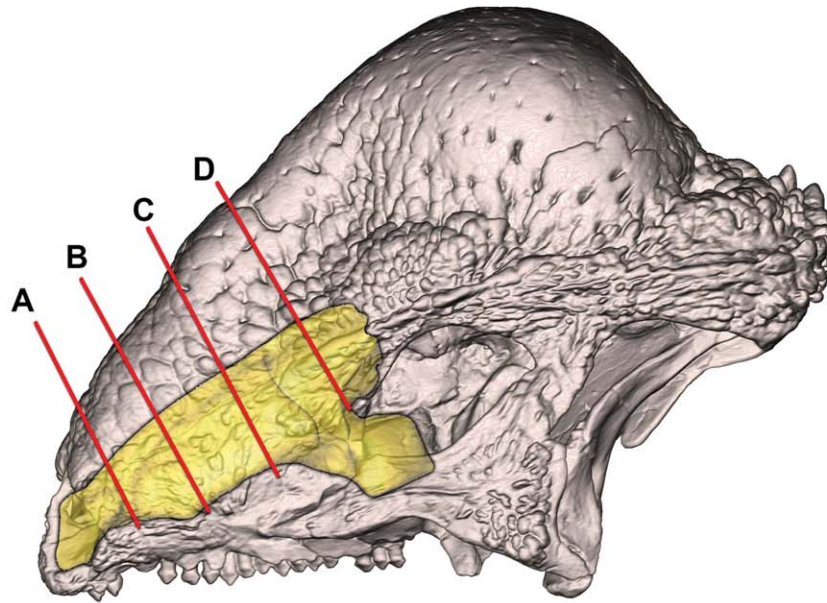
Fig. 23. Nasal airways in extant diapsids highlighting regions of airway constriction and olfactory segregation. **A:** Skulls of an ostrich (*Struthio camelus*, OUV 10636, top), alligator (*Alligator mississippiensis*, OUV 10389, middle), and iguana (*Iguana iguana*, OUV 10603 bottom). **B:** Axial cross sections taken at locations shown in the silhouettes in A. **C:** Simplified representation of airflow through nasal capsule at regions near airway constrictions. Airways in C reflect skull positions in A.

air further into the olfactory chamber and producing results more in line with what is seen in extant amniotes. Thus, of the five nasal conformations tested for *S. validum*, the branched concha conformation produced results that agreed best with airflow patterns in extant diapsids.

Sniffing

Given the lack of realistic olfactory airflow under many of the modeling scenarios just discussed, it must

be asked whether sniffing would have been a more appropriate scenario to model. Sniffing is a distinct breathing pattern apart from regular respiration. It consists of rapid, ballistic inspirations and expirations that produce substantially higher airflow rates than observed under resting respiration (Craven et al., 2010). These rapid oscillations serve to push large volumes of air into the olfactory recess where odorant molecules differentially settle out along the olfactory epithelium (Mozell, 1970). Perhaps, then, olfactory flow is only substantial during a sniffing bout. Whereas airflow into the



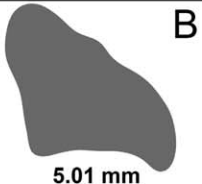

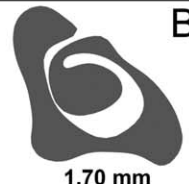


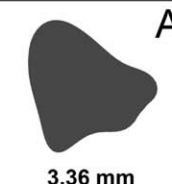
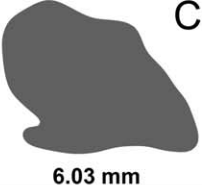

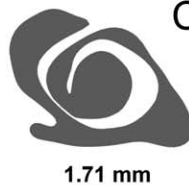
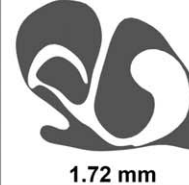


Bony-Bounded	Paranasal septum	Scrolled Concha	Branched Concha	Septum-Concha	Shared Regions
 B 5.01 mm	 B 3.87 mm	 B 1.70 mm	 B 1.78 mm	 B 2.36 mm	 A 3.36 mm
 C 6.03 mm	 C 4.50 mm	 C 1.71 mm	 C 1.72 mm	 C 2.25 mm	 D 2.60 mm

Fig. 24. Example cross-sectional measurements through the nasal capsule of *S. validum* (UALVP 2) showing the average distance from the center of the airfield to the nearest wall in all five nasal morphologies. Lettered red lines indicate locations of cross sections throughout the nasal capsule. As nasal morphology changed only within the CNP (B, C) a single average is shown for all five nasal morphologies in their shared regions of interest (A, D).

olfactory chamber was likely much higher during sniffing in *Stegoceras*, much as it is in extant animals (e.g., Craven et al., 2010); sniffing is a behavior that typically occurs only after a stimulus has been detected (e.g., Dial and Schwenk, 1996; Craven et al., 2010). Thus, air must still first reach the olfactory epithelium in order to stimulate sniffing behavior. Although classically viewed as being restricted to the olfactory chamber, olfactory epithelium may extend far rostrally from the olfactory chamber (e.g., Saint-Girons, 1976), thus allowing an olfactory stimulus to be detected earlier, and perhaps reducing the need to push air first into the olfactory chamber. Olfactory epithelium has been observed to be distributed differentially along the nasal capsule of extant tetrapods (Schoenfeld and Cleland, 2005). More rostrally located olfactory receptor neurons are sensitive to highly sorptive odorant molecules, whereas less sorp-

tive molecules require more retention time in the airway and are not absorbed until much farther into the olfactory recess (Schoenfeld and Cleland, 2005). Although ultimately dependent on the concentrations and types of odorants being inspired, given the regional sorptivity of olfactory epithelia, a full, or at least partial, pass through the olfactory chamber may still be necessary to stimulate sniffing behavior, which could explain why olfactory chamber airflow was observed in all extant diapsids during restful respiration that we have modeled using CFD (Fig. 23). Other computational analyses have also observed airflow within the olfactory chamber during restful breathing (Zhao et al., 2006; Jiang and Zhao, 2010). Thus, the flow patterns observed in many of our modeled *Stegoceras* nasal morphologies still appear valid as tests of overall nasal conformation despite using flow patterns associated with resting respiration rather than

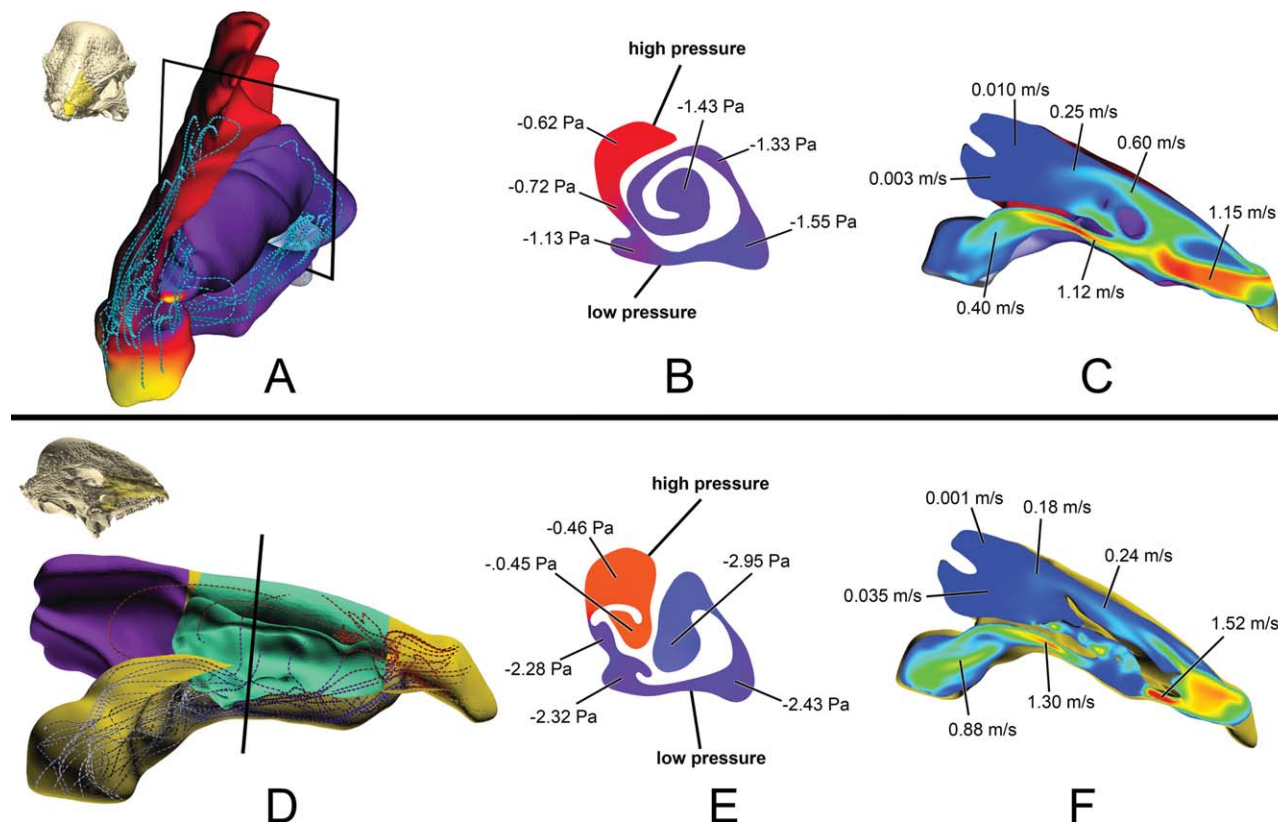


Fig. 25. Pressure and velocity distribution within the nasal capsule of the scrolled concha model (A–C) and branched concha model (D–F) of *S. validum* (UALVP 2). A: Placement of concha split the nasal capsule into a high-pressure medial side and low-pressure lateral side. B, E: Pressure was always higher in the olfactory chamber than the rest of the nasal capsule, with the connection between the high- and low-pressure regions being less complete in the scrolled model (B) com-

pared with the branched model (E). D: More complete separation in the branched concha produced a conveyor belt-like effect pushing inspired air further into the olfactory chamber. C, F: Cross sections through a medial view of the scrolled (C) and branched (F) models. The airfield is capable of maintaining momentum further into the olfactory chamber under the branched model.

sniffing. That is, although models incorporating sniffing might have produced even greater, more realistic olfactory flow, our intent again was not to restore airflow exactly (which is an unattainable goal) but rather to assess whether conchal structures attached to the preserved ridges had a positive impact on airflow, which could be done using resting respiration rather than invoking new assumptions about the airflow dynamics of dinosaur sniffing.

Osteological Evidence for Turbinates and Its Implications

Turbinates—olfactory or respiratory—are delicate structures that rarely mineralize in extant diapsids and even more rarely preserve in the fossil record. The systemic hypermineralization observed in pachycephalosaurids resulted in a relatively clear picture of the olfactory turbinates, implying an at least moderate if not well-developed sense of smell, which is concordant with the neurological finding of relatively large olfactory bulbs in the brain endocast. Evidence for respiratory turbinates in extinct taxa usually relies on proxies for their existence, namely, the presence of internal ridges along the bones of the nasal cavity (Hillenius, 1992,

1994; Ruben, 1996). The ridges noted on the ventral aspect of the nasal bones in *Stegoceras*, *Sphaerotholus*, and *Prenocephale* appear to meet the criteria used to assess turbinate placement in mammals, and to a lesser extent, birds (Fig. 16). Another criterion used to assess the presence of turbinates is the overall cross-sectional area of the nasal cavity (Ruben et al., 1996). It has been argued that animals lacking respiratory turbinates have nasal cavities that are smaller in cross-sectional area. However, this relationship is highly dependent on both the estimated mass of the individual, as well as the location within the nasal capsule in which the cross section was taken. Based on the data used to make the graph in Ruben et al. (1996), *Stegoceras* variably falls on the ectotherm line, the endotherm line, or above both lines depending on the mass estimate used and the location of the cross section. As a predictor of metabolic physiology, cross-sectional area of the nasal cavity currently appears problematic.

The results presented here suggest that the nasal capsule of *Stegoceras*—and presumably other pachycephalosaurids given the similar morphology of *Prenocephale*—housed well-developed nasal (presumably respiratory) turbinates for at least two reasons. First, the acknowledged OCs of turbinates are present in the form of

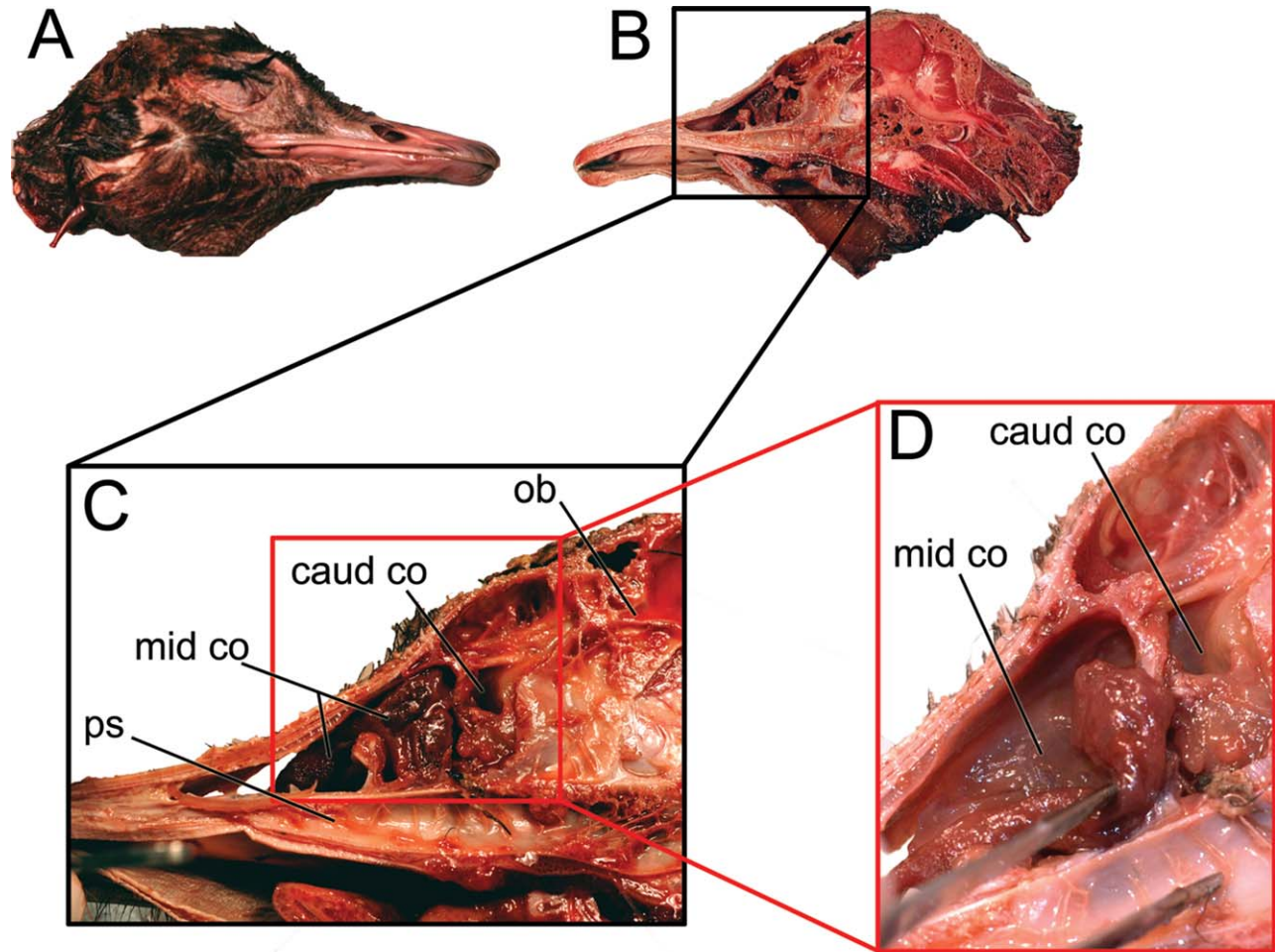


Fig. 26. Gross analysis of epithelium on the middle concha of an ostrich (*Struthio camelus*, OUV 10660). **A:** Right lateral view of ostrich head. **B:** Right medial view of sagittally sectioned ostrich head. **C:** Inset of ostrich nasal passage with nasal septum removed. **D:** Inset of cavum nasi proprium with medial branch of middle concha reflected to reveal yellow-colored olfactory epithelium similar to the olfactory epithelium seen on the caudal concha.

longitudinal ridges on the bones surrounding the cavum nasi proprium. And second, the CFD modeling analyses reveal that reasonably realistic nasal airflow can be restored when nasal conchae are included in the models. Respiratory conchae have been physiologically linked to reducing respiratory evaporative water loss (REWL), which is a critical function for endotherms due to their elevated ventilation rates, and thus have been used as prima facie evidence for elevated resting metabolic rates in the animals housing them (Hillenius, 1992; Ruben et al., 1996; Geist, 2000; Chinsamy and Hillenius, 2004). This apparent causal link has led to the intriguing proposition that respiratory conchae (or turbinates) may be used as indicators of metabolic status for extinct animals (Hillenius, 1994; Ruben, 1995; Ruben et al., 1996; Hillenius and Ruben, 2004). Given this line of reasoning, the inference of respiratory conchae in pachycephalosaurids would suggest that these dinosaurs had elevated rates of metabolism. The relatively recent discovery of potential respiratory turbinates in the distantly related tyrannosaur CMNH 7541 (Witmer and Ridgely, 2010) suggests

that respiratory conchae may have been widespread within Dinosauria, with the implication being that perhaps all dinosaurs had elevated metabolic rates.

However, this view of respiratory conchae as indicators of resting metabolism is not without contention (Seymour, 2004a, b; Padian and Horner, 2004). Opponents have noted examples of extant mammals and birds with reduced or absent respiratory conchae, indicating that not all tachymetabolic endotherms require respiratory conchae to offset heat and water loss. It is worth noting that opposition to the respiratory concha argument comes from the view that conchae are not absolutely necessary for tachymetabolic endothermy and so their presumed absence cannot absolutely refute hypotheses of endothermy in extinct taxa. Conversely, the uniqueness of respiratory conchae to endotherms has not been questioned. The original argument for respiratory turbinates/conchae and elevated metabolism (Hillenius, 1992) posited that the conchae in extant bradymetabolic reptiles were solely olfactory in nature. The function of turbinates or, more correctly, the

mucosa-covered conchae that reside on turbinates, is dependent on both the location of the concha within the airway as well as the epithelium that covers the conchae. Of these two criteria, only the former is accessible to paleontology. Conchae obtain respiratory status if they lie within the main flow of the respired airfield (Ruben et al., 1998). This can be grossly determined by looking at the shape of the nasal capsule and determining the general direction of flow from nostril to choana. In general, the olfactory chamber and paranasal sinuses are considered to be the two portions of the nasal passage that lie outside of the main airfield (more so for the latter). Thus, any conchal structure within the olfactory chamber would be considered to be olfactory-only in function, whereas structures lying within the main airfield have been considered respiratory-only in function. This black and white view of conchal function starts to blur upon viewing the histology of the mucosa on the conchae. For instance, the middle concha of birds is generally considered to be respiratory-only in function, based on its location within the nasal capsule (Ruben et al., 1998; Geist, 2000). However, histologically, this structure may be partly or largely covered in olfactory epithelium as is seen in some Columbiformes (Bang, 1971) as well as ostriches (Jin et al., 2008; Fig. 26).

The argument that extant reptiles lack respiratory conchae—or at least conchal structures that play a physiological role in heat and water balance—is questioned by our work on the conchal anatomy and histology in extant reptiles. Using only the criterion of position within the nasal capsule it becomes apparent that the preconcha of crocodylians should be classified as a respiratory concha. It lies directly in the line of the respired airfield as determined by gross analyses of airway shape as well as detailed CFD analysis of respired airflow (Bourke and Witmer, 2010; Fig. 27). Histologically, this region of the nasal capsule has been found to contain olfactory epithelium mixed with respiratory epithelium (Saint-Girons, 1976; Hansen, 2007). However, the extent of the olfactory epithelium is less pronounced on the preconcha than on the more caudally located concha. An extensive plexus along the ventral side of the airway, and a well vascularized preconcha mainly supplied by the medial nasal and sphenopalatine vessels offer further support for a thermoregulatory function of the crocodylian preconcha (Porter and Witmer, 2011; Fig. 27). The position of these well-vascularized surfaces in the airstream would have allowed evaporative cooling to cool blood within them and support physiological thermoregulation. The avian caudal concha and the crocodylian concha and postconcha are not as well vascularized, indicating a lesser role in physiological thermoregulation, likely due to reduced airspeeds decreasing the ability to support evaporation. Therefore, the preconcha of crocodylians based on anatomical location, relative vasculature, and potentially histology, warrants classification as a respiratory concha, pending experimental validation.

The single concha of squamates has routinely been cited as having solely an olfactory function (Ruben, 1995; Ruben et al., 1996, 1998; Hillenius and Ruben, 2004). However, much like the preconcha of crocodylians, this structure at least partially lies within the respiratory airfield. Our CFD analyses on iguanas and varanids have shown that the rostral and ventral portion of the

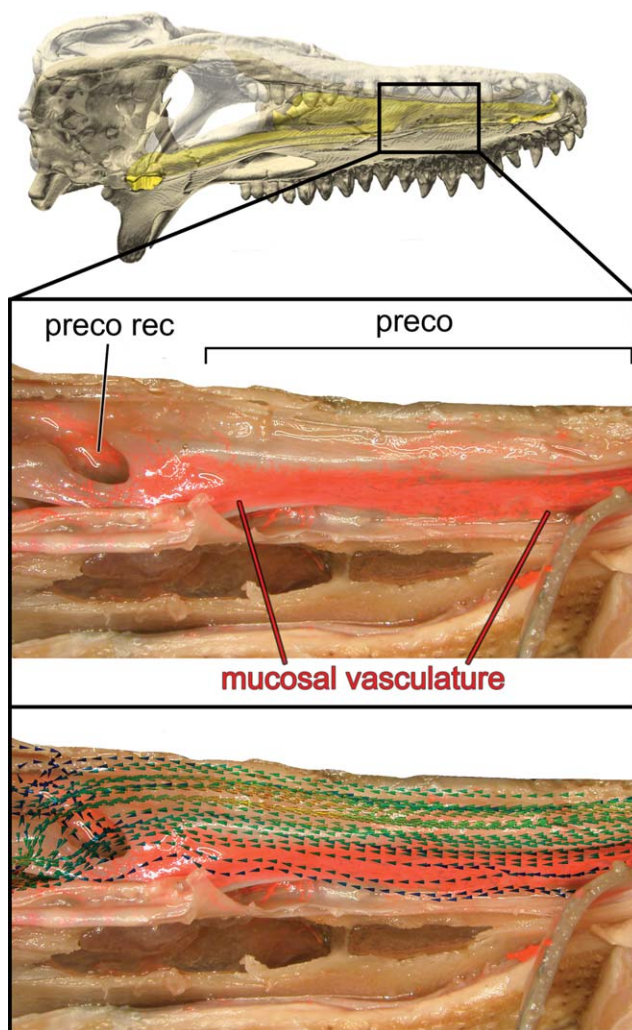


Fig. 27. Ventromedial view of left airway in *Alligator mississippiensis* (OUVC 10389). Inset: Dissection of latex-injected (pink) *Alligator* nasal capsule revealing extensive vasculature within the mucosa of the preconcha and tectum nasi (top). A separate vascular plexus was observed along the solum nasi as well (not shown). This region of the nasal capsule is in direct line with the path of respired air (bottom) suggesting that it serves a thermoregulatory function in *Alligator*.

squamate concha lies within the main airfield during both phases of respiration (Fig. 28). This rostral portion of the concha is more vascular than the caudal portion in iguanas (Fig. 28). Extensive studies on squamate nasal histology (Stebbins, 1948; Bellairs, 1949; Duvdevani, 1972; Gabe and Saint-Girons, 1976; Rehorek et al., 2000) have shown that this area of the nasal capsule is composed of respiratory epithelium, whereas olfactory epithelium makes up the caudal portion of the concha. Thus, the single concha of squamates must be viewed as a regionally segregated respiratory and olfactory turbinate.

Lastly, it is pertinent to note that the original argument for the role that respiratory conchae play in the evolution of endothermy was based on the presumed requisite coupling of high ventilation (respiration) rates with the high oxygen requirements of endothermy, as

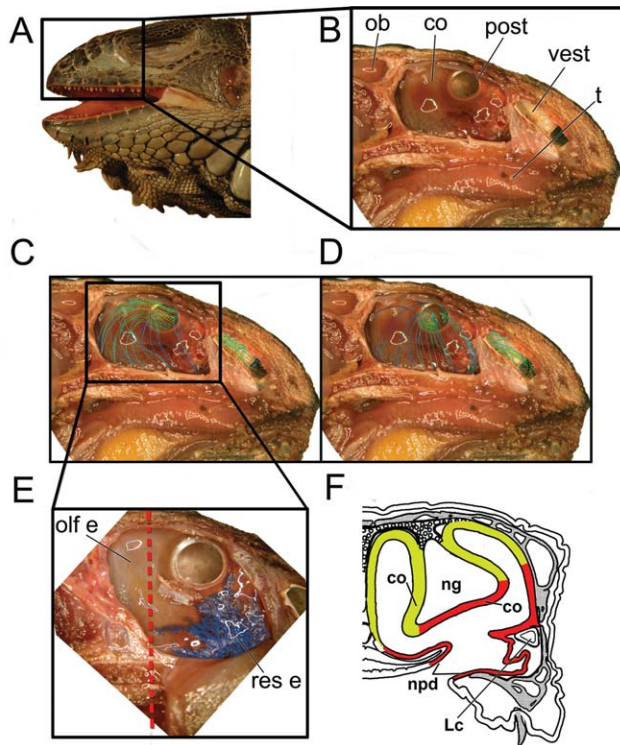


Fig. 28. Nasal morphology and airflow through the nasal capsule of *Iguana iguana* (OUVC 10684). **A**: Left lateral view of head highlighting nasal capsule location. **B**: Left medial view of sagittal section through nasal septum. **C**: Airflow pattern based on CFD analysis during inspiration and **(D)** during expiration. **E**: Expanded view of concha, showing the gross location of respiratory and olfactory epithelium. Vascular injection (blue) reveals extensive blood flow to the respiratory region of the concha. Red dotted line indicates the location of **(F)** the diagrammatic cross section through the concha revealing the histological location of epithelia along the nasal capsule. Yellow = olfactory epithelium. Red = respiratory epithelium. Diagram in **F** based on Gabe and Saint-Girons (1976).

seen in mammals (Hillenius, 1994; Ruben et al., 1996, 1998). However, extant birds—which may have average basal metabolic rates up to twice those of similarly sized mammals (McNab, 2009)—are able to meet these high oxygen demands not with high ventilation rates but rather through a respiratory system that is more efficient at extracting more oxygen per breath. As a result, birds breathe, on average, one- to two-thirds as often as similarly sized mammals (Calder, 1968; Frappell et al., 2001). Although comparable respiratory data are relatively few for reptiles, these low respiratory frequencies for birds are not that different from those of similarly sized—continuously breathing—lizards (Bennett 1973) and alligators (see Methods above). These disparate respiratory parameters call into question how important respiratory conchae are for endothermy in birds, and are reflected in the conflicting results of empirical studies on avian respiratory conchae (Tieleman et al., 1999; Geist, 2000; Michaeli and Pinshow, 2001).

In light of our findings on the diversity of nasal conchal structure, histology, blood flow, and airflow in diapsids, it is appropriate to be cautious about the physiological implications of the inference of respiratory

conchae in pachycephalosaurids or other dinosaurs. More experimental work is needed to explore the physiological significance of these intriguing anatomical findings in nonavian diapsids. It is possible that heat exchange in these conchal structures could play a more local role in selective brain temperature regulation (Witmer, 2001; Porter and Witmer, 2011), as either an alternative or an adjunct to a broader respiratory role in mitigating REWL.

ACKNOWLEDGEMENTS

For useful discussions over the course of the project, the authors thank B. Andres, D. Brinkman, D. Cerio, B. Craven, J. Davis, C. Early, R. Felice, J. Gauthier, E. Gorscak, A. Morhardt, M. Norell, H. O'Brien, E. Snively, and E. Vrba. Thanks to S. Anderson, D. Briggs, P. Dodson, and J. Lyson for comments on an early version of portions of the manuscript. M. Caldwell and P. Manning graciously carried specimens to Austin, Texas, for CT scanning. At UTCT, they thank M. Colbert and J. Maisano. Thanks to P. Currie for providing access to UALVP 2 for scanning. They also thank H. Rockhold and Ohio-Health O'Bleness Hospital (Athens, OH) for CT scanning. For scanning and providing the scan data of NMMNH P-27403, they thank C. Gerrard, G. Hatch, C. Pilbro, and especially T. Williamson. They thank M. and J. Sonsalla for donating MRF 360–362 to the Marmarth Research Foundation, and B. Benty and M. Fox for preparing them. They thank Michael Habib and Brent Craven for useful advice and critique on the manuscript.

LITERATURE CITED

- Aftosmis M, Gaitonde D, Tavares TS. 1994. On the accuracy, stability and monotonicity of various reconstruction algorithms for unstructured meshes. AIAA Pap 94-0415.
- Agarwal R. 1999. Computational fluid dynamics of whole body aircraft. *Annu Rev Fluid Mech* 31:125–169.
- Allison PA, Pye K. 1994. Early diagenetic mineralization and fossil preservation in modern carbonate concretions. *Palaios* 9:561–575.
- Almeida L, Campos R. 2011. Systematization, description and territory of the caudal cerebral artery of the brain in broad-snouted caiman (*Caiman latirostris*). *Pesq Vet Bras* 31:817–822.
- Angielczyk KD, Sheets HD. 2007. Investigation of simulated tectonic deformation in fossils using geometric morphometrics. *Paleobiology* 33:125–148.
- Arbour VM, Currie PJ. 2012. Analyzing taphonomic deformation of ankylosaur skulls using retro-deformation and Finite Element Analysis. *PLoS One* 7:e39323 doi,10.1371/journal.pone.0039323.
- Bang BG. 1960. Anatomical evidence for olfactory function in some species of birds. *Nature* 188:547–549.
- Bang BG. 1971. Functional anatomy of the olfactory system in 23 orders of birds. *Acta Anat* 79:1–76.
- Bang BG, Wenzel BM. 1985. Nasal cavity and olfactory system. In: King AS, McLelland J, editors. *Form and Function in Birds*. Vol.III. Elsevier. p 195–225.
- Baumel JJ. 1993. Systema cardiovasculare. In: Baumel JJ, editor. *Handbook of Avian Anatomy: Nomina Anatomica Avium*. Cambridge, MA: Nuttall Ornithological Club. New York. Academic Press. p 407–476.
- Baumel JJ, Witmer LM. 1993. Osteologia. In: Baumel JJ, King AS, Breazile JE, Evans HE, Vanden Berge JC, editors. *Handbook of Avian Anatomy: Nomina Anatomica Avium*. Publications of the Nuttall Ornithological Club. No. 23. p 45–132.

- Bellairs A D'A. 1949. Observations on the snout of *Varanus*, and a comparison with that of other lizards and snakes. *J Anat* 83 (Pt. 2):116–146.
- Bennett AF. 1973. Ventilation in two species of lizards during rest and activity. *Comp Biochem Physiol* 46A:653–671.
- Biswas R, Strawn RC. 1998. Tetrahedral and hexahedral mesh adaptation for CFD problems. *App Num Math* 26:135–151.
- Blacker T. 2001. Automated conformal hexahedral meshing constraints, challenges and opportunities. *Eng Comp* 17:201–210.
- Bourke JM, Witmer LM. 2010. The nose knows: the effects of nasal cavity anatomy on airflow in alligators. *J Vertebr Paleontol* 30 (2 supp):63A.
- Bourke JM, Witmer LM. 2011. Computer modeling of nasal airflow in two extant avian dinosaurs (turkey and ostrich), with implications for modeling airflow in extinct theropods. *J Vertebr Paleontol* 31 (2 supp):75A.
- Bourke JM, Witmer LM. 2012. Dorsal or rostral nostrils? Testing fleshy nostril position and airflow in sauropods using computational fluid dynamics. *J Vertebr Paleontol* 32 (1 supp):66A.
- Brown C, Russel AP. 2012. Homology and architecture of the caudal basket of Pachycephalosauria (Dinosauria: Ornithischia): the first occurrence of myorhabdoi in Tetrapoda. *PLoS One* 7:e30212.
- Brzustowicz J, Lounsbury T, Esclafer de la Rode JM. 2003. Improving racecar aerodynamics. *SAE Automot Eng* 111:95–98.
- Brzustowicz JP, Lounsbury TH, Esclafer de la Rode JM. 2002. Experimental and computational simulations utilized during the aerodynamic development of the Dodge Intrepid R/T race car. *SAE* 2002-01-3334.
- Burda DJ. 1966. Embryonic modifications of lacertilian intracranial arteries. *Am J Anat* 118:743–754.
- Burda DJ. 1969. Developmental aspects of intracranial arterial supply in the alligator brain. *J Comp Neuro* 135:369–380.
- Calder WA. 1968. Respiratory and heart rates of birds at rest. *The Condor* 70:358–365.
- Carrano MT, Hutchinson JR. 2002. Pelvic and hindlimb musculature of *Tyrannosaurus rex* (Dinosauria: Theropoda). *J Morphol* 253:207–228.
- Carrier DR, Farmer CG. 2000a. The evolution of pelvic aspiration in archosaurs. *Paleobiology* 26:271–293.
- Carrier DR, Farmer CG. 2000b. The integration of ventilation and locomotion in archosaurs. *Amer Zool* 40:87–100.
- Chen XB, Lee PH, Chong VFH, Wang DY. 2009. Assessment of septal deviation effects on nasal air flow: a computational fluid dynamics model. *Laryngoscope* 119:1730–1736.
- Chinsamy A, Hillenius WJ. 2004. Physiology of nonavian dinosaurs. In: Weishampel DB, Dodson P, Osmólska H, editors. *The Dinosauria*. 2nd ed. Berkeley: University of California Press. p 643–659.
- Coe M. 1978. The decomposition of elephant carcasses in the Tsavo (East) National Park, Kenya. *J Arid Environ* 1:71–86.
- Colbert EH. 1946. *Sebecus*, representative of a peculiar suborder of fossil Crocodylia from Patagonia. *Bull Am Mus Nat Hist* 87:221–270.
- Collins JC, Pilkington TC, Schmidt-Nielsen K. 1971. A model of respiratory heat transfer in a small mammal. *Biophys J* 11:886–914.
- Coombs WP, Jr. 1975. Sauropod habits and habitats. *Palaeogeogr Palaeoclimatol Palaeoecol* 17:1–33.
- Coombs WP, Jr. 1978. The families of the ornithischian dinosaur order Ankylosauria. *Palaeontology* 21:143–170.
- Craven BA, Neuberger T, Paterson EG, Webb AG, Josephson EM, Morrison EE, Settles GS. 2007. Reconstruction and morphometric analysis of the nasal airway of the dog (*Canis familiaris*) and implications regarding olfactory airflow. *Anat Rec* 290:1325–1340.
- Craven BA, Paterson EG, Settles GS. 2010. The fluid dynamics of canine olfaction: unique nasal airflow patterns as an explanation of macrosmia. *J R Soc Interface* 7:933–943.
- Craven BA, Patterson EG, Settles GS, Lawson MJ. 2009. Development and verification of a high-fidelity computational fluid dynamics models of canine nasal airflow. *J Biomech Eng* 131: 091002–1.
- Crole MR, Soley JT. 2010. Gross morphology of the intra-oral rhamphotheca, oropharynx and proximal oesophagus of the emu (*Dromaius novaehollandiae*). *Anat Hist Embryol* 39:207–218.
- Dial BE, Schwenk K. 1996. Olfaction and predator detection in *Coleonyx brevis* (Squamata: Eublepharidae), with comments on the functional significance of buccal pulsing in geckos. *J Exp Zool* 276:415–424.
- Doorly DJ, Taylor DJ, Schroter RC. 2008. Mechanics of airflow in the human nasal airways. *Resp Phys Neuro* 163:100–110.
- Dunlavey T, Mitchell C, Sheets HD. 2004. Retro-deformation is paramount to the accurate description of fossil taxa. *Geo Soc Am Abstr* 36:422.
- Duvdevani I. 1972. The anatomy and histology of the nasal cavities and the nasal salt gland in four species of fringed-toed lizards, *Acanthodactylus* (Lacertidae). *J Morphol* 137:353–364.
- Evans D, Witmer LM, Ridgely RC. 2009. Endocranial anatomy of lambeosaurine dinosaurs: a sensorineural perspective on cranial crest function. *Anat Rec* 292:1315–1337.
- Evans DC, Schott RK, Larson DW, Brown CM, Ryan MJ. 2013. The oldest North American pachycephalosaurid and the hidden diversity of small-bodied ornithischian dinosaurs. *Nat Commun* 4. doi: 10.1038/ncomms2749.
- Farmer CG. 2006. On the origin of avian air sacs. *Respir Physiol Neurobiol* 154:89–106.
- Farmer CG, Carrier DR. 2000a. Pelvic aspiration in the American alligator (*Alligator mississippiensis*). *J Exp Biol* 203:1679–1687.
- Farmer CG, Carrier DR. 2000b. Ventilation and gas exchange during treadmill locomotion in the American alligator (*Alligator mississippiensis*). *J Exp Biol* 203:1671–1678.
- Farmer CG, Sanders K. 2010. Unidirectional airflow in the lungs of alligators. *Science* 327:338–340.
- Fastovsky DF, Weishampel DB. 2005. *The Evolution and Extinction of the Dinosaurs*. 1st ed. Cambridge: Cambridge University Press.
- Foss JF. 1998. Basic engineering fluid mechanics. In Johnson RW, editor. *The Handbook of Fluid Dynamics*. Florida: CRC Press. p 5-1–5-99.
- FrapPELL PB, Hinds DS, Boggs DF. 2001. Scaling of respiratory variables and the breathing pattern in birds: an allometric and phylogenetic approach. *Phys Biochem Zool* 74:75–89.
- Gabe M, Saint-Girons H. 1976. Contribution a la morphologie comparee des fosses nasales et leurs annexes chez les lepidosoriens. *Mem du Mus Nat d'Hist Naturelle* 98:1–87.
- Geist NR. 2000. Nasal respiratory turbinate function in birds. *Physiol Biochem Zool* 73:581–589.
- Gilmore CW. 1924. On *Troodon validus* An orthopodous dinosaur from the Belly River Cretaceous of Alberta, Canada. *Bull Alberta Univ* 1:1–43.
- Guilherme JMG, Bailie N, Martins DA, Kimbell JS. 2007. Atrophic rhinitis: a CFD study of air conditioning in the nasal cavity. *J Appl Physiol* 103:1082–1092.
- Haas G. 1955. The jaw musculature in *Protoceratops* and in other ceratopsians. *Am Mus Nov* 1729:1–24.
- Hansen A. 2007. Olfactory and solitary chemosensory cells: two different chemosensory systems in the nasal cavity of the American alligator, *Alligator mississippiensis*. *BMC Neuro* 8:64.
- Hicks JW, White FN. 1992. Pulmonary gas exchange during intermittent ventilation in the American alligator. *Resp Physiol* 88:23–36.
- Hieronymus TL, Witmer LM, Tanke DH, Currie PJ. 2009. The facial integument of centrosaurine ceratopsids: Morphological and histological correlates of novel skin structures. *Anat Rec* 292: 1370–1396.
- Hillenius W. 1992. The evolution of nasal turbinates and mammalian endothermy. *Paleobiology* 18:17–29.
- Hillenius WJ. 1994. Turbinates in therapsids: evidence for Late Permian origins of mammalian endothermy. *Evolution* 48: 207–229.
- Hillenius WJ, Ruben JA. 2004. The evolution of endothermy in terrestrial vertebrates: who? when? why? *Phys Biochem Zool* 77: 1019–1042.
- Hinds DS, Calder WA. 1971. Tracheal dead space in the respiration of birds. *Evolution* 25:429–440.

- Hoi Y, Meng H, Woodward SH, Bendok BR, Hanel RA, Guterman LR, Hopkins LN. 2004. Effects of arterial geometry on aneurysm growth: three-dimensional computational fluid dynamics study. *J Neurosurg* 101:676–681.
- Holliday, CM. 2009. New insights into dinosaur jaw muscle anatomy. *Anat Rec* 292:1246–1265.
- Holliday CM, Witmer LM. 2008. Cranial kinesis in dinosaurs: intracranial joints, protractor muscles, and their significance for cranial evolution and function in diapsids. *J Vertebr Paleontol* 28: 1073–1088.
- Holmes WM, Cotton R, Xuan VB, Rygg AD, Craven BA, Abel RL, Slack R, Cox JPL. 2011. Three-dimensional structure of the nasal passageway of a hagfish and its implications for olfaction. *Anat Rec* 294:1045–1056.
- Hopson JA. 1979. Paleoneurology. In: Gans C, editor. *Biology of the Reptilia*. Vol.IX: Neurology A. New York: Academic Press. p 39–146.
- Horner JR, Goodwin MB. 2009. Extreme cranial ontogeny in the Upper Cretaceous dinosaur *Pachycephalosaurus*. *PLoS One* 4: e7652. doi:10.1371/journal.pone.0007626.
- Hugh-Jones P, Barter CE, Hime JM, Rusbridge MM. 1978. Dead space and tidal volume of the giraffe compared with some other mammals. *Resp Phys* 35:53–58.
- Hutchinson JR, Bates KT, Molnar J, Allen V, Makovicky PJ. 2011. A computational analysis of limb and body dimensions in *Tyrannosaurus rex* with implications for locomotion, ontogeny, and growth. *PLoS One* 6:e26037.
- Jackson DC, Schmidt-Nielsen K. 1964. Countercurrent heat exchange in the respiratory passages. *Physiology* 51:1192–1197.
- Jarvik E. 1942. On the structure of the snout of crossopterygians and lower gnathostomes in general. *Zool Bidr Upsala* 21:235–675.
- Jiang J, Zhao K. 2010. Airflow and nanoparticle deposition in rat nose under various breathing and sniffing conditions. *J Aerosol Sci* 41:1030–1043.
- Jin EJ, Peng KM, Wang JX, Du AN, Tang L, Wei L, Wang Y, Li SH, Song H. 2008. Study of the morphology of the olfactory organ of African ostrich chick. *Anat Histol Embryol* 37:161–165.
- Kimbell JS, Godo MN, Gross EA, Joyner DR, Richardson RB, Morgan KT. 1997. Computer simulation of inspiratory airflow in all regions of the F344 rat nasal passages. *Tox App Pharm* 145: 388–398.
- Ku DN. 1997. Blood flow in arteries. *Annu Rev Fluid Mech* 29:399–434.
- Langman VA, Maloij GMO, Schmidt-Nielsen K, Schroter RC. 1979. Nasal heat exchange in the giraffe and other large mammals. *Respir Physiol* 37:325–333.
- Lauder GV, Drucker EG, Nauen JC, Wilga CD. 2003. Experimental hydrodynamics and evolution: Caudal fin locomotion in fishes. In: Bels VL, Gasc J-P, Casinos A, editors. *Vertebrate biomechanics and evolution*. Oxford: BIOS Scientific Publishers. p 117–135.
- Lehman TM. 1996. A horned dinosaur from the El Picacho formation of west Texas, and review of ceratopsian dinosaurs from the American southwest. *J Paleont* 70:494–508.
- Longrich NR, Sankey J, Tanke D. 2010. *Texacephale langstoni*, a new genus of pachycephalosaurid (Dinosauria: Ornithischia) from the Upper Campanian Aguja Formation, southern Texas, USA. *Cretaceous Res* 31:274–284.
- Loudon C, Tordesillas A. 1998. The use of the dimensionless Womersley number to characterize the unsteady nature of internal flow. *J Theor Biol* 191:63–78.
- Maidment SCR, Porro LB. 2009. Homology of the palpebral and origin of supraorbital ossification in ornithischian dinosaurs. *Lethaia* 43:95–111.
- Maryańska T. 1977. Ankylosauridae (Dinosauria) from Mongolia. *Palaeo Polo* 37:85–151.
- Maryańska T, Chapman RE, Weishampel DB. 2004. Pachycephalosauria. In: Weishampel DB, Dodson P, Osmólska H, editors. *The Dinosauria*. 2nd ed. Berkeley: University of California Press. p 464–477.
- Maryańska T, Osmólska H. 1974. Pachycephalosauria, a new suborder of ornithischian dinosaurs. *Palaeo Polo* 30:45–102.
- McNab BK. 2009. Ecological factors affect the level and scaling of avian BMR. *Comp Biochem Physiol A* 152:22–45.
- Michaeli G, Pinshow B. 2001. Respiratory water loss in free-flying pigeons. *J Exp Biol* 204:3803–3814.
- Milsom WK. 1988. Control of arrhythmic breathing in aerial breathers. *Can J Zool* 66:99–108.
- Mirade PS, Daudin J-D. 2006. Computational fluid dynamics prediction and validation of gas circulation in a cheese-ripening room. *Int Dairy J* 16:920–930.
- Miyashita T, Arbour VM, Witmer LM, Currie PJ. 2011. The internal cranial morphology of an armoured dinosaur *Euoplocephalus* corroborated by X-ray computed tomographic reconstruction. *J Anat* 219:661–675.
- Motani R, Amenta N, Wiley DF. 2005. Possibilities and limitations of three dimensional retrodeformation of a trilobite and plesiosaur vertebrae. *Paleo Bios* 25:88.
- Mozell MM. 1970. Evidence for a chromatographic model of olfaction. *J Gen Physiol* 56:46–63.
- Murrish DE, Schmidt-Nielsen K. 1970. Exhaled air temperature and water conservation in lizards. *Resp Phys* 10:151–158.
- Nagy KA, Girard IA, Brown TK. 1999. Energetics of free-ranging mammals, reptiles, and birds. *Annu Rev Nutr* 19:247–277.
- O'Connor PM. 2006. Postcranial pneumaticity: an evaluation of soft-tissue influences on the postcranial skeleton and the reconstruction of pulmonary anatomy in archosaurs. *J Morphol* 267: 1199–1266.
- O'Connor PM. 2009. Evolution of archosaurian body plans: skeletal adaptation of an air-sac-based breathing apparatus in birds and other archosaurs. *J Int Biol* 311A:629–646.
- O'Connor PM, Claessens LPAM. 2005. Basic avian pulmonary design and flow-through ventilation in non-avian theropod dinosaurs. 2005. *Nature* 436:253–256.
- Oelrich TM. 1956. The anatomy of the head of *Ctenosauria pectinata* (Iguanidae). *Misc Pub Mus Zool Univ Mich* 94:1–122.
- O'Gorman EJ, Hone DWE. 2012. Body size distribution of the dinosaurs. *PLoS One* 7:e51925. doi:10.1371/journal.pone.0051925.
- Osborn HF. 1898. Additional characters of the great herbivorous dinosaur *Camarasaurus*. *Bull Am Mus Nat Hist* 10:219–233.
- Osmólska H. 1974. Nasal salt glands in dinosaurs. *Acta Palaeo Polo* 24:205–215.
- Ostrom JH. 1961. Cranial morphology of the hadrosaurian dinosaurs of North America. *Bull Am Mus Nat Hist* 122:1–78.
- Ostrom JH. 1962. The cranial crests of hadrosaurian dinosaurs. *Postilla* 62:1–29.
- Padian K, Horner JR. 2004. Dinosaur physiology. In: Weishampel DB, Dodson P, Osmólska H, editors. *The Dinosauria*. 2nd ed. Berkeley: University of California Press. p 660–671.
- Parsons TS. 1959. Nasal anatomy and the phylogeny of reptiles. *Evolution* 13:175–187.
- Parsons TS. 1967. Evolution of the nasal structure in the lower tetrapods. *Am Zool* 7:397–413.
- Parsons TS. 1970. The nose and Jacobson's organ. In: Gans C, Parsons TS, editors. *Biology of the Reptilia* 2. New York: Academic Press. p 99–191.
- Peczki J. 1995. Implications for body-mass estimates for dinosaurs. *J Vertebr Paleontol* 14:520–533.
- Porter WP, Witmer LM. 2011. Vascular anatomy and its physiological implications in extant and extinct dinosaurs and other diapsids. *J Vertebr Paleontol* 31:176A.
- Porter WP, Witmer LM. 2012. Vascular patterns in iguanas: blood vessels and cephalic sites of thermal exchange. In *Annual Meeting of the Society of Integrative and Comparative Biology*, Charleston, South Carolina.
- Rehorek SJ, Firth BT, Hutchinson MN. 2000. The structure of the nasal chemosensory system in squamate reptiles. 1. The olfactory organ, with special reference to olfaction in geckos. *J Biosci* 25: 173–179.
- Rieppel O, Gauthier J, Maisano J. 2008. Comparative morphology of the dermal palate in squamate reptiles, with comments on phylogenetic implications. *Zool J Linn Soc* 152:131–152.
- Roache PJ. 1994. Perspective: a method for uniform reporting of grid refinement studies. *J Fluid Eng* 116:405–413.

- Romer AS. 1922. The locomotor apparatus of certain primitive and mammal-like reptiles. *Bull Am Mus Nat Hist* 46:517–603.
- Romer AS. 1924. Pectoral limb musculature and shoulder-girdle structure in fish and tetrapods. *Anat Rec* 27:119–143.
- Romer AS. 1933. *Vertebrate Paleontology*. Chicago: University of Chicago Press.
- Ruben JA. 1995. The evolution of endothermy in mammals and birds: from physiology to fossils. *Annu Rev Physiol* 57:69–95.
- Ruben JA. 1996. Evolution of endothermy in mammals, birds and their ancestors. In: Johnston IA, Bennett AF, editors. *Animals and Temperature: Phenotypic and Evolutionary Adaptation*. Cambridge: Cambridge University Press. p 347–376.
- Ruben JA, Hillenius WJ, Geist NR, Leitch A, Jones TD, Currie PJ, Horner JR, Espe III G. 1996. The metabolic status of some Late Cretaceous dinosaurs. *Science* 273:1204–1207.
- Ruben JA, Jones TD, Geist NR. 1998. Respiratory physiology of the dinosaurs. *BioEssays* 20:852–859.
- Rudwick MJS. 1964. The inference of function from structure in fossils. *Br J Philos Sci* 15:27–40.
- Ruiz-Gironés E. 2011. Automatic hexahedral meshing algorithms: from structured to unstructured meshes. Ph.D. Dissertation, Universitat Politècnica de Catalunya, Barcelona Spain.
- Saint-Girons H. 1976. Données histologiques sur les fosses nasales et leurs annexes chez *Crocodylus niloticus* Laurenti et *Caiman crocodilus* (Linnaeus) (Reptilia, Crocodylidae). *Zoomorphologie* 84: 301–318.
- Schachner ER, Cieri RL, Butler JP, Farmer CG. 2013. Unidirectional pulmonary airflow patterns in the savannah monitor lizard. *Nature* 506:367–370.
- Schachner ER, Farmer CG, McDonald AT, Dodson P. 2011a. Evolution of the dinosauriform respiratory apparatus: new evidence from the postcranial axial skeleton. *Anat Rec* 294:1532–1547.
- Schachner ER, Lyson TR, Dodson P. 2009. Evolution of the respiratory system in nonavian theropods: evidence from rib and vertebral morphology. *Anat Rec* 292:1501–1513.
- Schachner ER, Manning PL, Dodson PD. 2011b. Pelvic and hind-limb myology of the basal archosaur *Poposaurus gracilis* (Archosauria: Poposauroidae). *J Morphol* 272:1464–1491.
- Schmidt-Nielsen K. 1997. *Animal Physiology*. 5th ed. Cambridge: Cambridge University Press.
- Schmidt-Nielsen K, Hainsworth RF, Murrish D. 1970. Counter-current heat exchange in the respiratory passages: Effect on water and heat balance. *Respir Physiol* 9:263–276.
- Schoenfeld TA, Cleland TA. 2005. The anatomical logic of smell. *Trends Neurosci* 28:620–627.
- Schott RK, Evans DC, Goodwin MB, Horner JR, Brown CM, Longrich NR. 2011. Cranial ontogeny in *Stegoceras validum* (Dinosauria: Pachycephalosauria): a quantitative model of pachycephalosaur dome growth and variation. *PLoS One* 6:e21092. doi: 10.1371/journal.pone.0021092.
- Schott RK, Evans DC, Williamson TE, Carr TD, Goodwin MB. 2009. The anatomy and systematics of *Colepiocephale lambei* (Dinosauria: Pachycephalosauridae). *J Vertebr Paleontol* 29:771–786.
- Sedlmayr JC. 2002. Anatomy, evolution, and functional significance of cephalic vasculature in Archosauria. Ph.D. Dissertation, Ohio University, Athens, OH.
- Sereno PC. 2000. The fossil record, systematics and evolution of pachycephalosaurs and ceratopsians from Asia. In: Benton MJ, Shishkin MA, Unwin DM, Kurochkin EN, editors. *The age of dinosaurs in Russia and Mongolia*. Cambridge: Cambridge University Press. p 480–560.
- Seymour RS. 2004a. Evidence for endothermic ancestors of crocodyles at the stem of archosaur evolution. *Physiol Biochem Zool* 77: 1051–1067.
- Seymour RS. 2004b. Reply to Hillenius and Ruben. *Physiol Biochem Zool* 77:1073–1075.
- Simpson GG, Eftman HO. 1928. Hind limb musculature and habits of a Paleocene multituberculata. *Am Mus Nov* 333:1–19.
- Snively E, Cox A. 2008. Structural mechanics of pachycephalosaur crania permitted head-butting behavior. *Paleontol Electron* 11:3A17.
- Snively E, Russell AP. 2007. Functional variation of neck muscles and their relation to feeding style in Tyrannosauridae and other large theropod dinosaurs. *Anat Rec* 290:934–957.
- Snively E, Theodor JM. 2011. Common functional correlates of head-strike behavior in the pachycephalosaur *Stegoceras validum* (Ornithischia, Dinosauria) and combative artiodactyls. *PLoS One* 6:e21422. doi:10.1371/journal.pone.0021422.
- Stebbins RC. 1948. Nasal structure in lizards with reference to olfaction and conditioning of the inspired air. *Am J Anat* 83:183–221.
- Sullivan RM. 2000. *Prenocephale edmontonensis* (Brown and Schlaikjer) new comb. and *P. brevis* (Lambe) new comb. (Dinosauria: Ornithischia: Pachycephalosauria) from the Upper Cretaceous of North America. *N M Mus Nat Hist Bull* 17:177–190.
- Sullivan RM. 2003. Revision of the dinosaur *Stegoceras* Lambe (Ornithischia, Pachycephalosauridae). *J Vertebr Paleontol* 23:181–207.
- Sullivan RM. 2006. A taxonomic review of the Pachycephalosauridae (Dinosauria: Ornithischia). *N M Mus Nat Hist Sci Bull* 35:347–365.
- Tielemans BI, Williams JB, Michaeli G, Pinshow B. 1999. The role of the nasal passages in the water economy of crested larks and desert larks. *Physiol Biochem Zool* 72:219–226.
- Tsuihiji T. 2010. Reconstructions of the axial muscle insertions in the occipital region of dinosaurs: evaluations of past hypotheses on Marginocephalia and Tyrannosauridae using the extant phylogenetic bracket approach. *Anat Rec* 293:1360–1386.
- Vickaryous MK, Russell AP. 2003. A redescription of the skull of *Euoplocephalus tutus* (Archosauria: Ornithischia): a foundation for comparative and systematic studies of ankylosaurian dinosaurs. *Zool J Linn Soc* 137:157–186.
- Vogel S. 1994. *Life in Moving Fluids*. 2nd ed. New Jersey: Princeton University Press.
- Vogel S. 2003. Viscosity and the patterns of flow. In: Vogel S, editor. *Comparative Biomechanics: Life's Physical World*. New Jersey: Princeton University Press. p 117–138.
- Waibl H, Gasse H, Hashimoto Y, Burdas K-D, Constantinescu GM, Saber AS, Simoens P, Salazar I, Sotonyi P, Augsburg H, Bragulla H. 2012. *Nomina anatomica veterinaria*. 5th ed. International Committee on Veterinary Gross Anatomical Nomenclature. World Association of Veterinary Anatomists. Columbia, Missouri.
- Watabe M, Tsogtbaatar K, Sullivan RM. 2011. A new pachycephalosaurid from the Baynshire formation (Cenomanian-Late Santonian), Gobi Desert, Mongolia. *N M Mus Nat Hist Bull* 53:489–497.
- Wedel MJ. 2003. Vertebral pneumaticity, air sacs, and the physiology of sauropod dinosaurs. *Paleobiology* 29:243–255.
- Weishampel DB. 1981. The nasal cavity of lambeosaurine hadrosaurids (Reptilia: Ornithischia): comparative anatomy and homologies. *J Paleol* 55:1046–1057.
- Wheeler P. 1978. Elaborate CNS cooling structures in large dinosaurs. *Nature* 275:441–443.
- Williamson TE, Carr TD. 2002. A new genus of derived pachycephalosaurian from Western North America. *J Vertebr Paleontol* 22: 779–801.
- Witmer LM. 1995a. The extant phylogenetic bracket and the importance of reconstructing soft tissues in fossils. In: Thomason JJ, editor. *Functional morphology in vertebrate paleontology*. New York: Cambridge University Press. p 19–33.
- Witmer LM. 1995b. Homology of facial structures in extant archosaurs (birds and crocodylians), with special reference to paranasal pneumaticity and nasal conchae. *J Morphol* 225:269–327.
- Witmer LM. 1997a. The evolution of the antorbital cavity of archosaurs: a study in soft-tissue reconstruction in the fossil record with an analysis of the function of pneumaticity. *J Vertebr Paleontol* 17 (1 supp):1–73.
- Witmer LM. 1997b. Craniofacial air sinus systems. In: Currie PJ, Padian K, editors. *The Encyclopedia of Dinosaurs*. New York: Academic Press. p 151–159.
- Witmer LM. 2001. Nostril position in dinosaurs and other vertebrates and its significance for nasal function. *Science* 293:850–853.
- Witmer LM, Ridgely RC. 2008a. The paranasal air sinuses of predatory and armored dinosaurs (Archosauria: Theropoda and Ankylosauria) and their contribution to cephalic architecture. *Anat Rec* 291:1362–1388.

- Witmer LM, Ridgely RC. 2008b. Structure of the brain cavity and inner ear of the centrosaurine ceratopsid *Pachyrhinosaurus* based on CT scanning and 3D visualization. In Currie PJ, editor. *A New Horned Dinosaur from an Upper Cretaceous Bone Bed in Alberta*. Ottawa: National Research Council Research Press. p 117–144.
- Witmer LM, Ridgely RC. 2009. New insights into the brain, braincase, and ear region of tyrannosaurs (Dinosauria, Theropoda), with implications for sensory organization and behavior. *Anat Rec* 292:1266–1296.
- Witmer LM, Ridgely RC. 2010. The Cleveland tyrannosaur skull (*Nanotyrannus* or *Tyrannosaurus*): new findings based on CT scanning, with special reference to the braincase. *Kirtlandia* 57:61–81.
- Witmer LM, Ridgely RC, Dufeu DL, Semones MC. 2008. Using CT to peer into the past: 3D visualization of the brain and ear regions of birds, crocodiles, and nonavian dinosaurs. In: Endo H, Frey R, editors. *Anatomical Imaging: Towards a New Morphology*. Springer. p 67–87.
- Witmer LM, Sampson SD. 1999. Nasal conchae and blood supply in some dinosaurs: physiological implications. *J Vertebr Paleontol* 19 (3 supp):85A. Japan.
- Witzmann F. 2009. Comparative histology of sculptured dermal bones in basal tetrapods, and the implications for the soft tissue dermis. *Paleodiversity* 2:233–270.
- Womersley JR. 1955. Method for the calculation of velocity, rate of flow and viscous drag in arteries when the pressure gradient is known. *J Physiol* 127:553–563.
- Yam R, Yuen PL, Yung R, Choy T. 2011. Rethinking hospital general ward ventilation design using computational fluid dynamics. *J Hosp Infect* 77:31–36.
- Zhao K, Dalton P, Yang GC, Scherer PW. 2006. Numerical modeling of turbulent and laminar airflow and odorant transport during sniffing in the human and rat nose. *Chem Senses* 31:107–118.